Exploring the impact of hydrogen peroxide delivery methods on PaDa-I enzyme deactivation during styrene biotransformation within tandem catalysis framework

Prepared by:
Rufaro Mukwenya

In fulfilment of the requirements for the degree of
Master of Science

Supervisor: Dr Athanasios Kotsiopoulos
Co-supervisor: Dr Derik Wilbers

Department of Chemical Engineering
Faculty of Engineering and the Built Environment
University of Cape Town

February 2024

Plagiarism Declaration

I know the meaning of plagiarism and declare that all the work in the document, save for that which is properly acknowledged, is my own. This thesis/dissertation has been submitted to the Turnitin module and I confirm that my supervisor has seen my report and any concerns revealed by such have been resolved with my supervisor.

Signed by candidate

Signature

Abstract

Biocatalysis has become an attractive method for hydrocarbon activation due to its alignment with the principles of green chemistry. Enzymes are advantageous over traditional metal-based catalysts because they are obtained from renewable sources, typically require mild reaction conditions, and are highly selective. A few classes of enzymes have been identified as active in these transformations including oxygenases, oxidases, hydroxylases, peroxidases and peroxygenases. One of the most promising classes of enzymes are unspecific peroxygenases (UPOs). These enzymes are able to use hydrogen peroxide (H_2O_2) as the oxidant and electron donor without the need for expensive co-factors. The main challenge is the deactivation of UPOs in reaction systems containing excess H_2O_2. A potential approach to circumvent this deactivation is to produce the hydrogen peroxide *in-situ* in a one-pot tandem catalytic system. However, this system is poorly understood with very little kinetic data reported in the literature.

In this study, different hydrogen peroxide delivery methods and concentrations were investigated to minimise enzyme deactivation. The delivery methods were once-off addition where the hydrogen peroxide was added all at once, stepwise addition where it was added at regular intervals and continuous addition where it was fed gradually at a controlled rate using a syringe pump. In addition, the influence of reaction temperature and pH on the enzyme's stability were investigated. Thereafter, the obtained optimised process conditions were evaluated in a hydrocarbon biotransformation reaction, using styrene as the model substrate. The PaDa-I enzyme (UPO variant) lost approximately 90% of its initial activity during the early stages of the reaction. This was significantly higher than the 50% and 40% activity lost when the enzyme was exposed to hydrogen peroxide and styrene as sole substrates. Despite the significant activity loss, a turnover number of 3 070 $mol_{product}\,mol_{protein}^{-1}$ was achieved employing semi-continuous addition which was determined to be the best H_2O_2 delivery method.

A full kinetic study investigating the deactivation of the PaDa-I enzyme was also performed. Three enzyme deactivation models were tested to model the experimental data by nonlinear regression - these kinetic models were first order, two-parameter and four-parameter models. It was established that the two-parameter model best fit the experimental data. This kinetic model described a deactivation pathway where the enzyme is not completely deactivated, but rather transformed to less reactive intermediates over time upon exposure to excess hydrogen peroxide. The crucial kinetic parameter obtained from this model was the ratio of the final (less active form) and initial specific enzyme activity α_1. The α_1 value of 0.07 obtained for the styrene biotransformation was approximately an order of magnitude lower compared to the studies using hydrogen peroxide and styrene as sole substrates. Further insights on the kinetics of this biotransformation revealed that hydrogen peroxide behaved as a non-competitive inhibitor. This suggested that hydrogen peroxide was bound to an allosteric site on the enzyme, which distorted the structure of the enzyme making it less effective for styrene oxidation. The H_2O_2 concentration or delivery rate should therefore be reduced to further minimise this inhibition. The findings in this study will form the basis for future tandem systems that combine *in-situ* H_2O_2 production with hydrocarbon biotransformation using UPOs.

Acknowledgements

I would like to extend my gratitude to all the amazing people that were part of this academic journey:

To the C*change DST-NRF Centre of Excellence in Catalysis and the Centre for Bioprocess Engineering Research (CeBER) for providing the financial means and conducive research environment that facilitated the completion of this project.

To my supervisor, Dr Thanos Kotsiopoulos, I would like to express my sincere gratitude for your unwavering support, invaluable guidance, patience, and constructive feedback in shaping the direction of my research.

To my co-supervisor, Dr Derik Wilbers, thank you for your hands-on guidance and support both in the lab and in improving my writing skills. I appreciate your kind and encouraging words that kept me motivated throughout.

To CeBER lab manager, Mr Tich Samkange, I am grateful for all the help you provided especially during the stressful moments in the lab. I always looked forward to the fun stories you told and for constantly cheering me on to keep going.

To my fellow postgraduate colleagues, I am grateful for the camaraderie, shared laughter and support you gave me. Some days I would struggle but you would encourage me to prioritise my mental health, take a break, reset, and come back stronger.

To my friends and family, thank you for the constant moral support and standing by me throughout this journey. Many thanks go to my mom and dad - thank you for believing in me, motivating me and praying for me.

And lastly, to the Almighty for giving me strength.

Table of contents

List of illustrations

List of figures

List of schemes

List of tables

Glossary

Biocatalysis	The use of enzymes to perform chemical conversions of organic compounds
Biotransformation	The process of converting one set of chemicals into another using biological systems
Catalytic efficiency	A measure of how efficiently an enzyme converts substrate to product
Chemocatalysis	The use of chemical catalysts to facilitate and accelerate chemical reactions without being consumed in the process
Circumneutral	pH values close to neutral, around 6.0 to 8.0
Deactivation	The loss of catalytic activity of an enzyme
Enzyme stability	The ability of an enzyme to maintain its activity under certain conditions
Hydrocarbon	A compound composed solely of hydrogen and carbon atoms
In-situ	Within the reaction system
Inhibition	The reduction of enzyme activity by a molecule (inhibitor)
Michaelis-Menten	A kinetic model describing the rate of enzymatic reactions
One-pot process	Process whereby all reactants are placed in one reactor for successive chemical reactions
Oxidant	Compound that acts as an oxidising agent
Oxidation	The addition of oxygen to a compound or the removal of hydrogen from a compound
Oxyfunctionalisation	A chemical process involving the introduction of oxygen-containing functional groups to the substrate molecule
Residual activity	The remaining enzyme activity after exposure to certain conditions
Tandem catalysis	Technique whereby multiple catalysts perform sequential transformation of the substrate via two or more distinct mechanisms
Turnover number	The number of substrate molecules converted to product per enzyme/protein molecule in a given time
Unspecific peroxygenase	A versatile enzyme that belongs to the family of heme-containing proteins that catalyse various oxidative reactions

Abbreviations

*Aae*UPO	Unspecific peroxygenase from *Agrocybe aegerita*
BioPd	Biofabricated catalyst containing palladium
E. coli	*Escherichia coli*
GC	Gas chromatography
GOx	Glucose oxidase
MeOH	Methanol
NADPH	Nicotinamide adenine dinucleotide phosphate hydrogen
NADH	Nicotinamide adenine dinucleotide hydrogen
NBD	5-nitro-1,3-benzodioxide
P450	Class of heme-containing monooxygenases that catalyse a range of diverse oxidative reactions, whose absorbance is at 450 nm when bound to carbon monoxide
S. cerevisiae	*Saccharomyces cerevisiae*
TON	Turnover number
UPO	Unspecific peroxygenase

Nomenclature

α_1	Ratio of specific activities of the active intermediate and initial enzyme forms
α_2	Relative specific activity of the second intermediate and initial enzyme forms
β	Specific activity of initial enzyme state
β_1	Specific activity of the first intermediate enzyme form
β_2	Specific activity of the second intermediate enzyme form
A_t	Enzyme activity at time t
A_0	Enzyme activity at time t = 0
AARD	Average absolute relative deviation
AIC	Akaike's information criterion
BIC	Bayesian information criterion
E	Initial enzyme form
E_1	First intermediate enzyme form
E_2	Second intermediate enzyme form
E_d	Deactivated enzyme form
$f(x_i)$	Predictive model value
K	Total number of estimated regression parameters
k_1, k_2	First-order deactivation rate constants (min^{-1})
k_{cat}	Molecule conversions per unit time ($mol_{product}\ mol_{enzyme}\ s^{-1}$)
K_I	Inhibition constant (mM)
K_M	Michaelis-Menten constant (mM)
$\log L(\theta)$	Log-likelihood estimator
n	Total number of observations
R^2	Coefficient of determination
S	Substrate concentration
t	Time (min or h)
v	Rate of reaction (mM min^{-1})
v_{max}	Maximum rate of reaction (mM min^{-1})
χ^2	Chi-square
U	The amount of enzyme that converts 1 µmol of 5-nitro-1,3-benzodioxide (NBD) to 1 µmol of 4-nitrocatechol in 1 min at 25 °C and pH 7.0
y_i	Experimental value
$\bar{y}$	Average of experimental values

1 Introduction

1.1 Background

In recent years, there has been steady development towards using biocatalysis for the oxidation of hydrocarbons to produce high value oxygenates (Bell *et al.*, 2021; Hobisch *et al.*, 2021; Pyser *et al.*, 2021; Winkler *et al.*, 2021; Yi *et al.*, 2021). Hydrocarbons are readily available in crude oil and natural gas, and they include alkanes and alkenes (Ayala and Torres, 2004). Hydrocarbons are often very inert due to the high dissociation energy of the C-H bonds. In particular aliphatic alkanes have C-H bond dissociation energies (BDE) in the range of 400-450 kJ/mol while alkenes are only slightly more reactive (C-H BDE 350-400kJ/mol) (Blanksby and Ellison, 2003). For this reason, conventional oxidation processes utilizing these as substrates often require harsh operating conditions to achieve substantial productivity (Soussan *et al.*, 2016). For example, the steam reforming process of methane to methanol conventionally occurs at temperatures as high as 470 °C (Ayala and Torres, 2004) and the commercial hydroformylation of alkenes to aldehydes requires pressures as high as 30 MPa (Franke *et al.*, 2012). As an alternative, the biotransformation of hydrocarbons has the potential to lower the energy requirement of such oxidative processes as the enzymes used in these reactions operate at ambient conditions. In addition, enzymatic reactions often proceed with high chemo- and regioselectivity, requiring less laborious and expensive purification steps (Polizzi *et al.*, 2007; Schrewe *et al.*, 2013).

Some of the enzymes that have been identified as biocatalysts with good catalytic performance in hydrocarbon oxyfunctionalisation are the PaDa-I variant from the unspecific peroxygenase (UPO) group of enzymes as well as the cytochrome P450 monooxygenase, CYP102A1 (Burek *et al.*, 2019; Hollmann *et al.*, 2011). These enzymes both contain heme-dependent domain groups and follow similar catalytic cycles using hydrogen peroxide (H_2O_2) as the oxidant. This is referred to as the peroxide shunt pathway (Cirino and Arnold, 2003; Hrycay and Bandiera, 2012; O'Reilly *et al.*, 2011). Hydrogen peroxide is considered a green oxidant that produces water as the only by-product. Furthermore, it may prove simpler to optimise reaction systems using H_2O_2 (especially at large scale) because of its independence from complex electron transport chains involving cofactors (Bormann *et al.*, 2015; Hobisch *et al.*, 2021; Valderrama *et al.*, 2002). In contrast, the natural pathway for CYP102A1 requires molecular oxygen and NAD(P)H, an expensive cofactor with additional costs associated with its regeneration (Munro *et al.*, 2013; O'Reilly *et al.*, 2011). The substrates that are normally catalytically oxidized by these enzymes include fatty acids, carboxylic acids, aromatics and a few medium-long chain alkanes (Samanta, 2008).

The main challenge with such reactions is that stoichiometric amounts of H_2O_2 required for full conversion of the substrate often inhibit the activity of enzymes through oxidative deactivation (Burek *et al.*, 2019; Valderrama *et al.*, 2002). Low H_2O_2 concentrations (3-5 wt%) are often required to maintain enzyme activity in this oxidation reaction (Puértolas *et al.*, 2015). The delivery of H_2O_2 can be improved through periodic dosage of H_2O_2 to the reaction mixture at low concentrations or through implementing an *in-situ* H_2O_2 generation system using gold-palladium based catalysts or biocatalysts such as oxidases. These delivery systems ensure that the oxidant is available at low enough concentrations to prolong the stability of the often expensive enzymes and thus potentially leading to better overall catalytic performance and a more economical process.

1.2 Context of project

The rising awareness of energy consumption and waste generation in current industrial hydrocarbon oxyfunctionalisation processes has led to intensive research into more eco-friendly synthetic routes. As previously mentioned, current oxidative processes often require expensive chemo-catalysts which operate occur under harsh reaction conditions and may be poorly selective. In contrast enzymatic biocatalysis is highly promising in this regard, complying with almost all twelve guidelines of green chemistry (Sheldon and Woodley, 2018). Most enzymatic processes in biocatalysis are often performed in an aqueous medium at mild operating conditions, thus making the process energy efficient. Additionally, enzymes are obtained from renewable sources and produce significantly less (and often not toxic) waste materials (Sheldon and Woodley, 2018; Truppo, 2017; Winkler *et al.*, 2021). With this in mind, many industries including pharmaceutical, food, cosmetic, and agrochemical industries have successfully incorporated biocatalytic steps in efforts to advance towards sustainable manufacturing processing (Dong *et al.*, 2018; Hollmann *et al.*, 2011; Truppo, 2017; Woodley, 2008).

Another way of establishing more sustainable routes is through the combination of reaction steps into a single reactor or one-pot systems which could further reduce waste production and solvent consumption (Gröger and Hummel, 2014; Sheldon and Woodley, 2018). Cascade reactions - a reaction whereby chemical bonds are formed sequentially such that subsequent reactions can only occur once the intermediate product of the preceding reaction is formed - are promising candidates for incorporation into one-pot processes. An example of this is the combination of the Wacker oxidation of styrene to acetophenone and its subsequent enzymatic reduction to (R)-1-phenylethanol (Scheme 1.1) (Sato *et al.*, 2015). In this case, the reaction occurs in a one-pot system which proceeds without changing the reaction conditions, adding reagents or isolating intermediates (Denard *et al.*, 2013). The advantage of this is that there are potentially fewer unit operations required; therefore the production costs in terms of both capital and operational expenditure could be reduced.

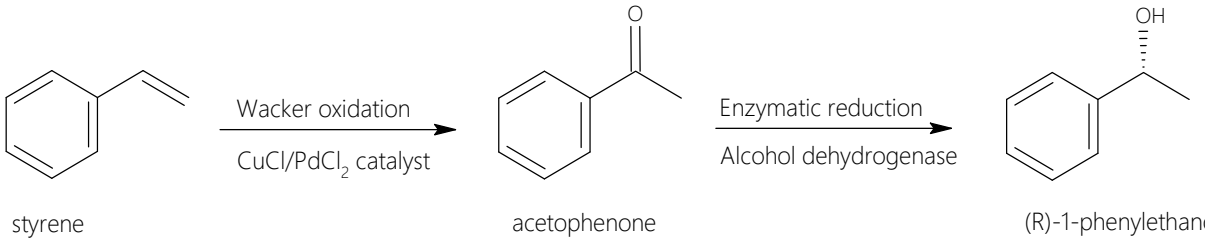

Scheme 1.1: Cascade reaction scheme of the Wacker oxidation of styrene to acetophenone followed by its reduction to (R)-1-phenylethanol (Sato *et al.*, 2015)

As shown in the scheme above, one-pot processes may combine traditional heterogeneously catalysed reaction steps with biocatalytic processes in tandem (Gröger and Hummel, 2014). Currently, studies have been made towards developing tandem systems whereby enzyme-driven oxyfunctionalisation is combined with heterogeneously catalysed *in-situ* H_2O_2 production (Churakova *et al.*, 2011; Freakley *et al.*, 2019; Ni *et al.*, 2016; Pesic *et al.*, 2019). Such one-pot chemo-biocatalytic processes often attempt to utilize the high chemoselectivity of enzymes in combination with the high catalytic activity of these catalysts towards H_2O_2 synthesis (Scheme 1.2).

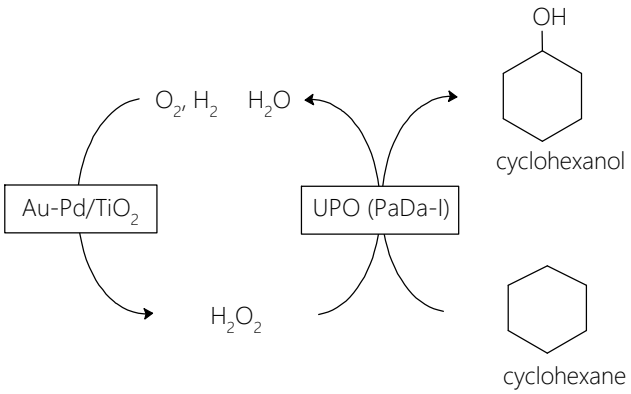

Scheme 1.2: A combination of heterogeneous catalysis and biocatalysis to oxidise cyclohexane to cyclohexanol using H_2O_2 produced *in-situ* (Freakley *et al*., 2019)

In the chemo-bio tandem system shown above, a titania supported gold-palladium catalyst was used to supply H_2O_2 to the PaDa-I variant to oxidise cyclohexane to cyclohexanol. This tandem system ensures that the oxidant is delivered to the enzyme at low enough peroxide concentrations that will not inhibit the enzyme thus potentially increasing long term stability and productivity of the enzyme.

1.3 Overall objective

The oxyfunctionalisation of hydrocarbons can be achieved using peroxide-driven enzymes such as unspecific peroxygenases (PaDa-I) and cytochrome P450 monooxygenases (CYP102A1). The enzyme performance; however, is significantly lowered at high concentrations of H_2O_2 as a result of enzyme deactivation. One of the strategies to improve this is to combine *in-situ* H_2O_2 generation with the enzymatic oxyfunctionalisation in a one-pot process such that low concentrations of the peroxide are delivered to the enzyme. This could potentially improve the productivity by reducing enzyme inactivation. There is; however, limited understanding of the overall process. The kinetics of the rate of H_2O_2 production, the rate of H_2O_2 uptake by the enzyme and concurrently the rate of enzyme deactivation are poorly understood. The main objective of this thesis therefore is to investigate how different peroxide delivery approaches impact the enzyme activity and whether that influences the overall productivity. Determining the deactivation kinetics associated with the different approaches brings insight on how the enzyme operates and how to further optimise the reaction for the oxyfunctionalisation of hydrocarbons.

1.4 Scope and limitations

There are several types of enzymes that can be used for the oxyfunctionalisation of hydrocarbons. However, in this study will be restricted to investigating the activity of a commercially available unspecific peroxygenases (PaDa-I variant). In this project, it is attempted to decouple the process steps currently employed in the *in-situ* delivery of H_2O_2 to PaDa-I (Churakova *et al*., 2011; Freakley *et al*., 2019; Ni *et al*., 2016; Pesic *et al*., 2019). The focus is to establish an optimal H_2O_2 delivery approach and evaluate the enzyme deactivation kinetics associated with such a system. This will then serve as a guideline when developing future heterogeneous catalysts for *in-situ* H_2O_2 generation in tandem chemo-bio systems. To this end the oxidant will be dosed into the reaction medium rather than being generated *in-situ*.

1.5 Thesis structure

The thesis begins with a review of the relevant literature in Chapter 2 which gives a brief overview on hydrocarbon activation biocatalytic processes. The implementation of tandem catalysis as a sustainable synthetic route for these processes are also reviewed in this chapter. This is followed by a discussion on the two catalytic reaction steps, *in-situ* H_2O_2 generation and enzyme-driven oxyfunctionalisation, whilst highlighting the impact of different delivery approaches on enzyme stability and performance. The literature review is concluded by outlining the gaps in the existing knowledge, thereafter, developing a problem statement, hypothesis and key questions. The experimental methods developed to address these research questions are detailed in Chapter 3. This is followed by the experimental results highlighting the impact of H_2O_2 delivery, H_2O_2 concentration, pH and temperature on the stability of the enzyme in Chapter 4. The deactivation kinetics of the enzyme under these reaction conditions are subsequently analysed and discussed in Chapter 5. In Chapter 6, the oxidation of styrene to styrene oxide, a model hydrocarbon biotransformation reaction, is evaluated using the different H_2O_2 delivery methods. The combined styrene and hydrogen peroxide-driven inhibition on styrene oxide production is also included in this chapter. Lastly, the hypothesis and key questions are evaluated and presented in Chapter 7, giving the overall concluding remarks and recommendations.

2 Literature review

Enzymes are promising biocatalysts that functionalise a wide range of substrates with high selectivity and minimal waste production (Polizzi *et al.*, 2007; Schrewe *et al.*, 2013; Soussan *et al.*, 2016). This is an attractive feature as industry is shifting towards environmentally friendly synthesis routes (Sheldon and Woodley, 2018; Truppo, 2017). A particularly important reaction is the oxidation of hydrocarbons. This may be accomplished biocatalytically using either unspecific peroxygenases or cytochrome P450s, with H_2O_2 as the oxidant (Burek *et al.*, 2019; Hollmann *et al.*, 2011; Whitehouse *et al.*, 2012). This is highly advantageous as no secondary cofactors are needed and water is the only byproduct. These enzymes are however inactivated in the presence of high concentrations of H_2O_2 (Bormann *et al.*, 2015; Valderrama *et al.*, 2002). Researchers have therefore explored the use of one-pot tandem systems where H_2O_2 is produced *in-situ* and delivered to the enzyme at a low concentration in the hope of circumventing enzyme deactivation (Freakley *et al.*, 2019; Ni *et al.*, 2016; Tieves *et al.*, 2019; Zhang *et al.*, 2017). The effect of H_2O_2 delivery on reaction and deactivation kinetics is however unclear. Knowledge of these kinetic parameters can potentially be used to further optimise the system such that underutilised hydrocarbons are valourised at high yields without prematurely deactivating the enzyme. The literature review therefore begins by discussing the use of hydrocarbons as a potential substrate for enzyme-driven functionalisation followed by the description and benefits of one-pot tandem systems. Thereafter, different *in-situ* H_2O_2 delivery systems are assessed along with different enzymatic oxyfunctionalisation reactions, and the knowledge gaps in terms of enzyme (deactivation) kinetics are highlighted.

2.1 Biocatalysis overview

Hydrocarbons are abundantly available chemical substrates obtained from natural gas and crude oil (Bergman, 2007; Soussan *et al.*, 2016). These are often employed as substrates in thermal or steam cracking where heat and pressure are used to break down the long hydrocarbon chains into shorter chain alkenes (Fakhroleslam and Sadrameli, 2020). The Fischer-Tropsch process also generates alkane byproducts. During this process syngas from coal liquefaction is converted to a pool of different length hydrocarbon chains consisting mainly of alkanes and alkenes (Jahangiri *et al.*, 2014; Khodakov *et al.*, 2007). The short chain alkanes produced are of low value and not fully exploited as platform chemicals for further derivatization. Most hydrocarbon feedstocks are mainly used as fuels and in power generation (Bergman, 2007). This is due to the high dissociation energy of C-H and C=C bonds which limits reactivity and selectivity in hydrocarbon activation and/or functionalisation (Blanksby and Ellison, 2003). Traditional catalytic processes using these as substrates typically demand harsh operating conditions to achieve substantial output. Furthermore, the catalysts employed (often chemo-catalysts) are poorly selective, resulting in a mixture of primary products and byproducts that require further purification (Ayala and Torres, 2004; Franke *et al.*, 2012; Soussan *et al.*, 2016). Recent research has focussed on moving away from the currently employed energy-intensive, waste generating industrial routes towards more sustainable, green chemistry routes for hydrocarbon activation (Sheldon and Woodley, 2018; Soussan *et al.*, 2016; Winkler *et al.*, 2021). Biocatalysis has emerged as an environmentally friendly alternative, synthesis route (Dong *et al.*, 2018; Schrewe *et al.*, 2013; Yi *et al.*, 2021).

Biocatalysis has developed into a mature industry whereby different classes of enzymes are seen to catalyse a wide spectrum of reactions which are normally difficult to perform by conventional chemical routes (Dong *et al.*, 2018). These enzymes can be produced by host cells through protein recombination,

a process whereby genetic material of the cell is modified for the heterologous expression of desirable enzymes which are not naturally produced by the host cell (Bernhardt, 2006; Hrycay and Bandiera, 2012; Lundemo and Woodley, 2015). This recombinant technique can also be used to modify the protein production process, thus allowing for high yields of enzymes specific to the reaction of interest. This, in turn, may improve the biocatalytic conversion of the desired reaction. The modification technique can also be employed to improve the stability of the enzyme produced (Polizzi *et al*., 2007). Different bacteria can be used as host cells such as *Pseudomonas putida*, *Pichia pastoris*, *Saccharomyces cerevisiae* and *Escherichia coli*. However, *E. coli* is the most widely used because it is robust, it has a high growth rate, its metabolic pathway is known and it often yields higher levels of protein compared to other microorganisms (Rolf *et al*., 2019; Soussan *et al*., 2016).

When enzymes are produced intracellularly, they can be used without further processing together with its host cell for catalytic application as a whole cell system. This approach enhances the stability of the biocatalyst by providing a protected and more natural environment as compared to immobilised enzymes or other *in-vitro* systems (Lundemo and Woodley, 2015; Schrewe *et al*., 2013). One of the disadvantages of using whole cell catalysts; however, is that the cell wall provides a barrier in terms of diffusion of substrate and product into and out of the cell thus limiting the catalytic potential of the cell. This may be circumvented using solvents such as acetone which improves the permeability of the cell wall to reduce mass transfer limitations (Olaofe *et al*., 2013). Another challenge to using whole cell catalysts is that the substrate/product can be toxic to the host cell which slows down its metabolism potentially reducing production rates. This can be circumvented by using a suitable solvent to act as a substrate pool and product sink. Such solvents include bis(2-ethylhexyl) phthalate (BEHP) (Olaofe *et al*., 2013), acetonitrile (Kluge *et al*., 2012) and acetone (Peter *et al*., 2011). The solvent reduces the concentration of both substrate and product in the aqueous phase of the reaction mixture that contains the enzyme thus increasing productivity as inhibition is reduced.

Another approach to overcome mass transfer limitations is to use cell-free systems. This is the form in which extracellular enzymes are used as they are secreted by the host cell. Otherwise for intracellular enzymes, at the end of the protein production and cell harvest, the cell wall is physically disrupted through lysis. The cell contents obtained can then be used in the form of a crude extract cell-free system (Lundemo and Woodley, 2015). To further concentrate the enzyme, methods such as ion exchange chromatography and gel filtration can be employed (Westphal and Berkel, 2021). This purification process can become quite expensive and constitutes significantly to the overall cost in biocatalysis (Ferreira *et al*., 2018; Tufvesson *et al*., 2011). Nonetheless, cell free systems provide easier access and more direct contact with the substrate. In addition, less additional requirements that sustain cell viability are required as the DNA of the host cell is removed (Hodgman and Jewett, 2012). Therefore, this could potentially reduce the timeline of the development of biotransformation processes through enabling screening of biocatalysts with the best performance at a faster rate (Rolf *et al*., 2019).

The enzymes used in biocatalytic processes are biodegradeable catalysts produced from renewable resources that are readily available (Sheldon and Woodley, 2018). The enzyme technology developed thus far ensures that complex hydrocarbon transformations occur at ambient temperature and pressure at a high selectivity (Ayala and Torres, 2004; Polizzi *et al*., 2007; Schrewe *et al*., 2013). This not only has the potential to improve energy savings but also increases safety. These are all attractive features that align with some of the principles of green chemistry (Sheldon and Woodley, 2018; Truppo, 2017). A variety of enzyme classes have been discovered to facilitate hydrocarbon activation and

functionalisation - these classes include oxygenases, oxidases, hydroxylases, peroxidases and peroxygenases (Dong *et al.*, 2018). Cytochrome P450 monooxygenases and unspecific peroxygenases (UPOs) are some of the most promising groups of enzymes currently being investigated (Babot *et al.*, 2013; Bormann *et al.*, 2015; Guengerich *et al.*, 2016; Hobisch *et al.*, 2021; Munro *et al.*, 2018; Urlacher and Girhard, 2019; Whitehouse *et al.*, 2012). These are membrane-bound proteins that contain an iron heme domain at the active site and facilitate the insertion of oxygen into the hydrocarbon substrates (Ayala and Torres, 2004; Samanta, 2008). Cytochrome P450s usually require a cofactor such as NAD(P)H to facilitate the electron transport chain in the metabolic pathway (Denard *et al.*, 2014). This cofactor itself and its regeneration can be costly at industrial scale, and therefore proves challenging when making design upscale considerations (Guengerich *et al.*, 2016; Munro *et al.*, 2013; O'Reilly *et al.*, 2011). P450 enzymes need this cofactor only when using molecular oxygen as the oxidant, however, some P450s can also use other oxidants such as H_2O_2 for oxidation reactions, circumventing the need for costly cofactors. This is made possible through the peroxide shunt pathway (Munro *et al.*, 2018; Whitehouse *et al.*, 2012). The use of H_2O_2 is potentially highly advantageous. It is a green oxidant, with only water produced as the by-product in oxidation reactions (Bormann *et al.*, 2015; Hobisch *et al.*, 2021; Sheldon and Woodley, 2018). Additionally, it may be accessed from air and hydrogen gas, which are cheap and abundantly available raw materials. The main challenge, however, is that UPOs and P450s are deactivated by high H_2O_2 concentrations which drastically reduces the catalytic activity of the enzymes (Valderrama *et al.*, 2002). To prevent premature enzyme deactivation, H_2O_2 can be produced *in-situ* to drive the enzymatic oxidation reactions. Such a delivery system may be constructed as either a one-pot system (both H_2O_2 synthesis and enzymatic oxidation in one vessel) which could potentially lower operational expenses or a two-pot tandem system where the individual catalytic steps are separated (Puértolas *et al.*, 2015). The combination of *in-situ* H_2 generation with biocatalysis in tandem can be further developed and applied to complex catalytic pathways potentially improving hydrocarbon oxyfunctionalisation at an industrial level.

2.2 Tandem systems

Traditional synthetic routes often consist of multiple reaction steps to obtain the product, whereby each step may occur in a separate vessel. This can be problematic due to the costs associated with purification after each step, which in turn results in yield losses as well as waste generation. In addition, more equipment is required which incurs high initial capital costs (Denard *et al.*, 2013). A potential solution to this is employing tandem catalysis whereby substrate transformation occurs sequentially through two or more distinct reaction mechanisms (Fogg and dos Santos, 2004). Instead of the individual reactors for each reaction step, the transformation can be carried out sequentially in two reactors forming a two-pot tandem system or further reduced to a single reactor forming a one-pot tandem process (Figure 2.1). Tandem systems potentially require less work up or change in conditions. Such systems are potentially more sustainable and could result in a significant improvement to the space-time yields and efficiency of various transformations. It could also reduce solvent consumption and intermediate isolation steps required for purification (Bell *et al.*, 2021). Furthermore, it potentially enables new reactivity and the use of substrates that are otherwise unavailable when using a single catalyst (Afewerki and Córdova, 2016).

To successfully combine different catalytic reactions into a tandem process, a complementary set of reaction conditions is often required. This may require careful selection of catalytic partners and reaction conditions to match the reactivity of the catalysts (Gröger and Hummel, 2014). It is important to ensure that the activity of one catalyst is not significantly lower such that the subsequent catalytic process is starved of its substrate, which could lead to undesirable side reactions or decomposition. On the other hand, the rate of production of one catalyst should not be too high that it overwhelms the active site of the subsequent catalyst or the tandem reaction overall (Wasilke *et al.*, 2005). Additionally, due to lack of purification steps, each reaction step should proceed with high chemo and regioselectivity. Enzymes are ideal candidates for tandem catalysis as they are highly selective (Ayala and Torres, 2004; Soussan *et al.*, 2016).

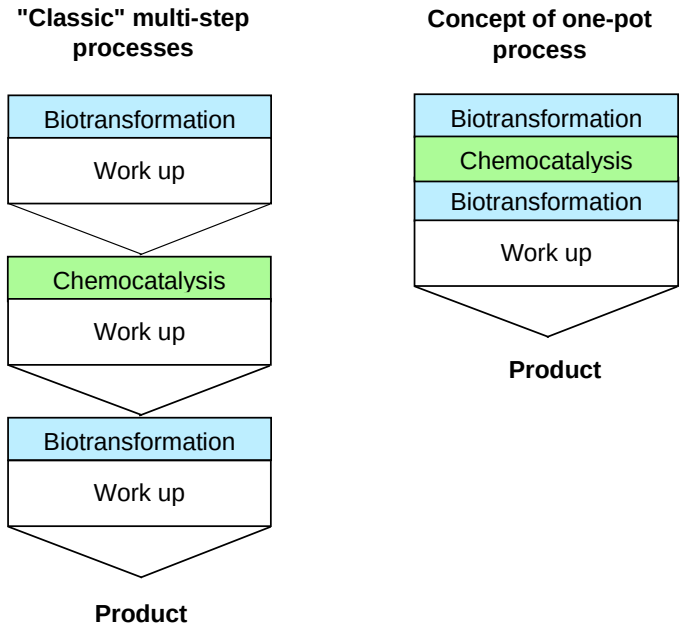

Figure 2.1: An adaptation on the comparison of multistep processes and one-pot processes (Gröger and Hummel, 2004)

The main challenge encountered in one-pot tandem catalysis is often the incompatibility of the individual reaction steps (Afewerki and Córdova, 2016; Denard *et al.*, 2014). The operating window is often very narrow (with regards to reaction conditions) to maintain compatibility. Different types of catalysts that can operate at the same conditions whilst maintaining optimum performance and high selectivity are rare (Denard *et al.*, 2014). This challenge is well illustrated when designing chemo-bio tandem systems. An important design factor that needs to be considered is that chemo-catalysts often require temperatures and pressures beyond the mild, ambient conditions that most biocatalysts prefer (Gröger and Hummel, 2014). In addition to that is the potential mutual inactivation that may occur when these catalysts are combined in the same vessel - the enzyme may cover the active sites of the chemo-catalyst as was observed when specific amino acids in alcohol dehydrogenase were found to inhibit a rhodium-based complex in the regeneration of cofactors required in enzymatic redox reactions (Hildebrand and Lütz, 2009). In addition, the reagents required by some chemo-catalytic systems are often incompatible with the biocatalytic systems (Denard *et al.*, 2014, 2013). For example, a one-pot system was developed whereby by the Suzuki cross-coupling of 4-bromoacetophenone with boronic acid catalysed by a Pd catalyst in triphenyl phosphine to form a biaryl ketone was subsequently reduced by alcohol dehydrogenase from *Rhodococcus sp.* to produce a biaryl alcohol (Scheme 2.1). The one-pot process yielded an overall conversion of 44% in contrast to the higher conversions >90% obtained when

the individual reactions were performed separately in a two-pot process. This prompted further investigations where the stability of the alcohol dehydrogenase was tested in the presence of the components in the cross-coupling reaction. Although the exposure time was not defined, it was revealed that the alcohol dehydrogenase was stable when exposed to the Pd catalyst only with a residual enzyme activity of 80%. The enzyme was less stable, however, in the presence of triphenyl phosphine and boronic acid where the residual enzyme activity was determined to be 56% and 14%, respectively. Burda *et al.* (2008) recommended removing triphenyl phosphine and using less boronic acid (1 equivalent instead of 1.75 equivalents) and this optimised one-pot tandem system achieved a higher overall conversion of 91%.

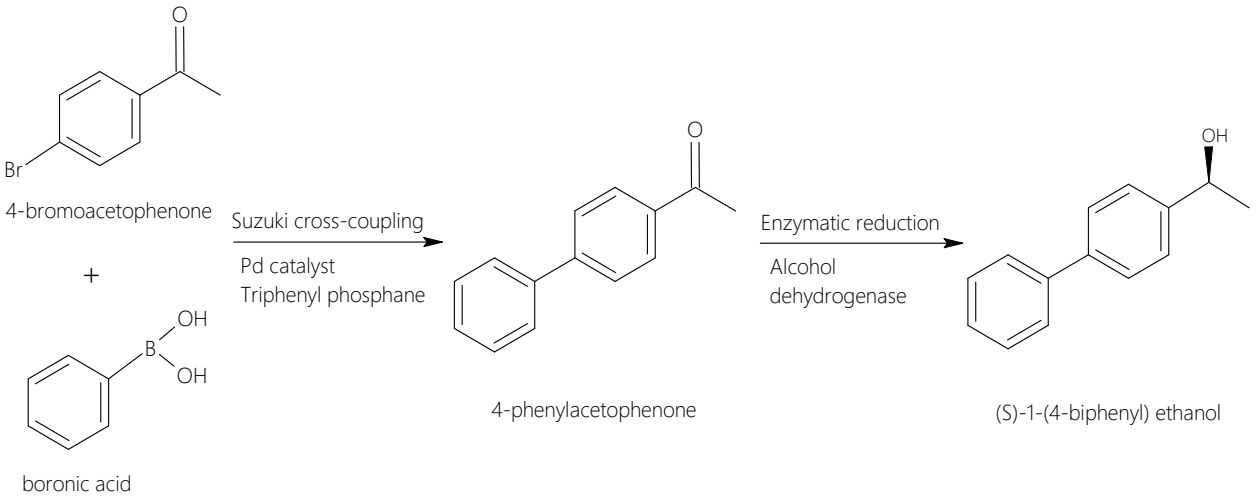

Scheme 2.1: Chemoenzymatic one-pot process of Suzuki cross-coupling and enzymatic reduction of 4-bromoacetophenone to (S)-1-(4-biphenyl) ethanol (Burda *et al.*, 2008)

There are other approaches to circumvent inactivation among different classes of catalysts in a one-pot tandem process. Physical barriers can be implemented between the catalysts using biphasic systems, enzyme immobilisation and the use of whole cells (Bormann *et al.*, 2015; Wasilke *et al.*, 2005). A biphasic system usually consists of immiscible organic and aqueous phases effectively partitioning reaction components according to solubility. This approach attempts to maintain stability of the different catalysts and to provide a substrate pool and product sink (Maurer *et al.*, 2005; Olaofe *et al.*, 2013) whilst still conducting a tandem transformation in a single reaction vessel. Enzyme immobilisation is another method whereby purified enzymes are isolated and attached to an insoluble material with the hope of increasing stability and potential reusability. This method, however, incurs additional costs in terms of catalyst preparation - it has been estimated that the cost of enzyme immobilisation is approximately four times as high as the cost of using crude enzyme (Bormann *et al.*, 2015; Tufvesson *et al.*, 2011). In contrast to immobilized enzymes, whole cells are relatively cheaper and provide a natural protective environment for the biocatalyst. Whole cell enzyme systems, however, are often controlled by the protein synthesis and cellular metabolism of the cell. There are also mass transfer limitations across the cell walls and membranes, especially of poorly water-soluble substrates and products such as organic compounds (Lundemo and Woodley, 2015; Schrewe *et al.*, 2013).

Despite these challenges, one-pot synthetic processes are becoming increasingly popular in the literature. The *in-situ* generation of hazardous chemicals that are subsequently consumed within the system is a particularly attractive application of one-pot synthesis. This eliminates the health and safety risks associated with the transportation of dangerous chemicals (Puértolas *et al.*, 2015). As previously

mentioned, several literature reports have investigated tandem one-pot processes for hydrocarbon oxyfunctionalisation (Denard *et al.*, 2013; Fogg and dos Santos, 2004; Freakley *et al.*, 2019; Gröger and Hummel, 2014; Wasilke *et al.*, 2005). Scheme 2.2 illustrates such a tandem system whereby H_2O_2 is produced *in-situ* as the oxidant for the subsequent enzyme-driven oxyfunctionalisation of hydrocarbons.

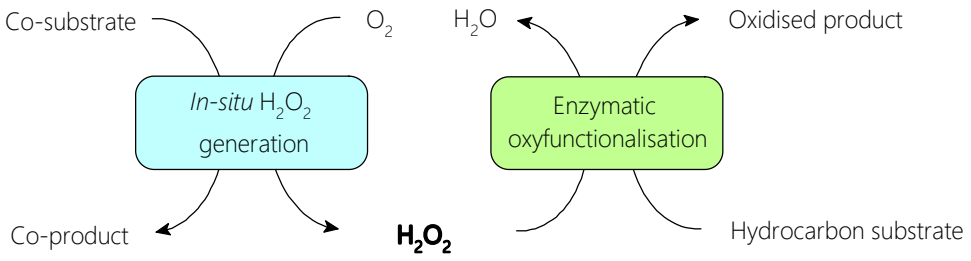

Scheme 2.2: An adaptation of a schematic showing a one-pot system of *in-situ* H_2O_2 generation coupled to enzymatic oxyfunctionalisation of hydrocarbons (Tieves *et al.*, 2019)

As previously mentioned, this approach negates the need for storage of hazardous H_2O_2 whilst also producing the oxidant from cheap and abundant reagents. The enzymes employed in such processes include unspecific peroxygenases and cytochrome P450 monooxygenases in the oxidation of hydrocarbon substrates such as aromatics, fatty acids and alkanes. Some H_2O_2 generation systems require a co-substrate in addition to molecular oxygen to produce H_2O_2. In such a scenario, it is then important to ensure that the co-substrate (and co-product, if any) will not deactivate/inhibit the enzyme. One-pot tandem systems are further reviewed where different *in-situ* H_2O_2 delivery systems are employed as well as how they influence the enzyme-driven oxyfunctionalisation of hydrocarbons.

2.2.1 *In-situ* hydrogen peroxide generation

As previously noted, UPOs and P450s can be used to oxidise hydrocarbons; however, the main limitation to this reaction is the irreversible oxidative inactivation of these enzymes caused by H_2O_2 (Bormann *et al.*, 2015; Valderrama *et al.*, 2002). Attempts to circumvent this challenge include the manipulation of these enzymes to achieve higher H_2O_2 tolerance through protein engineering (Whitehouse *et al.*, 2012). Another strategy is developing *in-situ* H_2O_2 generation systems to obtain a controlled supply of the oxidant at low concentrations that allow efficient catalytic turnover while minimising enzyme deactivation (Ni *et al.*, 2016).

There are several routes available for H_2O_2 production. Traditionally, it is produced indirectly via the anthraquinone process whereby a palladium or platinum-based catalyst is used to first hydrogenate then oxidise an alkyl anthraquinone, releasing H_2O_2 (Puértolas *et al.*, 2015). This process has high throughputs and concentrations of approximately 10^5 tpa and 35 – 50 wt%, respectively. Such concentrations of H_2O_2 are unsuitable to most bioreactors and would require dilution for external addition to bioreactors or one-pot tandem systems. This would include H_2O_2 dosage systems equipped with H_2O_2 sensors (Bormann *et al.*, 2015). Some of the challenges with this approach are high concentrations of H_2O_2 that would accumulate in the dead zones of the bioreactor. Additionally, large volumes of concentrated H_2O_2 raise problems associated with transportation and storage (Puértolas *et al.*, 2015). Therefore, different technologies for producing lower volumes at the desirable concentration of 3 - 5 wt% H_2O_2 have been developed including (Bormann *et al.*, 2015; Puértolas *et al.*, 2015): (i)

chemo-catalysis which involves the use of (noble) metal-based catalysts to catalyse the reduction of molecular O_2 by H_2; (ii) biocatalysis employing enzymes to reduce O_2 to H_2O_2; photocatalysis using visible light and flavin photocatalysts; (iii) electrochemistry whereby a cathode is used to reduce molecular oxygen to H_2O_2 and (iv) the chemical route whereby mild reducing agents such as organometallic hydrides or nicotinamide derivatives reduce O_2 to H_2O_2. The most important chemo-catalytic and biocatalytic routes toward H_2O_2 and their applicability to one pot tandem oxygenations are discussed in detail below.

Chemo-catalytic route

The direct synthesis of H_2O_2 may be accomplished using hydrogen and oxygen in the presence of a metal catalyst. This reaction is favourable at short residence times and sub-ambient temperatures of 1 - 2 °C (Samanta, 2008). Palladium (Pd) and gold (Au) metallic nanoparticles have been demonstrated to catalyse this reaction producing H_2O_2 in high yields (Crole *et al.*, 2016; Edwards *et al.*, 2014, 2007). The combination of these metals to form bimetallic nanoparticles has also been investigated and typically leads to higher stability of the catalyst and enhanced catalytic performance compared to monometallic nanoparticles (Hosseinkhani *et al.*, 2012). While H_2O_2 production is typically fast, product losses are incurred by the hydrogenation of H_2O_2 to water which is also catalysed by the Pd nanoparticle as well as the decomposition of H_2O_2 to water and oxygen via disproportionation (Scheme 2.3, **b** and **d**). Another challenge is obtaining a high rate of mass transfer of the gaseous H_2 and O_2 through the liquid reaction medium to the surface of the catalyst. This is due to the poor solubility of gaseous H_2 and O_2 in aqueous solutions (Samanta, 2008).

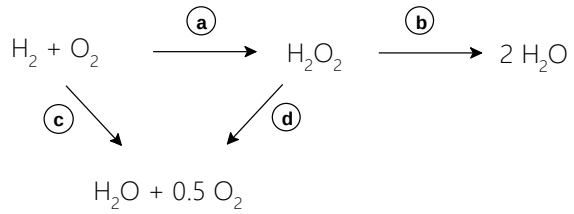

Scheme 2.3: The direct synthesis of H_2O_2 adapted from Crole *et al.* (2016)

Table 2.1 compares various supported gold-palladium catalysts in the production of H_2O_2. It was found that the nature of the support material greatly influenced both the rate of H_2O_2 production as well as H_2O_2 selectivity (Edwards *et al.*, 2014). Carbon proved to be the best support for H_2O_2 production, followed by titania and alumina. It was concluded that this was due to the acidic nature of the carbon surface which promoted the stabilisation of the H_2O_2 molecule. This might explain why the selectivity for H_2O_2 formation was highest using this support. The studies reviewed in Table 2.1 suggest that the use of gold-palladium nanoparticles for *in-situ* hydrogen production is highly promising for tandem chemo-bio catalysis. However, several practical issues would need to be overcome for incorporation into such a tandem process. In the investigation by Edwards *et al.* (2014) all experiments were performed at 2 °C, which may pose a challenge when combining this with the enzymes of interest (UPOs and cytochrome P450s) that typically operate between room temperature and 40 °C (Ayala and Torres, 2004; Polizzi *et al.*, 2007; Schrewe *et al.*, 2013). In another study using titania-supported AuPd catalysts (Crole *et al.*, 2016), it was determined that H_2O_2 production decreased at higher temperatures (50 mol kg_{cat}^{-1} h^{-1} at 20 °C compared to 64 kg_{cat}^{-1} h^{-1} reported at 2 °C, Table 2.1). The selectivity was not explicitly stated but at ambient temperature the rates of hydrogenation and decomposition were found to be significantly higher than those at sub-ambient temperature for titania supported AuPd catalysts. This suggests that

there is decreased selectivity to H_2O_2 production because the oxidation of hydrogen to water is thermodynamically favoured and the product losses are further accelerated by thermal decomposition of H_2O_2 at elevated temperatures. It would therefore be crucial to monitor H_2O_2 concentrations to ensure that it is sufficient for the H_2O_2-driven enzymatic reaction. To mitigate these H_2O_2 losses, acid or halide promoters can be added to the reaction medium to suppress further hydrogenation and nonselective water forming reactions from occurring. Halide ions in particular have been observed to poison the sites on the Pd particle that are responsible for the catalytic hydrogenation of H_2O_2 (Samanta, 2008). It has been determined the presence of hydrogen bromide in a H_2O_2 forming reaction catalysed by 0.6 wt% Pd/C inhibited further hydrogenation of the H_2O_2 product, reducing it by 57% at 1 ^{o}C and 29% at 17 ^{o}C (Landon *et al.*, 2003).

Table 2.1: Catalytic activity of gold/palladium catalysts on different supports

Catalyst	H_2O_2 selectivity (%)	H_2O_2 production (mol kg_{cat}^{-1} h^{-1})	Reference
2.5 wt% Au-2.5 wt% Pd/Al_2O_3	14	15	(Edwards *et al.*, 2014)
2.5 wt% Au-2.5 wt% Pd/carbon	80	110	(Edwards *et al.*, 2014)
2.5 wt% Au-2.5 wt% Pd/TiO_2	70	64	(Edwards *et al.*, 2014)
2.5 wt% Au-2.5 wt% Pd/TiO_2[a]	-	50	(Crole *et al.*, 2016)
2.5 wt% Au-2.5 wt% Pd/TiO_2[b]	-	25	(Crole *et al.*, 2016)
2.5 wt% Au-2.5 wt% Pd/TiO_2[c]	-	67	(Crole *et al.*, 2016)

Reaction conditions: 2.5 wt% Au-2.5 wt% Pd, 30 min reaction time, 1 200 rpm, 2 ^{o}C, 66 wt% MeOH solvent; [a]: 20 ^{o}C, 66 wt% MeOH, [b] 20 ^{o}C, 100% H_2O solvent, [c]: 20 ^{O}C, 100% MeOH solvent

Another limitation of this reaction is the poor solubility of the gases in aqueous medium. This has been addressed by introducing methanol as a solvent in heterogeneously catalysed processes, because the solubility of hydrogen and oxygen is significantly higher in methanol (MeOH) than in water - approximately five-fold and eight-fold, respectively (Samanta, 2008). Increasing the concentration of methanol in the reaction medium improves the production of H_2O_2 (Crole *et al.*, 2016). Changing from a water-rich reaction medium to a methanol-rich reaction medium roughly doubles the productivity (Table 2.1). In terms of the competing reactions, it was noted that hydrogenation and decomposition occurred at similar rates in the H_2O-rich solvent whereas the hydrogenation rate was higher in the MeOH-rich solvent due to the increased availability of H_2 within the reaction mixture (Table 2.2). It was established that optimal performance was obtained at a mass ratio 66 wt% methanol/34 wt% water. These optimized conditions may be problematic in a tandem chemo-bio system as methanol could potentially inhibit enzyme function. For UPOs, it was determined that the wild-type variant from *Agrocybe aegerita* retained only 40% enzyme activity when incubated with 50% (v/v) MeOH over 48 h. Contrastingly, the PaDa-I variant was more stable under the same conditions exhibiting approximately 95% residual enzyme activity (Molina-Espeja *et al.*, 2014).

Table 2.2: Effect of catalyst support on hydrogenation and decomposition of H_2O_2

H_2O_2 degradation route:			
Catalyst support	Hydrogenation (mol kg_{cat}^{-1} h^{-1})	Decomposition (mol kg_{cat}^{-1} h^{-1})	Reference
Al_2O_3	24	3	(Edwards *et al.*, 2014)
carbon	5	2	(Edwards *et al.*, 2014)
TiO_2	15	8	(Edwards *et al.*, 2014)
TiO_2[a]	600	450	(Crole *et al.*, 2016)
TiO_2[b]	790	110	(Crole *et al.*, 2016)

Reaction conditions: 2.5 wt% Au-2.5 wt% Pd, 30 min reaction time, 1 200 rpm, 2 °C, 66% MeOH solvent; [a]: 20 °C, 100% H_2O solvent, [b]: 20 °C, 100% MeOH solvent

Traditional heterogenous catalyst supports for gold-palladium nanoparticles require highly controlled synthesis conditions often employing high temperatures and pressures, increasing catalyst cost (Crole *et al.*, 2016; Edwards *et al.*, 2014). In contrast, bacterially bound AuPd nanoparticles utilize biomass as a support and are usually generated under ambient conditions which could potentially make bacterial supports an environmentally friendly alternative to conventional supports (Creamer *et al.*, 2007; Deplanche *et al.*, 2014; Foulkes *et al.*, 2016; Hosseinkhani *et al.*, 2012). Biofabricated catalysts are synthesised by the deposition of gold-palladium nanoparticles on the surface or periplasm of a microorganism, with the whole cell consequently used as the catalyst. Some research indicates that biofabricated catalysts can match or outperform their chemo-catalyst counterparts (Bennett *et al.*, 2013; Deplanche *et al.*, 2014; Zhu *et al.*, 2016). In addition, these biofabricated catalysts are more easily recovered from the reaction medium and retain catalytic activity compared to chemo-catalysts. The use of biofabricated catalysts has the potential to eliminate compatibility issues with reaction conditions in a pseudo bio-bio tandem system, as both catalysts would operate effectively under ambient conditions. Apart from biofabricated catalysts, biocatalysts have been considered for H_2O_2 generation.

Biocatalytic route

Oxidases are some of the first enzymes considered for H_2O_2 production in tandem with oxyfunctionalisation. This is mainly due to the compatibility of oxidases with UPO and P450 enzymes (Bormann *et al.*, 2015). In this route, oxidases are used to reduce molecular oxygen to H_2O_2. The required hydrogen source is obtained from a co-substrate which is specific to the enzyme. Glucose oxidase (GOx) is a popular choice (Bankar *et al.*, 2009; Burek *et al.*, 2019; Freakley *et al.*, 2019; Mano, 2019; Strelec *et al.*, 2018). GOx employs glucose as the co-substrate (Scheme 2.4) generating gluconic acid along with H_2O_2. GOx is a robust enzyme which is commercially available at affordable prices (Burek *et al.*, 2019). It has been reported that this enzyme operates optimally at room temperature and near-neutral pH 5.5 - 7 (Bankar *et al.*, 2009) with turnover numbers in excess of 1 163 $mol_{product}$ mol_{cat}^{-1} frequently reported (Table 2.3).

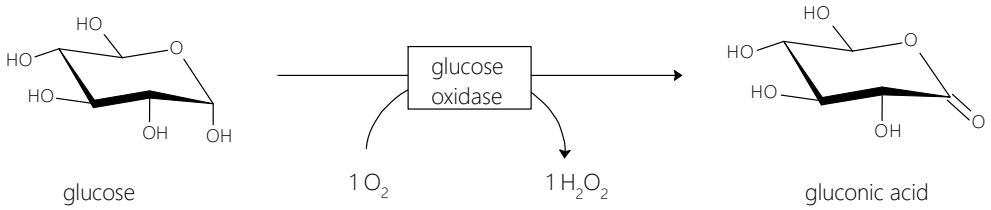

Scheme 2.4: A simplified schematic of H_2O_2 production by glucose oxidase with glucose as the co-substrate and gluconic acid as the co-product adapted from (Bankar *et al.*, 2009)

However, the performance of this system is deemed inefficient because only one equivalent of H_2O_2 is produced from one equivalent of glucose, whereas theoretically 12 equivalents of H_2O_2 should evolve from the complete oxidation of one equivalent of glucose (Ni *et al.*, 2016). Scaling this process to industrial size raises further issues. (Bormann *et al.*, 2015). Larger amounts of glucose within the reaction mixture would increase the viscosity leading to higher energy consumption for agitation. There would also be challenges with the generated co-product gluconic acid because the system would then require additional pH-control and the formed gluconic acid could potentially inhibit the H_2O_2-driven enzyme (Bankar *et al.*, 2009). Hence, current research has moved towards investigating other types of oxidases.

Table 2.3: Comparison of enzymatic hydrogen peroxide generation systems

Co-substrate	Enzyme(s)	TON[a]	Waste generation[b]	Reference
Glucose	Glucose oxidase	1 163	198	(Bankar *et al.*, 2009)
Methanol	Alcohol oxidase and	245 580	15	(Ni *et al.*, 2016)
	Formate dismutase	25 400		
Formic acid	Formate dehydrogenase and	39 000	44	(Pesic *et al.*, 2019)
	Old yellow enzyme	3 600		
Formic acid	Formate oxidase	318 000	-	(Tieves *et al.*, 2019)

Reaction conditions: pH 5.5 - 7, 25 - 30 °C; [a]: total turnover number in $mol_{product}\ mol_{enzyme}^{-1}$; [b] waste generation in $g_{co\text{-}product}\ g_{H2O2}^{-1}$

The use of primary alcohols and alcohol oxidases is another feasible H_2O_2 generation system that also operates at ambient, near-neutral conditions. The use of methanol as the co-substrate is potentially more efficient as significantly less waste is produced (15 g per mole H_2O_2) compared to the GOx system. However, the stoichiometric accumulation of the co-product formaldehyde which is carcinogenic poses a serious health concern and a threat to the environment if incorrectly disposed (Bormann *et al.*, 2015). A bi-enzymatic cascade has been proposed to circumvent the generation of formaldehyde, whereby alcohol oxidase from *Pichia pastoris* oxidised methanol to formaldehyde followed by the dismutation of formaldehyde into methanol and formic acid using formaldehyde dismutase from *Pseudomonas putida* (Ni *et al.*, 2016). The resulting double oxidation of methanol yields two equivalents of H_2O_2 from one equivalent of MeOH. In terms of catalytic activity, the H_2O_2 produced by this bienzymatic system yields a higher turnover number compared to the traditional glucose oxidase system (Table 2.3).

Formic acid can also be used as a co-substrate in the production of H_2O_2. In this system, one equivalent of formic acid produces one equivalent of H_2O_2. This is reported to produce less waste (44 g per mole H_2O_2) in terms of the co-product, carbon dioxide (Pesic *et al.*, 2019). Two different studies reported that dehydrogenases and oxidases, respectively, could be applied in this H_2O_2 generation system (Pesic *et al.*, 2019; Tieves *et al.*, 2019). The first approach involved a multi-enzymatic system where formate dehydrogenase coupled with old yellow enzymes from *Bacillus subtilis* were employed to produce H_2O_2. (Pesic *et al.*, 2019). The overall TON for this system (3 600 $mol_{product}\ mol_{cat}^{-1}$) was higher than what was reported for the traditional GOx system (1 163 $mol_{product}\ mol_{cat}^{-1}$). The challenge with this multi-enzymatic approach; however, is that the old yellow enzymes require NADH, which is an expensive cofactor. On the other hand, the second approach employed formate oxidase from *Aspergillus oryzae* (*Ao*FOx), a unique enzyme that produces its cofactor by self-oxidation (Tieves *et al.*, 2019). This feature may attribute

to the high turnover number (318 000 $mol_{product}$ mol_{cat}^{-1}) obtained compared to the other studies reviewed in Table 2.3.

Both chemo-catalytic and biocatalytic methods have been reported for *in-situ* H_2O_2 generation along with their associated advantages and disadvantages. The 2.5 wt% Au-2.5 wt% Pd/carbon chemo-catalyst and formate oxidase biocatalyst from *A. oryzae* are the high performing catalysts reviewed in each respective category. The Au-Pd/TiO_2 could potentially limit the H_2O_2 delivery rate as the dehydrogenation and decomposition of H_2O_2 are also catalysed at ambient conditions. Formate oxidase on the other hand operates at a higher selectivity for H_2O_2 production and requires similar operating conditions to the enzyme-driven functionalisation reaction, thus potentially making it a better candidate for a tandem system.

2.2.2 Enzymatic oxyfunctionalisation of hydrocarbons

Recent research has shifted focus towards unspecific peroxygenases (UPO), which were first isolated from a fungi, and cytochrome P450 monooxygenases from yeast and bacteria. These enzymes are stable and have high catalytic performance. Two such enzymes are PaDa-I and CYP102A1. The PaDa-I variant is an extracellular UPO evolved from *Agrocybe aegerita* and the CYP102A1 cytochrome P450 monooxygenase is an intracellular enzyme. These are both heme containing proteins with similar porphyrin ring structures (Munro *et al.*, 2018)., and can both use H_2O_2 as the oxidant for the biotransformation of hydrocarbons (Equation 2.1). Otherwise, P450 enzymes naturally use molecular O_2, as the oxygen source, and the cofactor NAD(P)H for electron transfer during oxygen insertion reactions (Equation 2.2).

$$RH + H_2O_2 \rightarrow ROH + H_2O \quad (2.1)$$

$$RH + O_2 + 2e^- + 2H^+ \rightarrow ROH + H_2O \quad (2.2)$$

The overall mechanism for UPO and P450 enzyme catalysed oxidation is illustrated in Scheme 2.5. The ferric resting state of the porphyrin ring structure consists of a distal water ligand which is displaced during substrate binding (**1**). Focusing on the P450 enzyme oxygen-dependent catalytic cycle thereafter, the heme iron (III) centre is reduced to yield a ferrous, substrate-bound protein (**2**). Molecular oxygen consequently binds to the enzyme forming a ferric dioxy complex (**3**). A second electron transfer along with a protonation facilitated by the cofactor NAD(P)H results in the ferric hydroperoxo complex often referred to as Compound 0 (**4** in Scheme 2.5). From this complex, the oxo-Fe (IV) porphyrin cation radical, Compound I, is formed through subsequent protonation and a water molecule removal (**5**). Compound I is a reactive intermediate which abstracts hydrogen from the substrate, yielding the ferryl hydroxo species Compound II and a substrate radical (**6**) which rapidly recombine to form the ferric enzyme state and hydroxylated product (**7**). The product dissociates from the protein and a water molecule coordinates to the heme thus regenerating the resting state (**8**). Compound 0 can alternatively be formed immediately after substrate binding (i.e. bypassing steps **2**, **3** and **4**) through what is called the hydrogen peroxide shunt pathway, as indicated by the blue, dashed arrow in Scheme 2.10. In this case, H_2O_2 is used instead as the source of oxygen and reducing equivalents. This is the natural catalytic pathway for UPOs, while some P450s can also divert to this pathway in the presence of H_2O_2.

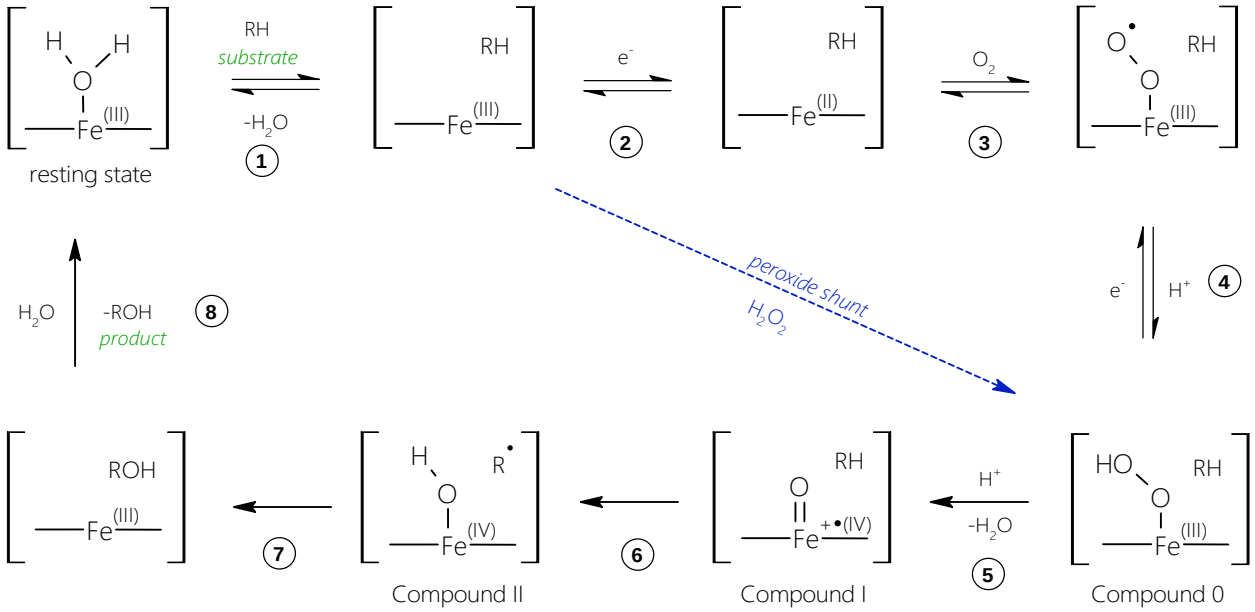

Scheme 2.5: An adaptation of the catalytic pathway for unspecific peroxygenases and cytochrome P450s (Krest *et al.*, 2013; Munro *et al.*, 2018; Ortiz De Montellano, 2010; Whitehouse *et al.*, 2012)

The use of H_2O_2 as the oxidant in hydrocarbon biotransformation processes may be a more viable large scale commercial route because, unlike the costly NAD(P)H cofactor along with its complex regeneration, H_2O_2 is inexpensive and only produces water as the by-product (Denard *et al.*, 2014; Munro *et al.*, 2013). Some of the known organic substrates for UPOs and P450s are aromatics, fatty acids as well as alkanes (Hobisch *et al.*, 2021; Hofrichter and Ullrich, 2014; Whitehouse *et al.*, 2012). The performance of these enzymes in oxyfunctionalisation reactions with different substrates have been evaluated using different manual H_2O_2 delivery approaches and *in-situ* H_2O_2 delivery in one-pot tandem processes.

Aromatic substrate

Aromatic compounds are important materials in the chemical industry finding application as solvents, fuels or as intermediates in chemical synthesis. In particular, the epoxidation of styrene to produce styrene oxide is an important step in the synthesis of biocides, cosmetics and engineering adhesives (Scheme 2.6) (Batra *et al.*, 2019). The conventional manufacturing route uses chemo-catalysts that produce the desired (*S*)-styrene oxide at approximately 50% enantiomeric excess (Groves and Myers, 1983). However, biocatalytic routes have been reported that improve the stereoselectivity such that no further purification is required. In addition, the biocatalysts, as previously mentioned, operate at mild conditions thus reducing energy consumption and harm to the environment (Mckenna *et al.*, 2013)

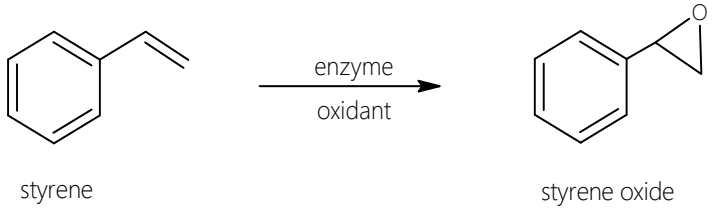

Scheme 2.6: The enzyme-driven epoxidation of styrene

CYP102A1 has also been effectively employed in the biocatalytic epoxidation of styrene. Some studies have explored the incorporation of chemically inert decoy molecules into the system to enhance CYP102A1 performance in this reaction within the peroxide shunt pathway (Dezvarei *et al*., 2019; Ma *et al*., 2018). This pathway is often less efficient in facilitating P450 enzyme catalysis compared to the standard NAD(P)H-dependent activity, primarily due to the enzyme inactivation induced by H_2O_2. The decoy molecules mimic the enzyme's natural substrates and partially occupy the substrate access channel. This triggers substrate recognition, thereby initiating the catalytic cycle for the biotransformation (Cong *et al*., 2015). Ma *et al*. (2018) tested the hydrogen-peroxide driven oxidation of styrene by seven full length mutant CYP102A1 enzymes in the presence and absence of a small decoy molecule called N-(**ω**-imidazolyl)-hexanoyl-L-phenylalanine (Im-C6-Phe). It was determined that the F87V variant performed best out of the seven strains and that it obtained an order of magnitude higher turnover numbers in the presence of Im-C6-Phe than in its absence. This suggests that the decoy molecule may have also acted as a barrier against the 20 mM H_2O_2 (added all at once) which potentially lowered the hydrogen peroxide-induced deactivation thus improving the product yield. Dezvarei *et al*. (2019), on the other hand, explored the impact of using a different decoy molecule (perfluorononanoic acid) with a CYP102A1 TE variant using a similar once-off delivery method but at a higher H_2O_2 concentration of 60 mM. In this case, the enzymatic activity was in fact reported to be lower in the presence of this decoy molecule though it was not quantified in the research. Hence, the productivity of the enzymes was only reported in the absence of the decoy molecules in Table 2.4. Comparing these two studies, the CYP102A1 TE variant performed slightly better than the CYP102A1 F87A variant as shown by the higher turnover number of 231 $mol_{product}\ mol_{enzyme}^{-1}$ compared to 120 $mol_{product}\ mol_{enzyme}^{-1}$. This was in spite of the former being exposed to a higher H_2O_2 concentration than the latter. This could be an indication that the TE variant of the enzyme is less prone to deactivation in the presence of H_2O_2, than the F87V variant, which could potentially mean that different enzyme mutants may have a different H_2O_2 tolerance. Data pertaining to the enzyme deactivation of each strain would provide a better understanding of this H_2O_2 tolerance, however that information was not available.

In another study whereby a UPO from *Agrocybe aegerita* (*Aae*UPO) was investigated, the same once-off delivery approach of H_2O_2 was employed as in the previously discussed P450 enzyme reaction systems (Kluge *et al*., 2012). Although a significantly lower H_2O_2 concentration of 1 mM was used, it was reported that a much higher turnover number (7 900 $mol_{product}\ mol_{enzyme}^{-1}$) as obtained for this *Aae*UPO compared to the P450 catalysed reactions over comparable reaction times. A higher TON was achieved despite the initial substrate concentration being lower in this *Aae*UPO system (1 mM) compared to the P450 systems (4 and 5 mM). When lower concentrations of H_2O_2 (0.44 - 0.74 mM) were delivered *in-situ* to a UPO variant (PaDa-I), a higher production of styrene oxide was reported as indicated by the highest TON in Table 2.4 (Freakley *et al*., 2019). This could potentially be due to less deactivation of the UPO enzymes as they were exposed to lower concentrations of H_2O_2 as well as an extended reaction period of 2 h compared to 10 min (Table 2.4). Freakley *et al*. (2019) went on to report that the PaDa-I variant maintained 50-55% of the initial enzyme activity after 4 h. It is, therefore, probable that the P450 enzymes were less catalytically efficient and stable in comparison, as they have a preference for O_2 compared to H_2O_2. They could therefore have been immediately deactivated when exposed to the higher H_2O_2 concentrations (20 and 60 mM), thereby lowering product formation rates. There is, however, insufficient data available in terms of monitoring the enzyme deactivation kinetics as the reaction proceeded, which would be crucial information used in optimising or improving this enzyme-driven epoxidation of styrene.

Table 2.4: Comparison of catalytic activity on the epoxidation of styrene

Enzyme	Styrene concentration	H_2O_2 delivery	TON[a]	Reaction time	Reference
CYP102A1 F87V	4 mM	20 mM (once-off addition)	120	30 min	(Ma *et al.*, 2018)
CYP102A1 TE	5 mM	60 mM H_2O_2 (once-off addition)	231	5 min	(Dezvarei *et al.*, 2019)
*Aae*UPO[b]	1 mM	1 mM H_2O_2 (once-off addition)	7 900	10 min	(Kluge *et al.*, 2012)
PaDa-I[c]	10 mM	0.44 - 0.74 mM (*in-situ*; chemo)	11 700	2 h	(Freakley *et al.*, 2019)

Reaction conditions: pH 6.0 - 8.0, ambient temperature; [a]: total turnover number measured in $mol_{product}$ mol_{enzyme}^{-1}; [b]: unspecific peroxygenase from *Agrocybe aegerita*; [c]: evolved unspecific peroxygenase variant from *Agrocybe aegerita*

Another important reaction that can be performed by UPOs is the oxidation of ethylbenzene to 1-phenylethanol (Scheme 2.7). This product is useful in the cosmetics, pharmaceutical and chemical industries (Li *et al.*, 2013).

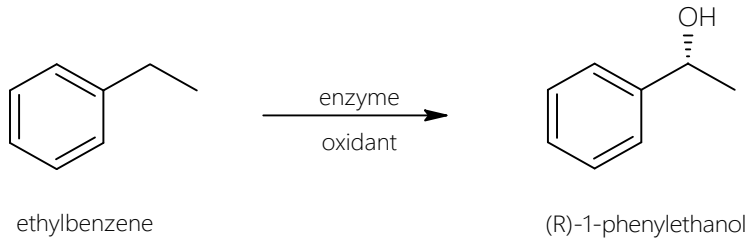

Scheme 2.7: The enzyme-driven oxidation of ethylbenzene

There are different manual delivery approaches and *in-situ* H_2O_2 generation systems that have been investigated to deliver the oxidant to the UPO enzyme to facilitate this oxidation reaction (Table 2.5). Among the studies reviewed in Table 2.5, Kluge *et al.* (2012) reported the lowest TON of 10 600 $mol_{product}$ mol_{enzyme}^{-1} for the biotransformation of ethylbenzene employing once-off H_2O_2 delivery. This may be attributed to the H_2O_2 delivery method employed or that a lower initial ethylbenzene concentration was used (1 mM) compared to the other systems reviewed (>10 mM) as shown in Table 2.5. Using *in-situ* H_2O_2 delivery, Freakley *et al.* (2019) reported a better enzyme performance with their chemo-enzymatic tandem system where the H_2O_2 concentration was between 0.44 - 0.74 mM at steady state. The higher TON obtained may also be attributed to the mutation of the strain of PaDa-I compared to the parent strain *Aae*UPO. Zhang *et al.* (2017) employed a photoenzymatic tandem system using *Aae*UPO and their system obtained even lower H_2O_2 concentrations of 0.16 mM which in turn resulted in TONs as high as 79 000 $mol_{product}$ mol_{enzyme}^{-1}. The extended reaction period of 72 h could also explain the discrepancy in TON. Furthermore, it is probable that the significantly lower H_2O_2 concentrations at steady state led to reduced enzyme deactivation which improved the enzyme stability. Only Freakley *et al.* 2019 reported a 50 - 55% enzyme activity loss after 4 h, however it remains unclear to what extent the enzymes remained active as a comprehensive deactivation kinetic study was not reported in either investigation.

Table 2.5: Comparison of catalytic activity on the oxidation of ethylbenzene

Enzyme	Ethylbenzene concentration	H_2O_2 delivery	TON[a]	Reaction time	Reference
*Aae*UPO[b]	1 mM	1 mM (once-off addition)	10 600	10 min	(Kluge *et al.*, 2012)
PaDa-I[c]	10 mM	0.44 - 0.74 mM (*in-situ*; chemo)	28 200	16 h	(Freakley *et al.*, 2019)
*Aae*UPO	15 mM	0.16 mM *in-situ* (photo)	79 000	72 h	(Zhang *et al.*, 2017)
*Aae*UPO	10 mM	*in-situ* (bio)	390 000	24 h	(Pesic *et al.*, 2019)
*Aae*UPO	100 mM	*in-situ* (bio)	31 800	24 h	(Tieves *et al.*, 2019)

Reaction conditions: pH 6.0 - 8.0, ambient temperature; [a]: total turnover number measured in $mol_{product}\ mol_{enzyme}^{-1}$; [b]: unspecific peroxygenase from *Agrocybe aegerita*; [c] evolved unspecific peroxygenase variant from *Agrocybe aegerita*

Multi-enzymatic tandem systems have also been developed to deliver H_2O_2 to a UPO for the biotransformation of ethylbenzene as recorded in Table 2.5 (Pesic *et al.*, 2019; Tieves *et al.*, 2019). For the studies reviewed for this biotransformation, the highest turnover number was obtained by the bio-bio tandem system developed by Pesic at al. (2019). When testing the sensitivity of their system to the *in-situ* H_2O_2 delivery rate, they increased the concentration of the H_2O_2-producing enzyme (old yellow enzyme) until they reached TONs as high as 390 000 $mol_{product}\ mol_{enzyme}^{-1}$ (Table 2.5). In their study, they did attempt to decouple the *in-situ* H_2O_2 generation system from the biotransformation system for better understanding of the overall tandem system - it is unclear what the H_2O_2 concentration was at steady state or at what old yellow enzyme concentration the system would eventually produce too much H_2O_2 such that it potentially inhibited the UPO. Tieves *et al.* (2019), on other hand, considered the ratio of the H_2O_2 generating enzyme (formate oxidase) to the UPO in their bio-bio tandem system. In this study, slight inhibition was observed at equimolar ratios whereas optimum performance was noted at a 1:5 ratio of the formate oxidase to the UPO. However, the kinetics regarding this inhibition were not evaluated. Furthermore, there was no monitoring of the steady state H_2O_2 concentration or evaluation of the enzyme kinetics to assess the impact the H_2O_2 delivery may have had on the UPO activity or stability. Nonetheless, this bio-bio tandem system achieved an order of a magnitude lower than the highest TON recorded in Table 2.5 which therefore suggests that there may have been other factors that influenced the UPO enzyme performance.

Fatty acid substrate

Fatty acids are readily available in the form of vegetable oils from biomass (Aranda *et al.*, 2021). UPO and P450 enzymes catalyse the hydroxylation of medium and long chain fatty acids at subterminal positions as indicated by the reaction mechanism in Scheme 2.8. The main product distribution for these enzymes have been reported as follows: the P450 CYP102A1 enzymes were reported to oxidise the fatty acid at positions furthest from the terminal carbon (ω-5, ω-4 and ω-3), whereas the UPO oxidised the hydrocarbon chain at positions closer to the terminal position at ω-1 and ω-2. The hydroxy derivatives obtained from this reaction find application in the cosmetic industry as well as in the production of additives in paint and coatings (Hammerer *et al.*, 2018).

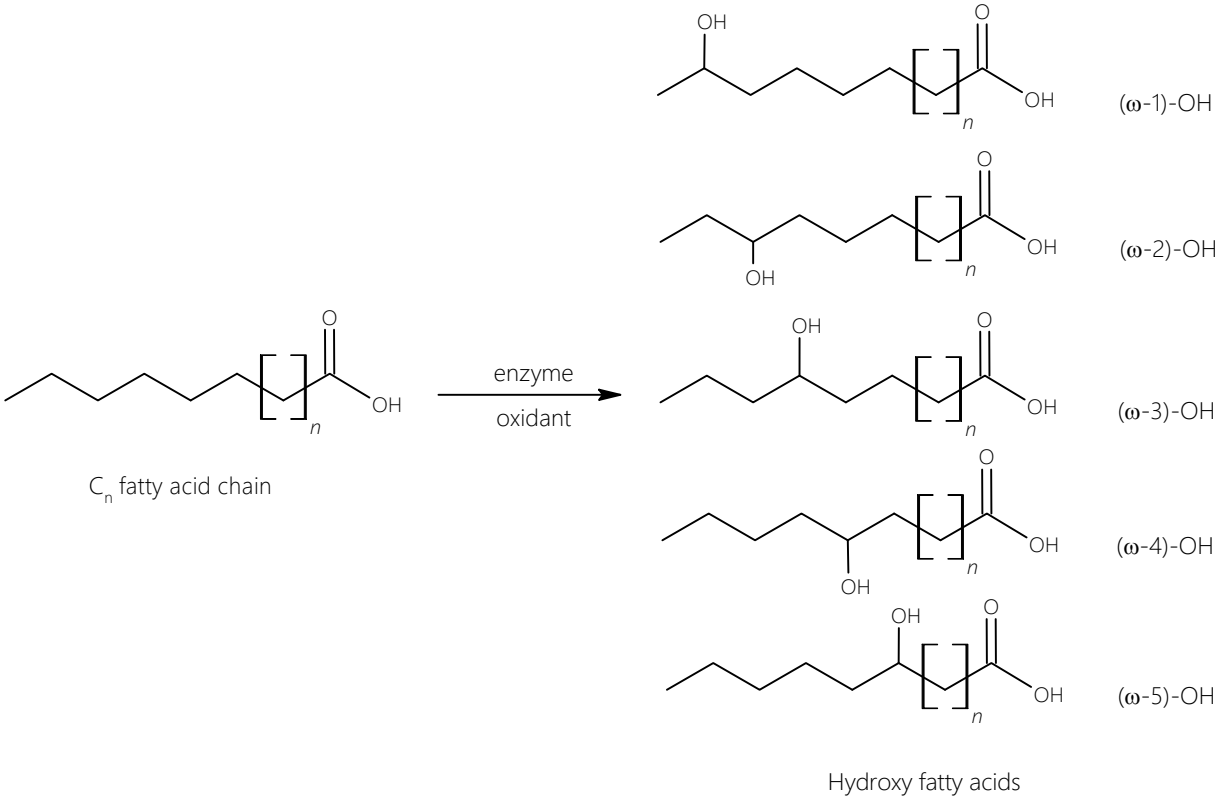

Scheme 2.8: The enzyme-driven oxidation of a fatty acid chain to its main possible hydroxy derivatives adapted from Gutiérrez *et al*. (2011)

Table 2.6 summarises the catalytic performance of several CYP102A1 variants and UPO enzymes in the oxidation of lauric acid. In one of the studies, the performance of the CYP102A1 F87A variant was evaluated using both the natural pathway and the peroxide shunt pathway using the same initial substrate concentration (2 mM) (Cirino and Arnold, 2002). It was reported that the enzyme performed five times better using molecular oxygen and NADPH than using 10 mM of H_2O_2 as the oxidant within the same short reaction time of 10 min. Cirino and Arnold (2002) speculated that this may have been due to the rapid enzyme inactivation that was induced by the H_2O_2 (once-off delivery), yet they did not monitor the enzyme stability over time throughout their investigation. Nevertheless, the F87A variant demonstrated an increased tolerance to H_2O_2 compared to the wild-type variant, which obtained a low TON of 2 $mol_{product}\ mol_{enzyme}^{-1}$ before it was completely deactivated at the same H_2O_2 concentration. The potential of protein engineering to improve H_2O_2 tolerance and concomitant increases in product yield is therefore highlighted in this study. This coupled with knowledge of the enzyme deactivation and inhibition kinetics could potentially improve the overall hydrogen-peroxide mediated biotransformation.

Cirino and Arnold (2003) went on to develop another variant of the enzyme, CYP102A1 21B3, and investigated its performance employing the same initial lauric acid concentration and once-off delivery method of H_2O_2 but at a lower concentration of 5 mM. This resulted in higher productivity as indicated by the higher turnover number of 280 $mol_{product}\ mol_{enzyme}^{-1}$. Furthermore, there may have been an improvement in the stability of the 21B3 variant which allowed for a reaction period of 30 min. In contrast, this enzyme variant lost all activity within 5 min when the H_2O_2 concentration was doubled to 10 mM. This observation provides some insight into the enzyme's stability, suggesting that higher H_2O_2 concentration could potentially lead to faster deactivation rates. In a different study where UPO was used instead, the reaction proceeded over an even longer reaction time of 2 h when exposed to a H_2O_2 concentration of 2.5 mM (once-off addition) (Gutiérrez *et al.*, 2011). It can be deduced that this lower

H_2O_2 concentration may have reduced the enzyme deactivation rate, however the studies outlined in Table 2.6 do not investigate or take into account enzyme deactivation in their analyses.

Table 2.6: Catalytic activity of CYP102A1 and UPO on the hydroxylation of lauric acid

Enzyme	Fatty acid concentration	Oxidant	TON[a]	Reaction time	Reference
CYP102A1 F87A	2 mM	NADPH + O_2	350	10 min	(Cirino and Arnold, 2002)
CYP102A1 F87A	2 mM	10 mM H_2O_2 (once-off addition)	70	10 min	(Cirino and Arnold, 2002)
CYP102A1 wild type	2 mM	10 mM H_2O_2 (once-off addition)	2	10 min	(Cirino and Arnold, 2002)
CYP102A1 21B3	2 mM	5 mM H_2O_2 (once-off addition)	280	30 min	(Cirino and Arnold, 2003)
*Aae*UPO[b]	1 mM	2.5 mM H_2O_2 (once-off addition)	n.d.	2 h	(Gutiérrez *et al.*, 2011)

Reaction conditions: pH 6.0 - 8.0, ambient temperature; [a]: total turnover number measured in $mol_{product}$ mol_{enzyme}^{-1}; [b]: unspecific peroxygenase from *Agrocybe aegerita*; [c] evolved unspecific peroxygenase variant from *Agrocybe aegerita*

Linear and cyclic alkane substrates

Typical reaction pathways for alkane activation include the abstraction of a hydrogen atom from the most reactive C-H bond. This tends to be at subterminal positions instead of the desirable terminal position (Scheme 2.9) (Bergman, 2007). Alkanes are not considered natural substrates for the UPO and P450 enzymes, however, these enzymes are catalytically active for alkane functionalisation. For CYP102A1, this is made possible with the aid of protein engineering (Glieder *et al.*, 2002). A recent study has shown that introducing a decoy molecule to a CYP102A1 variant aids the peroxide shunt pathway by acting as an acid-base co-catalyst (Chen *et al.*, 2019). On the other hand, the wild type unspecific peroxygenase from *Agrocybe aegerita Aae*UPO is capable of oxidising linear alkanes to alcohols without genetic modification (Peter *et al.*, 2011).

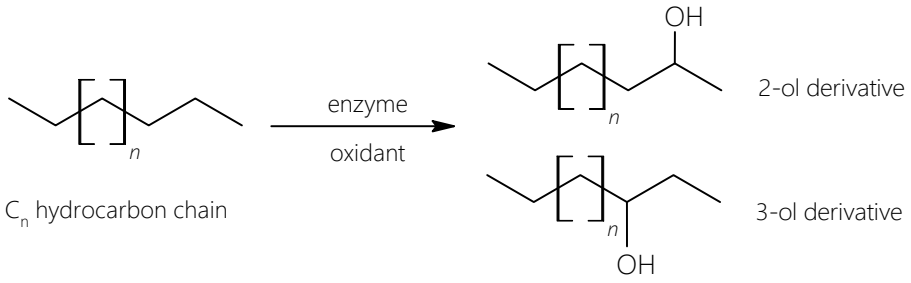

Scheme 2.9: The enzyme-driven hydroxylation of a linear alkane

The hydroxylation of n-propane, n-hexane and n-octane by UPOs and CYP102A1 variants was summarised in Tables 2.7 - 2.9. Chen *et al.* (2019) showed that H_2O_2-driven CYP102A1 F87A variants could facilitate the biotransformation of specific small chain alkanes. In the presence of a decoy molecule, N-(**ω**-imidazolyl)-hexanoyl-L-phenylalanine, the conversions of n-propane and n-hexane resulted in trace amounts of 1-propanol and 1-hexanol, respectively. The reaction did not proceed in

the absence of this decoy molecule as it is likely the enzyme did not recognise the alkanes as natural substrates or the H_2O_2 immediately deactivated the enzyme. In addition, it can be inferred that the F87A variants experienced less deactivation with the once-off delivery of 20 mM H_2O_2 compared to 60 mM H_2O_2 as a higher turnover (1 647 vs 1 050 $mol_{product}$ mol_{enzyme}^{-1}) and extended reaction period (30 vs 2 min) was achieved at the lower H_2O_2 concentration as per Tables 2.7 and 2.8. This observation may also have been due to the nature of the different substrates n-propane and n-hexane, respectively, that may have interacted with the enzyme in an inhibitory manner, as these are non-natural substrates. It is therefore important to understand how the substrate and oxidant individually influence the enzyme performance.

Table 2.7: Catalytic activity of CYP102A1 and UPO on the hydroxylation of n-propane

Enzyme	n-propane concentration	Oxidant	TON[a]	Reaction time	Reference
CYP102A1 139-3	1 mM	O_2 + NADPH	860	-	(Glieder *et al.*, 2002)
CYP102A1 F87A/T2681	4 mM	20 mM H_2O_2 (once-off addition)	1 647	30 min	(Chen *et al.*, 2019)
*Aae*UPO[b]	70 mM	4 mM h^{-1} H_2O_2 (continuous)[c]	997	60 min	(Peter *et al.*, 2011)

Reaction conditions: ambient temperature, pH 6.0 - 8.0; [a]: turnover number measured in $mol_{product}.mol_{enzyme}^{-1}$; [b]: unspecific peroxygenase from *Agrocybe aegerita*; [c]: continuous delivery via syringe pump

Table 2.8: Catalytic activity of CYP102A1 and UPO on the hydroxylation of n-hexane

Enzyme	n-hexane concentration	Oxidant	TON[a]	Reaction time	Reference
CYP102A1 139-3	1 mM	O_2 + NADPH	3 840	-	(Glieder *et al.*, 2002)
CYP102A1 F87A/T2681	4 mM	60 mM H_2O_2 (once-off addition)	1 050	2 min	(Chen *et al.*, 2019)
*Aae*UPO[b]	70 mM	4 mM h^{-1} H_2O_2 (continuous)	1 960	60 min	(Peter *et al.*, 2011)

Reaction conditions: ambient temperature, pH 6.0 - 8.0; [a]: turnover number measured in $mol_{product}.mol_{enzyme}^{-1}$; [b]: unspecific peroxygenase from *Agrocybe aegerita*; [c]: continuous delivery via syringe pump

In another study, Peter *et al.* (2011) investigated the impact of continuous H_2O_2 delivery on the enzyme catalytic performance of a UPO using similar small chain alkane substrates. The oxidant was delivered at 4 mM h^{-1} using a syringe pump. Interestingly, turnover numbers similar to the P450 variants were reported for the UPO, despite the UPO having a lower affinity to alkanes than P450s. In addition, the UPO system could extend to a longer reaction period where the enzyme retained some of its initial activity after 1 h. However, Peter *et al.* (2011) did not account for enzyme deactivation or its extent in their analysis. In a separate investigation, a photocatalyst was used for *in-situ* H_2O_2 delivery to an UPO with n-octane as the substrate. The hydrogen peroxide was delivered at 1.05 mM h^{-1} and its steady state concentration in the reaction mixture was maintained at 0.16 mM (Zhang *et al.*, 2017), which was significantly lower than the 4 mM introduced to the system by Peter *et al.* (2011). At these conditions, it was possible to run the reaction over an even longer period (70 h) yielding a high TON of 17 500 $mol_{product}$ mol_{enzyme}^{-1}. The tandem system developed by Zhang *et al.* (2017) also outperformed the NADPH-driven oxidation of n-octane using the CYP102A1 139-3 variant (Glieder *et al.*, 2002). Specifically,

it showed an approximately fivefold increase in TON. This suggests that the H_2O_2 concentration and its continuous supply to the enzyme may be a worthwhile venture into extending the enzyme's life span and potentially improving productivity. There is, however, a lack of clarity regarding the enzyme (residual) activity across all the studies presented in Tables 2.7 - 2.9.

Table 2.9: Catalytic activity of CYP102A1 and UPO on the hydroxylation of n-octane

Enzyme	n-octane concentration	Oxidant	TON[a]	Reaction time	Reference
CYP102A1 139-3	1 mM	O_2 + NADPH	3 020	-	(Glieder *et al.*, 2002)
*Aae*UPO[b]	70 mM	4 mM h^{-1} H_2O_2 (continuous)	1 280	60 min	(Peter *et al.*, 2011)
*Aae*UPO	15 mM	0.16 mM H_2O_2 (*in-situ*; photo)	17 500	70 h	(Zhang *et al.*, 2017)

Reaction conditions: ambient temperature, pH 6.0 - 8.0; [a]: turnover number measured in $mol_{product}.mol_{enzyme}^{-1}$; [b]: unspecific peroxygenase from *Agrocybe aegerita*; [c]: continuous delivery via syringe pump

Another non-natural substrate oxidised by these enzymes is cyclohexane to produce cyclohexanol (Scheme 2.10). The product of this reaction is important in the production of adipic acid and caprolactam (Musser, 2011). There are some studies that discuss the catalytic performance of CYP102A1 variants for this reaction using molecular oxygen as the oxidant (Glieder *et al.*, 2002; Maurer *et al.*, 2005). It was reported by Maurer *et al.* (2005) that the CYP102A1 R47L, Y51F variant remained active for approximately 4 days yielding a turnover number of 9 620 $mol_{product}$ mol_{enzyme}^{-1}. On the other hand, Glieder *et al.* (2002) studied the CYP102A1 139-3 variant which obtained a slightly lower TON (threefold decrease). The discrepancy may be attributed to the variations in enzyme mutations which could have affected the catalytic activity. These studies illustrate the catalytic ability of the CYP102A1 enzyme to oxidise cycloalkanes in the natural pathway, however there is no substantial research into using this same enzyme and substrate with H_2O_2 as the oxidant.

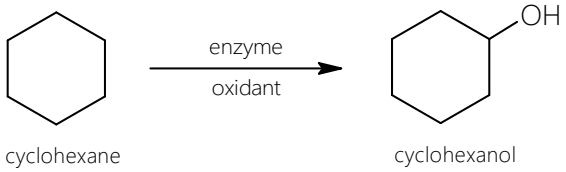

Scheme 2.10: The enzyme-driven oxidation of cyclohexane

On the other hand, there are several studies that reported successful H_2O_2-driven oxidation of cyclohexane using UPOs (Churakova *et al.*, 2011; Freakley *et al.*, 2019; Peter *et al.*, 2011; Zhang *et al.*, 2017). The photo-bio tandem system employed by Zhang *et al.* (2017) to deliver H_2O_2 to the UPO resulted in the highest cyclohexanol productivity with a TON of 65 000 $mol_{product}$ mol_{enzyme}^{-1} reported in Table 2.10. The *in-situ* H_2O_2 generation system consisted of gold-loaded titania used as a plasmonic photocatalyst which delivered H_2O_2 at 1.05 mM h^{-1} maintaining a steady-state concentration of 0.16 mM. The UPO was stable and active over 70 h which may have been due to the low H_2O_2 concentration available within the system. However, the residual activity was not monitored, which makes it unclear whether, or to what extent, enzyme deactivation may have occurred over time. A different photocatalyst was developed by Churakova *et al.* (2011) whereby flavin adenine mononucleotide (FMN) was used instead to deliver H_2O_2 to the UPO. The rate of H_2O_2 delivery (and concentration) was not specified for

this photocatalyst however the overall system was stable for only 5 h compared to 70 h and yielded more than a three-fold lower TON of 17 900 $mol_{product}$ mol_{enzyme}^{-1}. This may have been due to H_2O_2 concentrations that exceeded the enzyme's tolerance or the initial H_2O_2 production rates which inherently led to deactivation; however, these factors were not considered in their analysis. Alternatively, this photocatalytic route may have been less efficient or perhaps the nature of the photocatalyst involved may have affected enzyme performance, however Churakova *et al.* (2011) did not attempt to investigate the influence of the photocatalyst on the enzyme.

In a chemo-bio tandem system (Freakley *et al.*, 2019), the AuPd chemo-catalyst delivered H_2O_2 at a concentration low enough (approximately 0.3 mM h^{-1} initial rate, 0.44 mM - 0.74 mM at steady state) for the PaDa-I variant to remain active for 16 h, which resulted in a higher TON than the FMN photobiocatalytic system. In a more recent study, Stenner *et al.* (2023) determined that using an AuPd catalyst doped with Pt in a similar chemo-bio tandem system with PaDa-I resulted in a 1 mM h^{-1} initial H_2O_2 rate (1.50 mM at steady state) which achieved a cyclohexane conversion of 25.7%. In comparison, they reported a lower conversion of 17.4% using a AuPd catalyst - this may be attributed by the higher initial H_2O_2 delivery rate of approximately 1.50 mM h^{-1} (2.10 mM at steady state). This was significantly lower than the 4.6% conversion obtained when ca. 6 mM H_2O_2 was added to the reaction mixture by once-off delivery (Stenner *et al.*, 2023). They suggested that it might have been attributed to the destruction of the heme group, though they did not validate this with supporting analyses. The effect of reaction conditions on the deactivation of PaDa-I were further investigated in this study. It was established that the *in-situ* H_2O_2 generating system alone contributed to 18.1% activity loss, which increased to 24.7% when the organic substrate, cyclohexane, was added. Interestingly, the loss of enzyme activity further increased to 88.5% enzyme activity loss when once-off delivery of 200 ppm H_2O_2 was employed instead of the *in-situ* H_2O_2 delivery (Stenner *et al.*, 2023). This indicates that the delivery approach of the H_2O_2, and potentially organic substrates, may significantly affect the enzyme stability and catalytic activity. These factors are, therefore, crucial in developing and optimising the enzyme-mediated oxidation of cyclohexane.

Table 2.10: Comparison of catalytic activity on the oxidation of cyclohexane

Enzyme	Cyclohexane concentration	Oxidant delivery	Reaction time	TON[a]	References
CYP102A1 R47L, Y5IF	0.59 mM	NADPH + O_2	4 d	9 620	(Maurer *et al.*, 2005)
CYP102A1 139-3	2.5 mM	NADPH + O_2	-	3 910	(Glieder *et al.*, 2002)
*Aae*UPO[b]	30 mM	4 mM h^{-1} H_2O_2 (continuous)[d]	1 h	4 501	(Peter *et al.*, 2011)
*Aae*UPO	1 mM	H_2O_2 (*in-situ*; photo)	5 h	17 900	(Churakova *et al.*, 2011)
*Aae*UPO	15 mM	0.16 mM H_2O_2 (*in-situ*; photo)	70 h	61 500	(Zhang *et al.*, 2017)
PaDa-I[c]	10 mM	0.44 - 0.74 mM H_2O_2 (*in-situ*; chemo)	16 h	25 300	(Freakley *et al.*, 2019)
PaDa-I	10 mM	1.50 mM H_2O_2 (*in-situ*; chemo)	2 h	6 400	(Stenner *et al.*, 2023)

Reaction conditions: room temperature, pH 6.0 - 8.0; [a]: total turnover number measured in $mol_{product}.mol_{enzyme}^{-1}$; [b]: unspecific peroxygenase from *Agrocybe aegerita*; [c]: evolved unspecific peroxygenase variant from *Agrocybe aegerita*; [d]: continuous supply via syringe pump

In the case where H_2O_2 was manually delivered continuously to the parent strain *Aae*UPO at 4 mM h^{-1}, significantly lower turnovers were obtained compared to the tandem systems reported in Table 2.8 (Peter *et al.*, 2011). This may have been due to a less modified enzyme strain used in this study compared to the PaDa-I variant. Nevertheless, additional information was obtained through the evaluation of the Michaelis-Menten kinetic parameters of this system. The substrate affinity (K_M) was 18.4 mM and the turnover number per active site (k_{cat}) was 37 $mol_{product}$ $mol_{active\ site}$ s^{-1}. This study was repeated a few years later, with the H_2O_2 added in a stepwise manner whereby 1 mM H_2O_2 was added every minute over a total reaction time of 4 min (Peter *et al.*, 2014). There was an improvement in terms of catalytic performance as shown by a K_M value of 0.994 mM and k_{cat} of 72 $mol_{product}$ $mol_{active\ site}$ s^{-1}. This suggested that more of the active sites were available for the substrate and were not inhibited by H_2O_2. The kinetic model used in these studies was restricted to the unmodified Michaelis-Menten model which does not account for the suggested inhibition. It was, therefore, unclear how the different H_2O_2 delivery approaches (continuous and stepwise) influenced the overall enzyme kinetics.

Most published research has focused on maximizing product yield in biocatalysis, often disregarding critical factors such as the possibility of H_2O_2 or substrate-mediated inhibition or the H_2O_2 tolerance of the enzymes. Consequently, a few kinetic models have been developed with efforts to describe how substrates (and oxidants) influence the inhibition and deactivation of the enzyme.

2.2.3 Enzyme kinetics

To enhance the efficiency of hydrocarbon biotransformation using UPOs, it is crucial to obtain enzyme kinetic data. Such data is instrumental in gaining a better understanding of the biotransformation mechanism, specifically the interactions between the enzyme, substrate and oxidant. It also provides insights into the potential of enzyme inhibition and deactivation, that may be induced by the substrate and oxidant in the reaction medium.

Enzyme inhibition kinetics

The kinetics of an enzyme-driven hydrocarbon functionalisation reaction can be determined using the Michaelis-Menten model, which focuses on the interaction between enzymes and their substrates and the subsequent conversion of the substrate into a product. This model is a fundamental concept in enzyme kinetics that provides a mathematical framework to describe the rate of enzyme-catalysed reactions, as shown in Equation 2.3:

$$v = \frac{v_{max}\,[S]}{K_M + [S]} \tag{2.3}$$

where v is the reaction rate, S the substrate concentration, v_{max} the maximum reaction rate and K_M the Michaelis-Menten constant (Clarke, 2013).

This version of the model; however, does not account for any inhibition that hydrocarbon substrates or oxidants such as H_2O_2 potentially induce on UPOs and P450s. Three types of inhibition are often reported. These are competitive, non-competitive and uncompetitive inhibition (Clarke, 2013; Illanes *et al.*, 2008). Competitive inhibition occurs when the inhibitor competes with the substrate through binding to the active site of the enzyme. This may be reversed if the substrate concentration is high enough to minimise the effects of the competitive inhibitor (Illanes *et al.*, 2008). This catalytic pathway is modelled by the modified version of the Michaelis-Menten model shown in Equation 2.4, where I is the inhibitor concentration and K_I the inhibition constant (Clarke, 2013).

$$v = \frac{v_{max}\,[S]}{K_M\left(1+\frac{[I]}{K_I}\right)+[S]} \tag{2.4}$$

When the inhibitor binds to a part of the enzyme other than the active site (i.e. allosteric site), this is referred to as non-competitive inhibition. In this case, with the inhibitor bound to the allosteric site, the charge distribution over the enzyme is altered which impacts the affinity of the enzyme to the substrate. Increasing the substrate concentration, therefore, has no influence on this type of inhibition. In some cases, the modified Michaelis-Menten equation (Equation 2.5) predicts that non-competitive inhibition reduces the overall reaction rate (Illanes *et al.*, 2008).

$$V = \frac{v_{max}\,[S]}{(K_M+[S])\left(1+\frac{[I]}{K_I}\right)} \tag{2.5}$$

Uncompetitive inhibition occurs when the inhibitor binds to the enzyme only after the substrate has already bound to it (Clarke, 2013). This distorts the active site of the protein which hinders the catalytic activity of the enzyme and therefore cannot be overcome by increasing substrate concentration in the reaction environment. Equation 2.6 shows the modified Michaelis-Menten equation that models uncompetitive inhibition (Illanes *et al.*, 2008).

$$V = \frac{v_{max}\,[S]}{K_M+[S]\left(1+\frac{[I]}{K_I}\right)} \tag{2.6}$$

To improve and accurately predict enzyme performance in a biotransformation process, it is esssential to understand the catalytic response of the enzymes under varying substrate and oxidant concentrations. For instance, Mireles *et al.* (2021) observed ca. 50% higher substrate (2-benzyloxy ethanol) conversion by a PaDa-I variant upon decreasing the H_2O_2 concentration from 1 - 0.1 mM. In addition, they determined that the enzyme activity decreased by approximately 30% as the ether substrate, benzyloxyacetate, was increased from 0.2 - 4 mM. Therefore, other crucial aspects to evaluate are the H_2O_2-driven and potential substrate-induced deactivation of the enzyme.

Enzyme deactivation kinetics

Building on the biotransformation mechanism presented in Scheme 2.5, Valderrama *et al.* (2010) proposed a deactivation mechanism of heme peroxidases by H_2O_2. In this mechanism, exposure of the Compound II enzyme intermediate to excess H_2O_2 leads to the formation of a peroxy-Fe(III) porphyrin radical, Compound III (Scheme 2.11, **A**). It is proposed that Compound III causes enzyme deactivation through three possible pathways. The first pathway is an irreversible inactivation called heme bleaching whereby the peroxyl radical reacts with the porphyrin ring leading to the liberation of the iron metal centre (**B**) (Nagababu and Rifkind, 2004). In pathway **C**, the peroxyl radical on one enzyme molecule oxidises surrounding proteins such as amino acid side chains on another enzyme molecule, thus returning the former to ground state whilst deactivating the latter (Cai and Tien, 1989). Lastly, the decomposition of Compound III liberates the peroxyl radical, forming even more reactive hydroxyl radicals which then leads to protein oxidation.

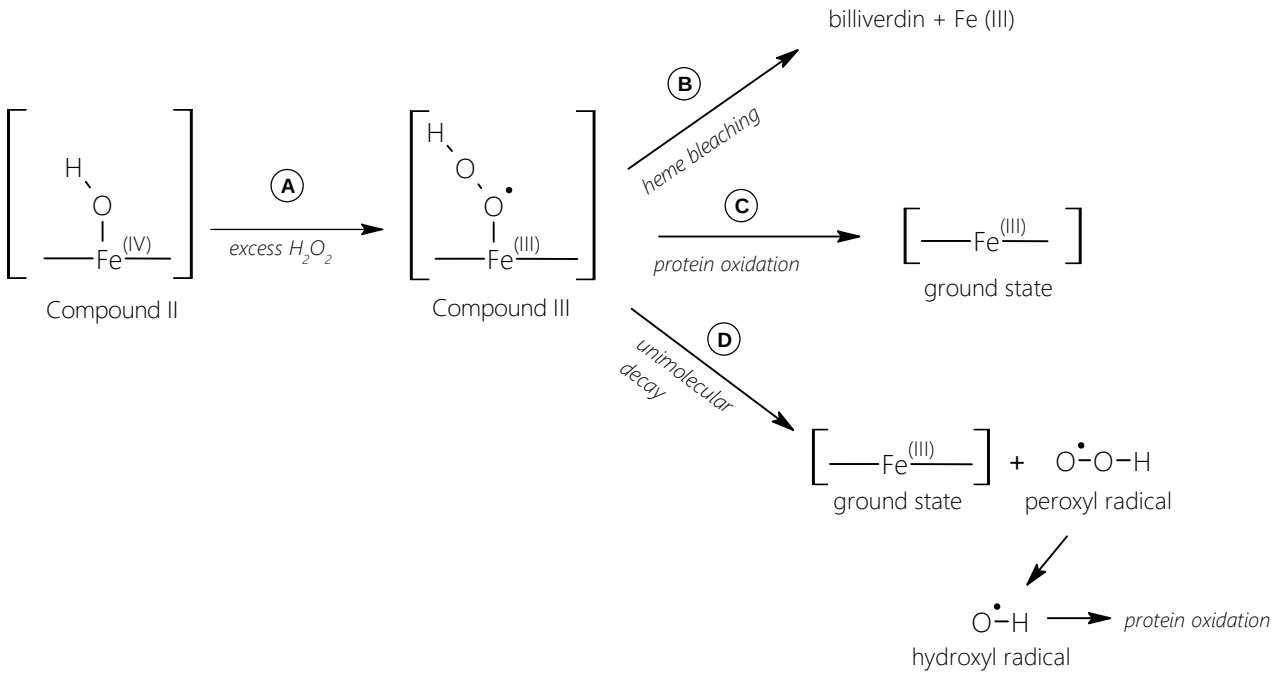

Scheme 2.11: An adaptation of the proposed enzyme deactivation mechanism for heme peroxidases (Valderrama, 2010)

In another study, the deactivation of horseradish peroxidase, an enzyme with a similar structure to UPOs and P450s, was investigated in the presence of H_2O_2 (Hernández-Ruiz *et al.*, 2001). In this enzyme deactivation mechanism, Compound I is formed when the enzyme is initially exposed to H_2O_2 (pathway **i** in Scheme 2.12). In the presence of excess H_2O_2, a Compound I·H_2O_2 enzyme intermediate is formed which can follow three possible pathways thereafter. It can engage a protective mechanism towards deactivation whereby the H_2O_2 is broken down to release oxygen, restoring the enzyme to its original ground state (**iii** in Scheme 2.12). Otherwise, Compound I·H_2O_2 could follow the other two pathways where the enzyme is either completely deactivated (**iv**) or forms less reactive enzyme intermediates which eventually lead back to recovering the enzyme ground state (**v**)-(**viii**).

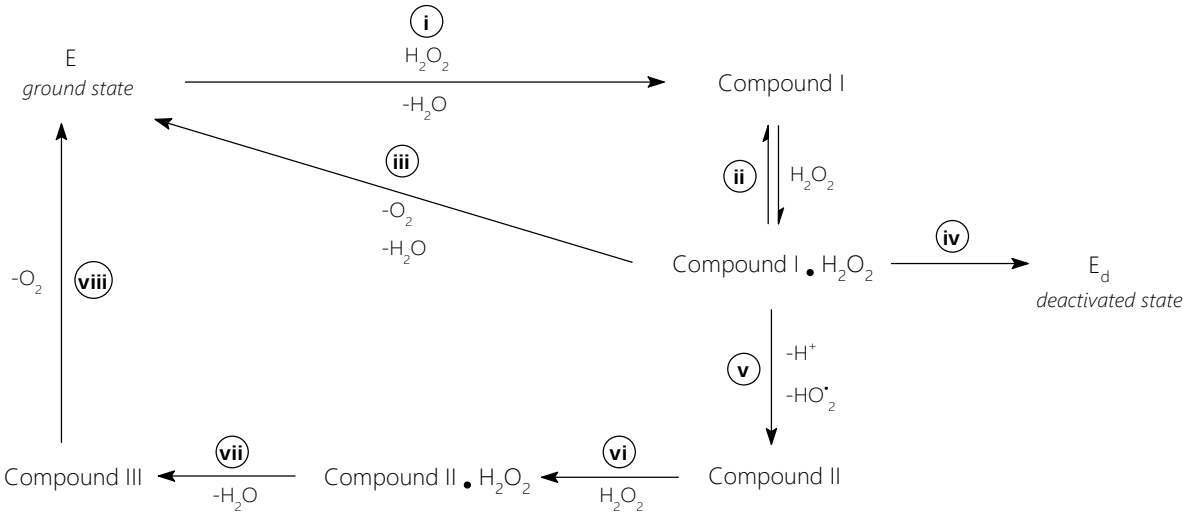

Scheme 2.12: Mechanism of the reaction of horseradish peroxidase with H_2O_2 adapted from Hernández-Ruiz *et al.* (2001)

Due to the limited knowledge of the deactivation mechanism specific to UPOs, there is a need to further interrogate the kinetics associated with enzyme deactivation. A kinetic model that may be relevant and applicable to UPO deactivation is the two-step series enzyme deactivation model (Henley and Sadana, 1986; Sadana and Henley, 1987a). This model was initially introduced to describe the enzyme deactivation kinetics for acetylcholinesterase exposed to varying pH values (circumneutral) and different concentrations of aster and NaCl. The mechanism presented in Equation (2.7) suggests that the enzyme is immediately deactivated (presumably upon contact with the H_2O_2 and/or substrate) forming the first enzyme intermediate deactivated state (E_1). Consequently, a second (slow) deactivation step occurs forming a second enzyme intermediate that is still active (E_2). From this mechanism, it is important to note that E, E_1 and E_2 are the different enzyme states that have different specific activities β, β_1 and β_2. Therefore, α_1 and α_2 effectively represent the ratio of the intermediate states relative to the initial enzyme state (Equations 2.8 and 2.9). The four-parameter equation that was developed to model this deactivation is shown in Equation (2.10), where k_1 and k_2 are first order deactivation constants (Henley and Sadana, 1986; Sadana and Henley, 1987a).

$$E \xrightarrow{k_1} E_1^{\alpha_1} \xrightarrow{k_2} E_2^{\alpha_2} \tag{2.7}$$

$$\text{where } \alpha_1 = \beta_1 / \beta \tag{2.8}$$

$$\text{and } \alpha_2 = \beta_2 / \beta \tag{2.9}$$

$$\frac{A_t}{A_0} = \left(1 + \frac{\alpha_1 k_1}{k_2 - k_1} - \frac{\alpha_2 k_2}{k_2 - k_1}\right) \exp(-k_1 t) - \left(\frac{k_1}{k_2 - k_1}\right)(\alpha_1 - \alpha_2) \exp(-k_2 t) + \alpha_2 \tag{2.10}$$

The reaction mechanism in Equation (2.11) is obtained if the enzyme undergoes a single-step deactivation, yet yields one final enzyme state, E_1, with a non-zero specific activity (Sadana and Henley, 1987a, 1987b). In this case, α_2 and k_2 would equal zero which reduces the four-parameter model to a two-parameter model as shown in Equation (2.12).

$$E \xrightarrow{k_1} E_1^{\alpha_1} \tag{2.11}$$

$$\frac{A_t}{A_0} = (1 - \alpha_1) \exp(-k_1 t) + \alpha_1 \tag{2.12}$$

Another mechanism is that the enzyme is completely inactivated in a single step to its deactivated state (E_d) as shown in Equation (2.13). In this case, the two-parameter model is further reduced to model first-order decay kinetics (Equation 2.14) (Sadana and Henley, 1987a).

$$E \xrightarrow{k_1} E_d \tag{2.13}$$

$$\frac{A_t}{A_0} = \exp(-k_1 t) \tag{2.14}$$

These models can potentially be used to evaluate the enzyme deactivation kinetics of UPOs exposed to hydrogen peroxide and potentially to assess whether the hydrocarbon substrate may also lead to deactivation. Furthermore, they may serve as a foundational basis for modelling and enhancing our understanding of the kinetics of PaDa-I enzyme.

2.3 Summary of key findings

A thorough review of the available literature on *in-situ* hydrogen production, hydrocarbon oxidation and tandem catalysis led to a number of key findings. Biocatalysis is potentially a sustainable synthesis route where the enzymes used require mild operating conditions and yield high product selectivity with minimal waste production. Hydrocarbons are part of the substrate scope for certain classes of enzymes, including unspecific peroxygenases and cytochrome P450s. These enzymes require H_2O_2 as the oxidant at low dosages to minimise enzyme deactivation and potentially prolong reaction time and hence productivity. One-pot systems have been developed whereby the H_2O_2 is produced *in-situ* instead of manually dosing the oxidant. There are several *in-situ* hydrogen peroxide generating systems that include chemo-catalysts and biocatalysts - these are potentially compatible with enzyme-driven oxyfunctionalisation in terms of operating at similar reaction conditions. In some of the studies it is unclear whether the rate of H_2O_2 generation (thus, delivery to the oxyfunctionalisation enzyme) by these different catalysts could potentially impact the overall enzyme performance. Furthermore, the H_2O_2 tolerance for UPOs and P450s is not clearly specified. In addition to highlighting part of the diverse range of substrates that can be oxidised by UPOs and cytochrome P450s which include aromatics, fatty acids and alkanes, the studies reviewed do not take into consideration whether these organic substrates might also inactivate the enzyme along with the H_2O_2. There is not much data available in terms of the reaction kinetics and/or enzyme deactivation kinetics. Moreover, the type of enzyme inhibition caused by H_2O_2 is unknown. Other factors such as temperature and pH could also potentially affect the enzyme activity. It is therefore important that the kinetics of such one-pot tandem systems are evaluated to optimise the process.

2.4 Defining the research project

2.4.1 Problem statement

Hydrocarbons are available in abundance as a resource but are currently underutilised as a substrate with the potential to produce high value materials. The unspecific peroxygenase PaDa-I variant is an enzyme that displays catalytic activity in the oxyfunctionalisation of hydrocarbons at milder conditions compared to conventional chemo-catalytic routes. This can be done in tandem with an *in-situ* hydrogen peroxide generating system to provide the oxidant to the enzyme. However, there is limited knowledge and understanding of the kinetics of the system in terms of the rate of hydrogen peroxide delivery to the enzyme along with the rate of enzyme deactivation.

2.4.2 Research project objectives

The objectives for this project are as follows:

- Research findings have indicated that exposure of the unspecific peroxygenase to excess H_2O_2 leads to severe enzyme deactivation (Karich *et al.*, 2016; Valderrama, 2010; Valderrama *et al.*, 2002). According to prior reports, H_2O_2 delivery strategies have been implemented to biocatalytic systems

to alleviate the rate of this deactivation. Instead of adding the oxidant all at once (Chen *et al.*, 2019; Gutiérrez *et al.*, 2011; Kluge *et al.*, 2012; Ma *et al.*, 2018), Peter *et al.* (2011) introduced H_2O_2 to their biocatalytic system at a controlled flow rate using a syringe pump. They also employed stepwise delivery whereby H_2O_2 was added at regular intervals (Peter *et al.*, 2014). In other studies, the H_2O_2 was produced *in-situ* in a one-pot system where the oxidant was steadily delivered to the enzyme (Churakova *et al.*, 2011; Freakley *et al.*, 2019; Pesic *et al.*, 2019; Tieves *et al.*, 2019; Zhang *et al.*, 2017). In this thesis, however, the effect of manually dosing H_2O_2 through once-off, stepwise and continuous delivery methods on the stability of the PaDa-I enzyme will be studied. Additionally, the investigation will also assess the impact of varying the H_2O_2 concentrations at 10 mM, 20 mM and 40 mM. This will determine the optimal delivery rate of H_2O_2 that will minimise enzyme deactivation.

- Most enzymes are sensitive towards the conditions of the reaction mixture - such conditions typically include temperature and pH (Bechtold and Panke, 2012; Bhatia, 2018; Doran, 1995). It has been reported that the PaDa-I variant, in particular, operates optimally at ambient temperatures and circumneutral pH levels (Hofrichter *et al.*, 2010; Kluge *et al.*, 2012; Molina-Espeja *et al.*, 2015; Peter *et al.*, 2011; Zhang *et al.*, 2017). It is important to investigate whether these reaction conditions will also have an impact on the activity of the enzyme. Therefore, the influence of temperatures 20 °C, 25 °C and 30 °C and pH levels 6.0, 7.0 and 8.0 on the enzyme stability will be studied.
- Research efforts have primarily focused on the product yields in their biocatalytic systems, neglecting to explore the extent of enzyme deactivation over time (Chen *et al.*, 2019; Churakova *et al.*, 2011; Kluge *et al.*, 2012; Pesic *et al.*, 2019; Tieves *et al.*, 2019; Zhang *et al.*, 2017). The enzyme deactivation kinetics will therefore be evaluated when employing once-off, stepwise and continuous H_2O_2 delivery to PaDa-I. This evaluation will be conducted both in the absence and presence of a hydrocarbon substrate, with styrene serving as the model substrate. Furthermore, the kinetics associated with enzyme inhibition will be determined. The knowledge gained from the kinetics will provide guidance for developing optimisation strategies in biotransformation systems.

2.4.3 Research hypothesis

The PaDa-I enzyme has the catalytic ability to oxidise hydrocarbons and convert them to valuable oxygenates using hydrogen peroxide as the oxidant. However, this enzyme is deactivated by hydrogen peroxide within a short time frame when a high concentration of this oxidant is added at once. The stability and catalytic performance of these enzymes can therefore be enhanced by adding low concentrations of hydrogen peroxide either at regular intervals or low flow rates because the rate of delivery of the oxidant will minimise the rate of enzyme deactivation.

2.4.4 Key research questions

The hypothesis formulated gives rise to these key questions:

1. How does varying the H_2O_2 concentration at 10 mM, 20 mM and 40 mM affect the enzyme activity?
2. How does varying the H_2O_2 delivery method at once-off, stepwise and continuous addition affect the enzyme activity?
3. How does varying the reaction temperatures (20 °C, 25 °C and 30 °C) and pH levels (6.0, 7.0 and 8.0) influence the enzyme activity?

4. In the presence of a hydrocarbon substrate, what is the optimal hydrogen delivery approach that will reduce enzyme deactivation?
5. In the presence of a hydrocarbon substrate, does H_2O_2 behave as a competitive, non-competitive or uncompetitive inhibitor to the enzyme?

3 Methodology

To address the research objectives and key questions, the stability of the PaDa-I enzyme was initially tested in the absence of a hydrocarbon substrate by investigating the impact of the following reaction conditions: H_2O_2 delivery method, H_2O_2 concentration, pH and temperature. The optimal reaction conditions were then selected and employed to the biotransformation of styrene, a known natural substrate for UPOs (Babot *et al.*, 2013; Bormann *et al.*, 2015; Hobisch *et al.*, 2021; Hofrichter and Ullrich, 2014). The data collected from these experiments were then used to determine the enzyme deactivation kinetics, product formation and H_2O_2 utilisation.

All reagents used to prepare the reaction mixture were obtained from Merck (T/A Sigma Aldrich) or Kimix Chemicals and were used without further purification. All solvents used were obtained from Merck and were of the highest grade available (98 - 99.9%). The experiments were performed using PaDa-I purified enzyme which was purchased from EvoEnzyme (EC 1.11.2.1, UPO). The enzyme was supplied as a crude extract at pH 7.0 for optimal peroxygenase activity. The enzyme, with a molecular weight of 51.1 kDa, was stored at 4 °C in a 100 mM potassium phosphate buffer maintained at pH 7.0. In terms of the experimental set-up, all experiments were performed in a Radley's 6 Plus Carousel reactor (Figure 3.1). To determine the oxidised product and residual substrate concentrations, GC analysis was performed on a Varian 3900 equipped with an Agilent VF-5ms (60 m x 0.32 mm x 0.45 mm) column and an FID detector. The residual enzyme activity was monitored by UV-Vis spectra which was recorded on a Thermo Genesys 105 UV-Vis spectrometer.

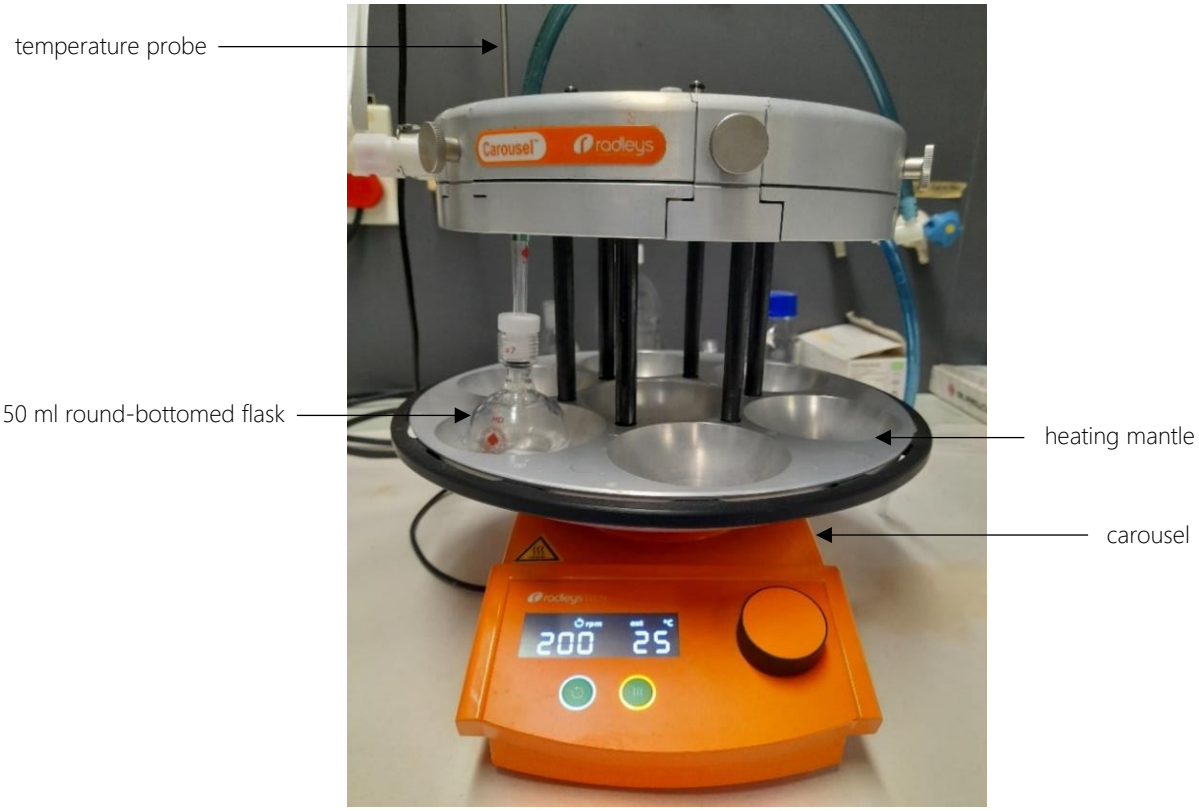

Figure 3.1: Radleys 6 Plus Carousel set up for experimental work

3.1 Experimental approach

With reference to some of the studies outlined in the literature review, tandem one-pot systems ensure that H_2O_2 is produced and steadily delivered to the enzyme for biotransformation reactions (Churakova *et al.*, 2011; Freakley *et al.*, 2019; Stenner *et al.*, 2023; Tieves *et al.*, 2019; Zhang *et al.*, 2017). Given the notable sensitivity of unspecific peroxygenases such as PaDa-I to H_2O_2 concentration and rate of exposure (Valderrama *et al.*, 2002), three delivery systems were investigated in this study. These included, the stepwise addition of the oxidant where the H_2O_2 was introduced at regular intervals, and continuous addition where the H_2O_2 was gradually fed and controlled by a syringe pump. Once-off addition of the oxidant to the reaction system was selected as the base case method of delivery where all the H_2O_2 was added at once. The hydrogen peroxide concentrations were selected on the basis of the hydrocarbon substrate concentration of 20 mM (Karich *et al.*, 2016; Wilbers *et al.*, 2021; Zhang *et al.*, 2017). The stoichiometric ratio of the substrate to the oxidant (Equation 2.2) was investigated at 2:1, 1:1 and 1:2 which translated to H_2O_2 concentrations of 10 mM, 20 mM and 40 mM (Figure 3.2). The base case H_2O_2 concentration was 20 mM, where the reaction was neither substrate nor oxidant limited at equivalent stoichiometric quantities of the oxidant and substrate.

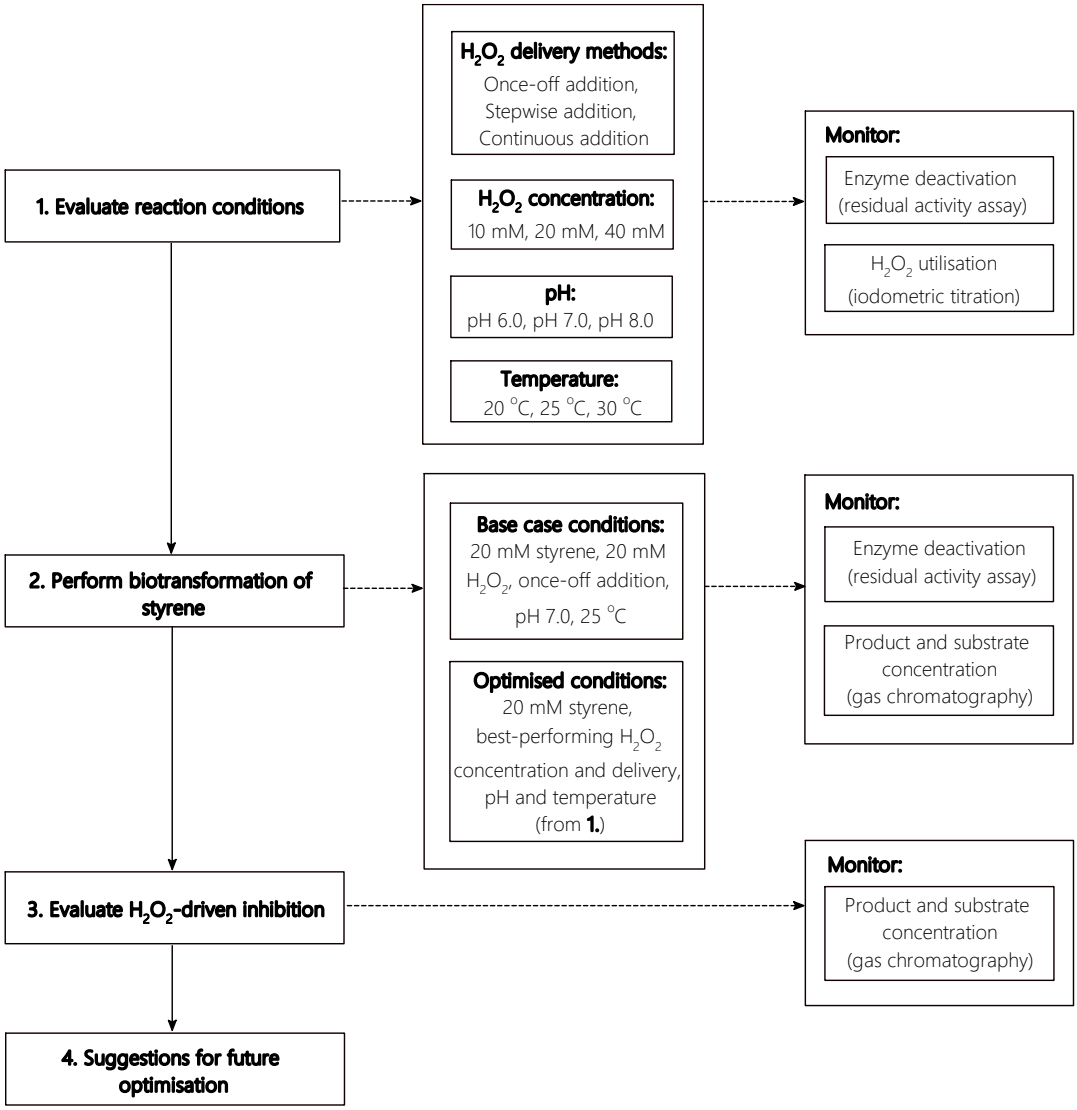

Figure 3.2:The approach developed for experimental work

The pH and temperature were investigated to determine the potential influence of these conditions on the stability of the enzyme (Figure 3.2). The UPO facilitates the oxidation of hydrocarbons within a narrow range of operating conditions which are typically ambient and circumneutral conditions. As such, the pH values investigated were selected within the near-neutral range of pH 6.0, 7.0 and pH 8.0, with pH 7.0 as the base case condition as recommended by EvoEnzyme. An ambient temperature range of 20 °C, 25 °C and 30 °C was investigated as enzymes are known to operate at mild conditions (Ayala and Torres, 2004; Polizzi *et al*., 2007; Schrewe *et al*., 2013). The best-performing reaction conditions where then evaluated with an emphasis on achieving the enzyme's highest stability. The optimised conditions were subsequently employed for the biotransformation of styrene. The influence of H_2O_2 concentration on the biotransformation was also investigated to assess the potential hydrogen peroxide-driven inhibition of the enzyme. The enzyme's catalytic performance was examined by monitoring the residual enzyme activity, H_2O_2 utilisation and the oxidised product concentration. The methodologies associated with these experiments are described in this chapter.

3.1.1 Hydrogen peroxide delivery studies

Hydrogen peroxide delivery experiments were performed in 50 ml round bottomed flasks. In a typical experiment, the reaction vessel was charged with 100 mM potassium phosphate buffer (pH 7.0) to ensure a total final volume of 20 ml and 1.7 U ml^{-1} PaDa-I enzyme (20 µl 2.8 $mg_{protein}$ ml^{-1} enzyme stock solution). One enzyme unit is defined as the amount of enzyme that converts 1 µmol of 5-nitro-1,3-benzodioxide (NBD) to 1 µmol of 4-nitrocatechol in 1 min at 25 °C and pH 7.0 (discussed in detail in Section 3.3.1). The flasks were thereafter placed on the Radleys 6 Plus Carousel (Figure 3.1) with the temperature of the heating mantle set to 25 °C and the agitation speed of the magnetic stirring bar at 200 rpm as described by Freakley *et al*. (2019). The H_2O_2 was subsequently introduced into the flasks using different delivery methods. These included once-off, stepwise and continuous addition to achieve final H_2O_2 concentrations of 10 mM, 20 mM and 40 mM over a 2 h reaction period. Table 3.1 shows the different H_2O_2 delivery rates that were tested for each delivery approach. The total volume of hydrogen peroxide solution added to the system was maintained at 2 ml for each of the experiments. This was accomplished using stock solutions of 100 mM, 200 mM and 400 mM H_2O_2, respectively.

Table 3.1: The different H_2O_2 delivery systems and concentrations

Once-off (mM)	Stepwise (mM per 30 min)	Continuous (mM h^{-1})
10.0	2.5	5.0
20.0	5.0	10.0
40.0	10.0	20.0

A Gilson adjustable volume pipette was used for the once-off and stepwise delivery systems. The oxidant delivery rate was 0.5 ml (H_2O_2 stock solution) every 30 min when a stepwise addition was employed. In the continuous delivery system, the H_2O_2 was fed to the reaction vessel at 1 ml h^{-1} using a NE-300 Just Infusion™ syringe pump. These experiments were run in duplicate for 2 hours in which samples for analysis were collected in 5 min intervals in the first 15 minutes, and thereafter at 30 minute intervals. Analyses included determining the residual enzyme activity (Section 3.3.1), residual hydrogen peroxide concentration (Section 3.3.2) and monitoring the pH over the course of the reaction.

3.1.2 pH studies

The optimal pH conditions were determined by varying the pH between 6.0 - 8.0 and employing once-off delivery of 20 mM H_2O_2 to the PaDa-I enzyme/buffer mixture. Samples were collected in duplicate to establish reproducibility and at the same intervals as detailed in Section 3.1.1. Stock solutions of 100 mM potassium phosphate buffer were prepared at pH 6.0, pH 7.0 and pH 8.0 and these were used for each respective experimental run.

3.1.3 Temperature studies

To determine the best-performing temperature, the reaction temperature was varied between 20 - 30 ^{o}C using once-off addition of 20 mM H_2O_2 as the method of delivery to the enzyme/buffer mixture. The samples were collected at the same frequency and predetermined times as described in Section 3.1.1. To set the reaction temperature to 20 ^{o}C, the round-bottomed flask was immersed in a water bath connected to a chiller to maintain the temperature at the desired set point. The Radley's Carousel heating mantle was used to maintain temperatures at 25 ^{o}C and 30 ^{o}C, respectively.

3.2 Enzyme catalytic performance

3.2.1 Biotransformation reactions

The biotransformation of styrene experiments were performed in round-bottomed flasks at the base case conditions initially (Figure 3.2). The reaction mixture contained a total final volume of 20 ml 100 mM potassium phosphate buffer pH 7.0 and an enzyme concentration of 12 U ml^{-1} (130 µl 2.8 $mg_{protein}$ ml^{-1} PaDa-I enzyme stock solution). 20 mM styrene was then added to the reaction mixture followed by once-off delivery of 20 mM H_2O_2 (2 ml of 200 mM H_2O_2 stock solution). These experiments were conducted at 25 ^{o}C and 200 rpm. The reaction time was extended to 24 h until pseudo-steady state conditions were achieved. The stepwise and semi-continuous delivery methods were also employed at the same H_2O_2 concentration to investigate whether the H_2O_2 delivery would influence the rate of styrene oxide production. The round-bottomed flask was carefully opened and resealed to add 5 mM H_2O_2 (0.5 ml 200 mM H_2O_2) every 30 min over the first 2 h only. For semi-continuous addition, a similar approach was used where 0.83 mM H_2O_2 (83 µl 200 mM H_2O_2) was added every hour over the entire 24 h period. These biotransformation experiments were performed in duplicate and samples were collected sacrificially at 5 min, 30 min, 1 h, 2 h, 4 h, 8 h, 16 h and 24 h. Analyses included residual peroxygenase activity, substrate and product analysis by gas chromatography and monitoring of the pH.

3.2.2 Inhibition studies

To decouple the potential inhibition by the substrate and oxidant on enzyme activity, preliminary experiments were performed to determine the influence of styrene and H_2O_2 concentration on the rate of styrene oxide formation. The reaction conditions for these experiments were similar to those discussed in Section 3.2.1 with an initial styrene concentration of 20 mM; however, the H_2O_2 was added to the reaction mixture at concentrations 10 mM, 5 mM and 2.5 mM by once-off delivery. This was repeated at different initial styrene concentrations 10 mM, 5 mM and 2.5 mM. Samples were collected after one hour and analysed to determine the substrate and product concentrations.

3.3 Analytical methods

3.3.1 Residual peroxygenase activity assay

The residual activity of the enzyme was determined using a peroxygenase activity assay that employs 5-nitro-1,3-benzodioxide (NBD) as the substrate. This assay was performed by first withdrawing an aliquot of 80 µl of the reaction mixture and adding it to 500 µl of 100 mM potassium phosphate buffer (pH 7.0), 310 µl deionised water and 100 µl of 5 mM NBD (dissolved in acetonitrile). Thereafter, 10 µl of 100 mM H_2O_2 was added to initiate the reaction. The reaction mixture was incubated in a dry bath incubator for 5 min at 25 °C. The successful conversion of NBD yielded a bright yellow colour representing the product 4-nitrocatechol as per the reaction mechanism in Scheme 3.1. Thereafter, 100 µl of 10 M NaOH was added to quench the reaction and affect a colour change in the solution from yellow to a pink/red mixture.

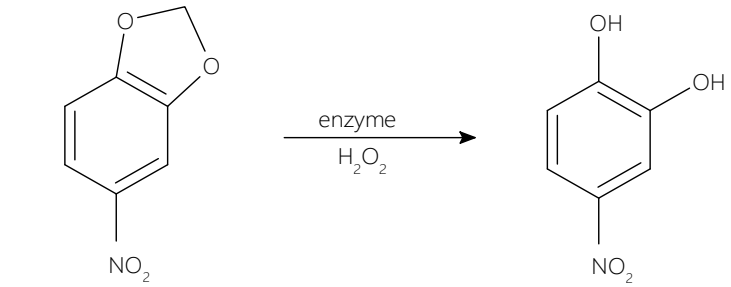

5-nitro-1,3-benzodioxide 4-nitrocatechol

Scheme 3.1: Reaction scheme for the NBD peroxygenase activity assay

Product formation was quantified by measuring the absorbance at a wavelength of 514 nm using ε_{514} = 11 400 M cm^{-1} as the extinction coefficient for 4-nitrocatachol (Poraj-Kobielska *et al.*, 2012). The percentage residual enzyme activity was calculated relative to the measured activity of the enzyme/buffer mixture before the addition of H_2O_2 or styrene substrate. The specific enzyme activity was calculated in terms of the moles of 4-nitrocatechol product formed per minute per unit mass of total protein ($\mu mol_{nitrocatechol}\ min^{-1}\ mg_{protein}^{-1}$ or $U\ mg_{protein}^{-1}$).

3.3.2 Iodometric titration

Residual H_2O_2 concentration was determined by the iodometric titration method adapted from (Jeffery *et al.*, 1989). A 500 µl sample was withdrawn from the reaction mixture and added to a conical flask containing 30 ml of 1 wt% potassium iodide dissolved in 1 M sulfuric acid. The flask was covered with aluminium foil and incubated at room temperature for 15 minutes. After incubation, 2 mM sodium thiosulphate was then rapidly titrated against the liberated iodine until a pale, straw-like yellow colour was observed. Starch indicator was then added turning the solution blue-black, and the titration was continued until the solution reached a colourless endpoint. The titre obtained was then used to calculate the residual H_2O_2 concentration as shown in Equation 3.1:

$$\text{Residual } H_2O_2 \text{ concentration} = \frac{(\text{Volume}_{titre} \times \text{Concentration}_{titre})}{\text{Volume}_{sample}} \quad (3.1)$$

3.3.3 Gas chromatography

For substrate and product quantification in oxidation reactions, the biotransformation experiments were stopped by the addition of ethyl acetate (2 x 10 ml) containing 20 mM 1-decanol as internal standard. The reaction mixture was then transferred to a clean, dry 50 ml falcon tube. The tube was vortexed for 5 min and then centrifuged at 4 000 rpm for 5 min to separate the organic and aqueous phases. Thereafter, 1 ml of the organic layer was transferred to a clean, dry gas chromatography (GC) vial. Experiments were analysed by injecting 1 µl of sample into a GC equipped with an Agilent VF5-ms column. Nitrogen was used as the carrier gas (flow rate 1 ml min^{-1}). The temperature program used during the analysis included setting the oven to 60 ^{o}C where it was held for 2 min, before the temperature was ramped to 120 ^{o}C at 1.5 ^{o}C min^{-1} over the following 32 min and again ramped to 200 ^{o}C at 15 ^{o}C min^{-1} and held at 200 ^{o}C for 2 min. The total run time was approximately 40 min. Analytes were identified by comparison of the retention times with those of the appropriate GC reference standards. The concentration of the analytes was determined using the calculated relative response factors along with standard curves for each compound (see Appendix A.1 for standard curves).

3.4 Statistical analysis

In assessing the suitability of the kinetic models reviewed in the literature (Section 2.2.3), each model's ability to predict system performance was evaluated by calculating and comparing several statistical metrics: the coefficient of determination (R^2), chi-square (χ^2) value and average absolute relative deviation (AARD). Equations 3.2 - 3.4 represent these statistical metrics, where y_i was the experimental value, $\bar{y}$ the average of the experimental values, $f(x_i)$ the predictive model value and n the total number of observations.

$$R^2 = 1 - \frac{\sum\left(y_i - f(x_i)\right)^2}{\sum\left(y_i - \bar{y}\right)^2} \tag{3.2}$$

$$\chi^2 = \sum \frac{\left(y_i - f(x_i)\right)^2}{f(x_i)} \tag{3.3}$$

$$AARD = \frac{100}{n} \left| y_i - f(x_i) \right| \tag{3.4}$$

Further statistical analysis was carried out to establish the most suitable kinetic model for the experimental data. This was achieved by calculating and evaluating the Akaike's Information Criterion (AIC) and the Bayesian Information Criterion (BIC) (Burnham and Anderson, 2002). The equations for these statistical criteria are presented in Equations 3.5 and 3.6:

$$AIC = -2 \log L(\theta) + 2K \tag{3.5}$$

$$BIC = -2 \log L(\theta) + K \log(n) \tag{3.6}$$

where K represented the total number of estimated regression parameters within the model and the log-likelihood estimator, denoted as logL(θ), was expressed as shown in Equations 3.7 and 3.8 (Burnham and Anderson, 2002):

$$\log L(\theta) = -\frac{1}{2} n \log(\sigma^2) - \frac{n}{2} \log(2\pi) - \frac{n}{2} \tag{3.7}$$

$$\text{where } \sigma^2 = \frac{\sum\left(y_i - f(x_i)\right)^2}{n} \tag{3.8}$$

4 Assessing the PaDa-I enzyme stability under different reaction conditions

Enzymes are sensitive proteins that exhibit a change in catalytic behaviour under different reaction conditions including pH, type of buffer, ionic strength and temperature (Bhatia, 2018; Doran, 1995; Punekar, 2018). Knowledge of how these conditions effect the stability and catalytic activity of enzymes such as the PaDa-I UPO are crucial for designing catalytic biotransformation processes.

The effects of temperature, pH and H_2O_2 concentration along with the oxidant delivery methods on the PaDa-I enzyme were evaluated to determine the optimal reaction conditions for use in the oxidative biotransformation of small organic molecules such as styrene. It has previously been shown that the UPO favours ambient temperatures and near-neutral pH for the catalytic transformation of hydrocarbon substrates such as styrene, cyclohexane and fatty acids (Dong *et al.*, 2018; Hobisch *et al.*, 2021; Hollmann *et al.*, 2011). It is, however, unclear how the stability of the UPO is affected by these conditions. Different reaction temperature or pH may be required to ensure prolonged enzyme stability that may potentially extend productivity over time. In addition, various authors have shown that the H_2O_2 required for hydrocarbon biotransformation also deactivates the enzyme when it is delivered at high concentrations (Bormann *et al.*, 2015; Valderrama *et al.*, 2002). This deactivation likely occurs through bleaching of the heme domain and oxidation of intrinsic and surrounding protein molecules (Section 2.2.2). It is crucial to account for this deactivation when conducting these studies, given the high cost of the enzyme (Ferreira *et al.*, 2018; Tufvesson *et al.*, 2011).

The residual activity of the PaDa-I enzyme was therefore monitored while varying the temperature (20 °C, 25 °C and 30 °C) and pH (pH 6.0, 7.0 and 8.0) of the reaction solution. Furthermore, the enzyme was exposed to a range of H_2O_2 concentrations (10mM, 20 mM and 40 mM) using different delivery methods; namely, once-off, stepwise and continuous addition. Each condition was investigated in isolation, with all other parameters kept constant at the base case conditions outlined in Section 3.1. These base conditions were derived from several literature sources (Karich *et al.*, 2016; Polizzi *et al.*, 2007; Schrewe *et al.*, 2013; Zhang *et al.*, 2017) and consisted of a reaction temperature of 25 °C, pH 7.0, 20 mM H_2O_2 concentration and a once-off H_2O_2 delivery approach. For these experiments, the stability of the enzyme was assessed by monitoring the enzyme activity through a residual peroxygenase activity assay (Section 3.3.1). The residual enzyme activity was measured relative to the initial enzyme activity. The initial measurement was taken from the enzyme/potassium phosphate buffer before the addition of hydrogen peroxide. In each case, 100% residual enzyme activity represented 1.7 U ml^{-1} (8.7 U $mg_{protein}^{-1}$), where 1 U was the amount of enzyme that converted 1 µmol of 5-nitro-1,3-benzodioxide (NBD) to 1 µmol of 4-nitrocatechol in 1 min at 25 °C and pH 7.0. In addition, the residual H_2O_2 concentration was measured by iodometric titration (Section 3.3.2) to assess oxidant consumption over time by the enzyme. The results of these experiments are presented and discussed in this chapter.

4.1 Effect of temperature on enzyme stability

The peroxygenase activity of the PaDa-I variant was monitored over time at different reaction temperatures (20 °C, 25 °C and 30 °C) as shown in Figure 4.1. In the control experiment (in the absence of H_2O_2), it was observed that the enzyme lost approximately 15% of its initial peroxygenase activity when an equivalent volume (2 ml) of 100 mM potassium phosphate buffer pH 7.0 was added to the mixture, instead of the H_2O_2. This decrease in activity may be attributed to the formation of bubbles upon addition of the buffer, which could initially physically disrupt the enzyme's structure. As the reaction proceeded beyond 30 min, the residual enzyme activity remained constant under all three temperatures investigated, with the 30 °C experimental runs exhibiting a 5% lower residual enzyme activity compared to those at 25 °C and 20 °C (Figure 4.1 a). A similar observation was made by Stenner *et al.* (2023) whose investigation included the deactivation of a PaDa-I variant in the same buffer solution. The reaction temperature in their experiments was 20 °C with a similar incubation time of 2 h. Although the substrate used for determining the residual enzyme activity was 2,2'-azino-bis(3)-ethylbenzothiazoline-6-sulfonic acid (ABTS) and not NBD, they also reported an enzyme activity loss of 3.3% after 2 h. It is probable that the enzyme may inherently experience a slight decrease in stability over time even in the absence of the oxidant and substrate, which indicates how sensitive the enzyme may be to any sudden changes in the reaction environment.

Figure 4.1 b on the other hand illustrates how sensitive the enzyme was when it was incubated in 20 mM H_2O_2 delivered by once-off addition. In the presence of H_2O_2, the enzyme lost more than half of its initial activity across the three temperatures investigated. Within the first 30 min, a slight recovery was observed at the three reaction temperatures investigated as seen by the minor fluctuation above the initial drop in peroxygenase activity as the H_2O_2 was added. Thereafter, the enzyme remained at steady state where similar residual enzyme activity was measured until the end of the monitoring time. Like the control experiment, by the end of the reaction the enzyme activity was slightly lower at 30 °C (~35%) compared to 25 °C and 20 °C (40%). This was potentially due to the decomposition of H_2O_2 at the higher temperature.

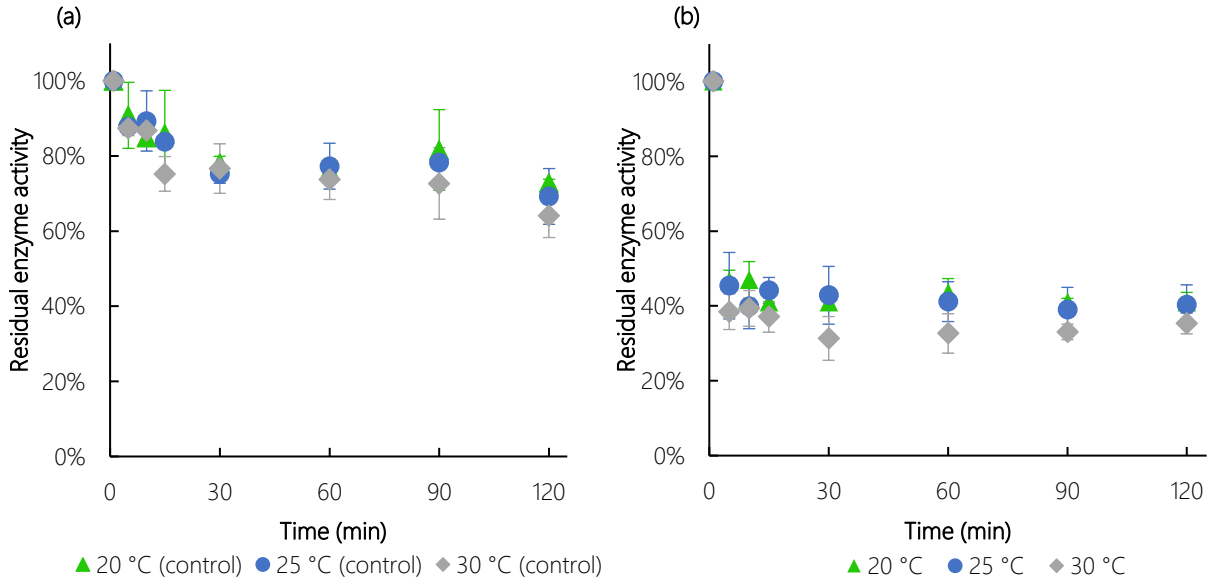

Figure 4.1: The residual peroxygenase activity of PaDa-I in the absence (a) and presence (b) of 20 mM H_2O_2 once-off addition at 20 °C (▲), 25 °C (●) and 30 °C (◆). Reaction conditions: 20 ml 100 mM potassium phosphate buffer pH 7.0, 1.7 U ml^{-1} (NBD) PaDa-I, 200 rpm, 25 °C.

In an investigation by Tieves *et al.* (2019), they tested the sensitivity of the bio-bio tandem process to temperature by comparing the overall substrate conversion. The tandem system consisted of formate oxidase which was used to produce H_2O_2 *in-situ* for the biotransformation of ethylbenzene by a UPO.. It was determined that product formation was optimal at 25 °C where around 10% conversion was reported. This was followed by an 8% conversion at 20 °C, 7% conversion at 30 °C and only 1% conversion at 40 °C (Tieves *et al.*, 2019). These observations are in agreement with the residual enzyme activity profiles plotted in Figure 4.1 and show that the enzyme was more stable at 25 °C and 20 °C where more product was formed at the lower temperatures tested. The system is, however, complex as formate oxidase used in this one-pot system may have also contributed to the overall productivity. The authors made no attempt to decouple the systems thus the stability of individual enzymes in the tandem system was not evaluated. Neither did they provide information on the H_2O_2 concentration achieved at each temperature investigated. Nevertheless, the clear observation made in Figure 4.1 shows that H_2O_2 indeed inhibits the enzyme catalytic ability as evidenced by the significantly lowered residual enzyme activity. Around 30-35% of the initial peroxygenase activity was lost over the course of the control experiment compared to the 60-65% loss when exposed to 20 mM H_2O_2.

In addition to monitoring the enzyme activity over time, the H_2O_2 concentration was also measured at the three temperatures in the absence (control experiment, Figure 4.2 **a**) and presence of the PaDa-I enzyme (Figure 4.2 **b**). When there was no enzyme present in the reaction mixture, the H_2O_2 concentration was constant over the 2 h reaction period at 20 °C and 25 °C. In contrast, a slight decrease in concentration (about 2%) was observed at 30 °C that could be attributed to decomposition of the H_2O_2 (Crole *et al.*, 2016). When the UPO was present in the reaction mixture, the residual H_2O_2 concentration steadily decreased over time at seemingly similar rates across the three temperatures investigated. The concentration profiles in Figure 4.2 **b** along with the residual enzyme activity profiles in Figure 4.1 **b** indicated that the H_2O_2 transformed by the enzyme may have directly resulted in the lowered enzyme activity that was measured. Though the enzyme is temperature sensitive, oxidant addition appeared to be chiefly responsible for enzyme deactivation under the conditions evaluated.

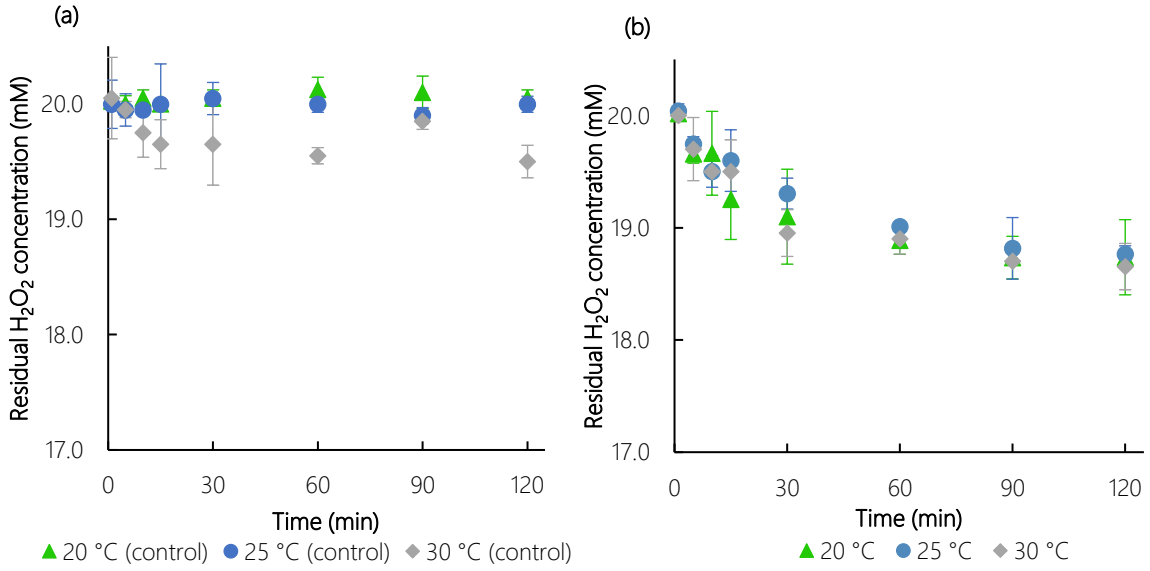

Figure 4.2: The residual hydrogen peroxide concentration profiles in the absence (a) and presence (b) of PaDa-I enzyme at 20 °C (▲), 25 °C (●) and 30 °C (◆). Reaction conditions: 20 ml 100 mM potassium phosphate buffer pH 7.0, 1.7 U ml^{-1} (NBD) PaDa-I, 20 mM H_2O_2 once-off addition, 200 rpm.

4.2 Effect of pH on enzyme stability

Reaction pH is another parameter that can greatly affect enzyme stability. Consequently, the effect of pH on the residual enzyme activity over time was investigated at three different pH values (pH 6.0, 7.0 and 8.0). The plots in Figure 4.3 show that, although marginal, a higher residual enzyme activity was maintained at pH 8.0, followed by pH 7.0 and lastly pH 6.0. Experiments were conducted in the absence (control, Figure 4.3 **a**) and presence (Figure 4.3 **b**) of H_2O_2. In the control experiments, where no H_2O_2 was added, an initial 30% loss in enzyme activity at pH 7.0 and pH 6.0 was observed while only 20% of the initial activity was lost at pH 8.0. Thereafter, the enzyme appeared to adjust to the conditions of the reaction mixture as the enzyme activity steadily increased between 5 and 30 minutes by approximately 20% at pH 7.0 and pH 8.0 and by 10% at pH 6.0 (Figure 4.3 **a**). Molina-Espeja *et al.* (2014) reported a similar observation where the enzyme activity increased by 20% after a 2-4 h incubation period - they referred to this phenomenon as hyperactivation. Over the course of the reaction, the enzyme activity gradually decreased and at the end of the 2 h incubation period, 82%, 76% and 74% residual peroxygenase activities at pH 8.0, 7.0 and 6.0, were measured.

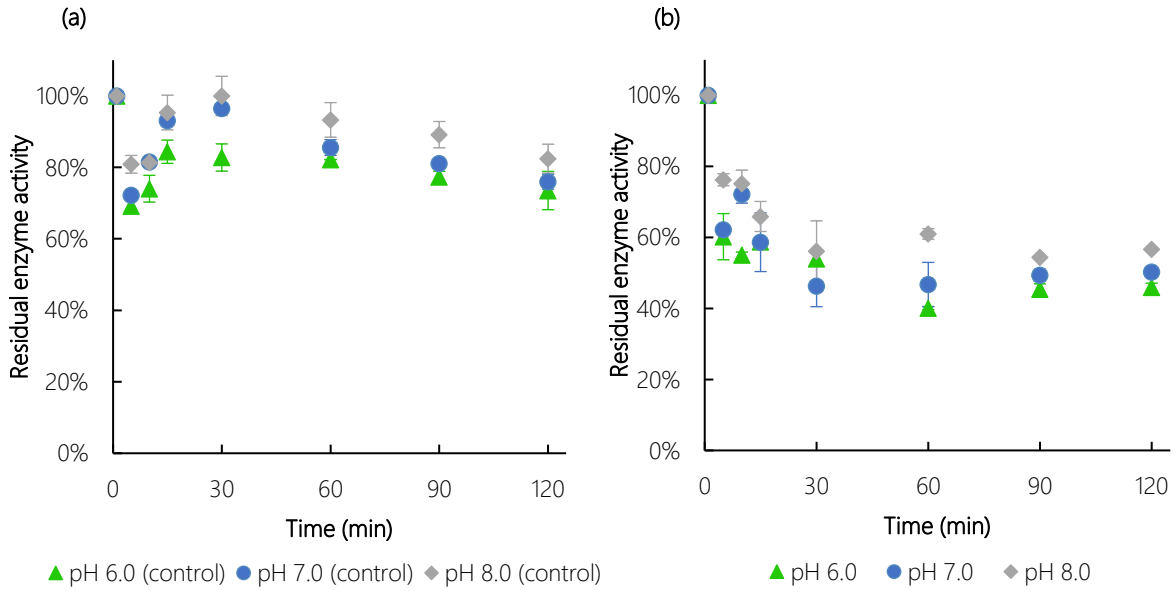

Figure 4.3: The residual peroxygenase activity of PaDa-I in the absence (a) and presence (b) of 20 mM H_2O_2 once-off addition at pH 6.0 (▲), pH 7.0 (●) and pH 8.0 (◆). Reaction conditions: 20 ml 100 mM potassium phosphate buffer, 1.7 U ml^{-1} (NBD) PaDa-I, 200 rpm, 25 °C

On the other hand, when exposed to 20 mM H_2O_2, the enzyme activity rapidly decreased after 5 min. This resulted in activity losses of approximately 40% at pH 7.0 and 6.0 and 30% at pH 8.0 (Figure 4.3 **b**). Across all three pH values investigated, the enzyme activity continued decreasing up until 30 minutes, after which the enzyme activity remained steady for the rest of the incubation period. At the end of 2 h, the residual enzyme activity was the highest at pH 8.0 (57%) followed by pH 7.0 and 6.0 (about 50%). This strongly suggested that pH 8.0 was the optimum pH value for further experimentation. In contrast to these findings, Molina-Espeja *et al.*, (2014) investigated the optimal pH for a PaDa-I variant and determined the peroxygenase activity was highest at pH 6.0, followed by pH 7.0 and pH 8.0. They reported that, relative to pH 6.0, the enzyme retained about 60% and 50% of its activity at pH 7.0 and 8.0, respectively (Molina-Espeja *et al.*, 2014). Notably, Molina-Espeja *et al.* (2014) assessed peroxygenase activity at a single point after 10 min whereas in this study the enzyme's stability was measured over

time, specifically in terms of its residual enzyme activity. It is also possible that the evolution pathway used to develop that PaDa-I variant differed slightly to the approach employed in the commercially available EvoEnzyme. Nevertheless, in each case the UPO seemed to favour near-neutral pH conditions.

In the absence of the enzyme from the reaction mixture, the H_2O_2 concentration remained constant at 20 mM H_2O_2 at the different pH values for the control experiments (Figure 4.4 **a**), which indicated that the hydrogen peroxide concentration was not affected by a change of pH in the tested range. An interesting observation; however, was made in terms of the H_2O_2 utilisation at the different pH values. The least amount of H_2O_2 was used by the enzyme at pH 8.0, followed by pH 7.0 and lastly pH 6.0 (Figure 4.4 **b**). This trend, when considered alongside the residual activity profiles in Figure 4.3 **b**, suggests that the enzyme experiences reduced deactivation when it consumes less H_2O_2. However, decreased oxidant usage may potentially lead to reduced enzyme productivity when a hydrocarbon substrate is introduced to the reaction mixture.

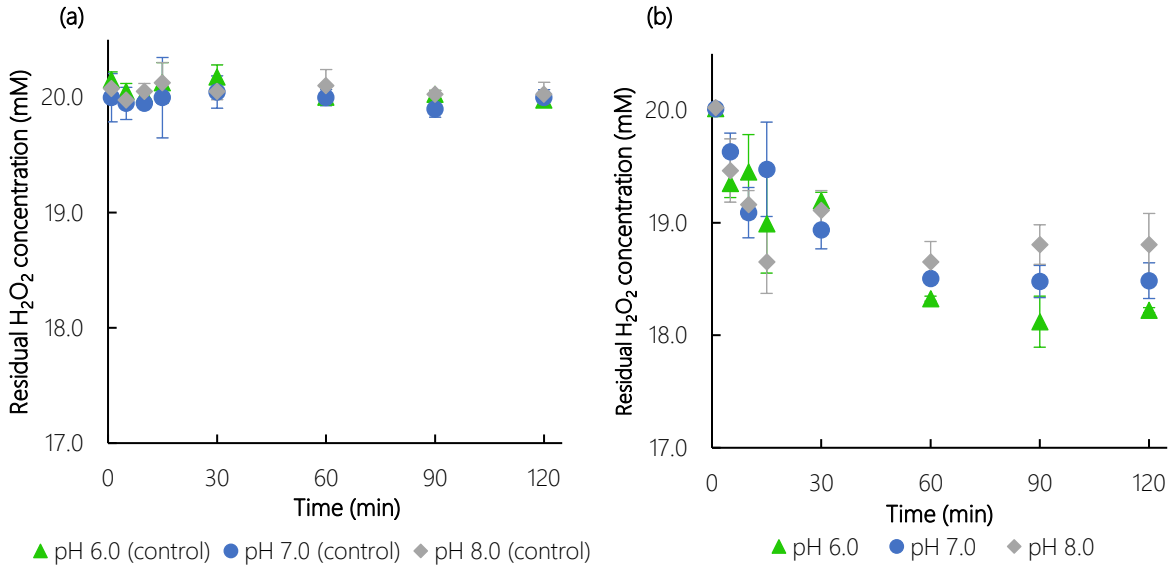

Figure 4.4: The residual H_2O_2 concentration profiles in the absence (a) and presence (b) of PaDa-I enzyme at pH 6.0 (▲), pH 7.0 (●) and pH 8.0 (◆). Reaction conditions: 20 ml 100 mM potassium phosphate buffer, 1.7 U ml^{-1} (NBD) PaDa-I, 20 mM H_2O_2 once-off addition, 200 rpm.

An enzyme similar to UPO, horseradish peroxidase, was investigated by Hernández-Ruiz *et al.* (2001). The horseradish peroxidase was exposed to H_2O_2, in this investigation. It was proposed that the enzyme could engage a protective mechanism whereby the enzyme liberated oxygen in response to the H_2O_2. Otherwise, it would simply be deactivated or form less reactive intermediates (*viz.* Section 2.2.3 and Scheme 2.12). Beyond pH 6.4, the horseradish peroxidase produced bubbles of oxygen and retained higher residual enzyme activity which indicated the protective mechanism (Hernández-Ruiz *et al.*, 2001). Bubble formation was; however, not observed in these experiments (herein). It is therefore possible that the PaDa-I enzyme may have instead produced less reactive intermediates, which could account for the measurable residual activity. This effect may likely have been more dominant at pH 8.0 compared to pH 7.0 and pH 6.0 - the pH of the reaction mixture may have affected the active site of the enzyme thus influencing the way it bound to the substrate H_2O_2.

Overall, the pH studies showed that the stability of the enzyme was more significantly influenced by the addition of H_2O_2 than the pH of the reaction mixture under the conditions tested. By the end of the 2 h

incubation time, the enzyme retained approximately 50% peroxygenase activity in the presence of H_2O_2 compared to approximately 80% in the control experiments at pH values 6.0, 7.0 and 8.0.

4.3 Effect of hydrogen peroxide concentration and delivery approach on enzyme stability

The stability of the enzyme was further evaluated by investigating the effect of different H_2O_2 concentrations and delivery systems. The H_2O_2 delivery approaches that were investigated included once-off, stepwise and continuous addition, whereby the H_2O_2 was added all at once, sequentially at regular intervals and gradually at a controlled flow rate, respectively. Equivalent volumes of potassium phosphate buffer (pH 7.0) were added to the enzyme/buffer mixture using the three aforementioned feeding schemes to serve as the control experiments (Figure 4.5).

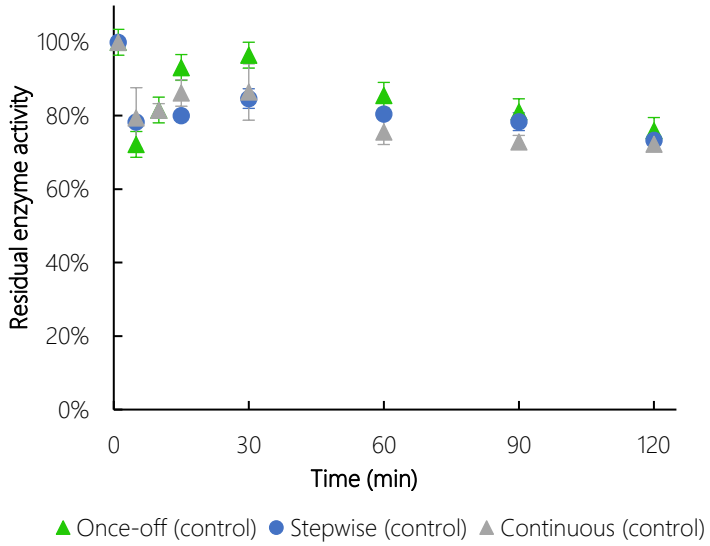

Figure 4.5: The residual peroxygenase activity of the PaDa-I enzyme in the absence of H_2O_2, using delivery methods once-off (▲), stepwise (●) and continuous (◆) addition of potassium phosphate buffer pH 7.0. Reaction conditions: 20 ml 100 mM potassium phosphate buffer pH 7, 1.7 U ml^{-1} (NBD) PaDa-I, 200 rpm, 25 °C.

All delivery approaches appeared to follow the same trend where an initial loss in enzyme activity was observed in the first 5 minutes. The lower residual enzyme activity measured for the once-off addition control experiment (72%) could be due to the higher volume of potassium phosphate buffer added to the system compared to the other feeding schemes (~79%). Over time, the enzyme had recovered and after 30 minutes, 97% residual activity was measured after the once-off addition of buffer, which was similar to the hyperactivation phenomenon noted in the pH studies (*viz*. Appendix B.1). This contrasted with the observation made for the stepwise and continuous delivery approaches where the activity did recover but only up to around 86% of the initial enzyme activity. This may be a result of sequential interference whilst feeding the phosphate buffer in a stepwise and continuous manner. This is especially evident by the slightly lower activity of the enzyme at 60 min and 90 min for the continuous delivery method, even though by the end of the 2 h incubation period the enzyme exhibited similar residual activities of approximately 72% across the three delivery methods. These observations highlight that the delivery approaches may influence the enzyme stability to a certain extent even in the absence of the H_2O_2.

As previously noted, when H_2O_2 was added to the enzyme/buffer mixture, the enzyme immediately lost some of its initial catalytic activity (>20%). Figure 4.6 illustrates that during the initial stages of the reaction, the extent of activity loss increased with H_2O_2 concentration using the once-off addition delivery method, as expected. A significantly larger decrease in activity (40%) was observed upon the once-off addition of 40 mM H_2O_2 compared to 20 mM and 10 mM (30% and 20%, respectively). Thereafter, recovery of peroxygenase activity was observed as the enzyme adjusted to the H_2O_2 in the system similar to what was observed in the control experiments. There was; however, a steady decline in enzyme activity in the first 30 min. By the end of the 2 h reaction the enzyme had lost approximately 40% of its initial peroxygenase activity. At that point it was observed that the enzyme had the lowest residual activity of 49% in the presence of 40 mM H_2O_2 compared to 20 mM H_2O_2 (59%) and 10 mM H_2O_2 (63%).

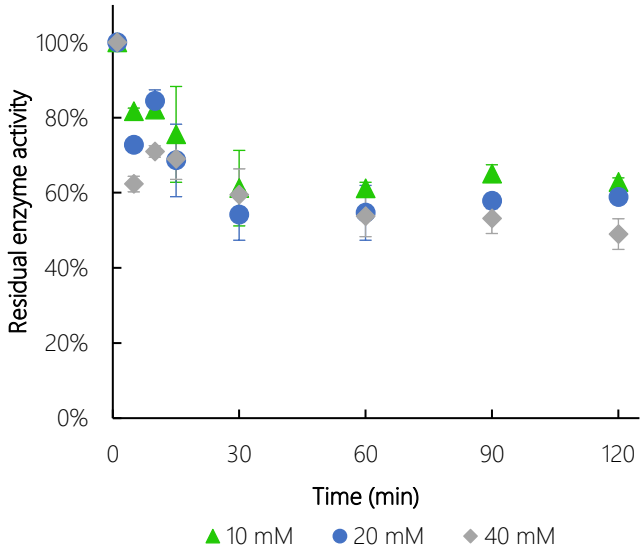

Figure 4.6: The residual peroxygenase activity of the PaDa-I enzyme using once-off delivery of H_2O_2 at concentrations 10 mM (▲), 20 mM (●) and 40 mM (◆). Reaction conditions: 20 ml 100 mM potassium phosphate buffer pH 7.0, 1.7 U ml^{-1} (NBD) PaDa-I, 20 mM H_2O_2, 200 rpm, 25 ^{o}C.

This trend of increasing loss in enzyme activity with increasing H_2O_2 concentrations was also observed by other authors investigating the oxidation of ethers by a PaDa-I variant (Mireles *et al.*, 2021). For a H_2O_2 concentration range between 0.1 - 1 mM, they reported the lowest residual activity at 1 mM H_2O_2 (30%) and the highest at 0.1 mM (90%). In another recent study that investigated the oxidation of cyclohexane by PaDa-I, it was determined that the enzyme lost 68% activity in a reaction mixture containing 50 ppm H_2O_2 which increased to 88% at 200 ppm H_2O_2. It was suggested that the hydrogen peroxide (added through once-off delivery) resulted in the generation of oxygen-based radicals that specifically targeted the enzyme's heme-centre (Stenner *et al.*, 2023). Although it is worth noting that the deactivation studies in those papers did not decouple the effect of H_2O_2 concentration alone (i.e. in the absence of the substrate) on the PaDa-I enzyme activity. Nevertheless, both studies illustrate the influence of increasing H_2O_2 concentration through using the once-off delivery approach on the enzyme activity. This is in agreement with the observations made in the current study.

Following once-off addition, the stepwise and continuous H_2O_2 delivery methods were investigated. During these experiments H_2O_2 was fed to the enzyme/buffer reaction mixture to final H_2O_2 concentrations of 10 mM, 20 mM and 40 mM respectively. Tables 4.1 and 4.2 compare the effect of the

different delivery methods on residual enzyme activity after 5 and 30 minutes of incubation. It was observed that manually dosing the H_2O_2 gradually and in low quantities reduced enzyme activity loss. Continuous H_2O_2 addition to the enzyme/buffer mixture resulted in ca. 10% more peroxygenase activity being retained compared to the stepwise and once-off delivery methods, particularly in the earlier stages of the reaction. Table 4.1 shows that the less H_2O_2 delivered to the system led to a higher residual enzyme activity after 5 min. As the reaction proceeded and more H_2O_2 was added during stepwise and continuous addition, the enzyme lost more activity (Table 4.2), likely as a result of deactivation induced by the hydrogen peroxide. Unlike in the control experiments, the enzyme failed to recover and the residual activity continued decreasing between 5 and 30 minutes in the presence of H_2O_2. This trend was observed at all H_2O_2 concentrations irrespective of the delivery method employed (Tables 4.1 and 4.2).

Table 4.1: A comparison of residual peroxygenase activity of PaDa-I relative to the concentration of H_2O_2 present in the system after 5 min

H_2O_2 (mM) after 5 min			Residual enzyme activity (%) after 5 min		
Once-off	Stepwise	Continuous	Once-off	Stepwise	Continuous
9.7±0.2	2.4	0.3	70 ± 1	67 ± 2	83 ± 1
19.6±0.2	5.1	0.7 ± 0.1	62	64 ± 3	74 ± 1
39.4±0.2	10.2 ± 0.8	1.4 ± 0.2	53 ± 2	64 ± 7	68 ± 4

Reaction conditions: 20 ml 100 mM potassium phosphate buffer pH 7.0, 1.7 U ml^{-1} (NBD) PaDa-I, 20 mM H_2O_2, 200 rpm, 25 ^{o}C

Table 4.2: A comparison of residual peroxygenase activity of PaDa-I relative to the concentration of H_2O_2 present in the system after 30 min.

H_2O_2 (mM) after 30 min			Residual enzyme activity (%) after 30 min		
Once-off	Stepwise	Continuous	Once-off	Stepwise	Continuous
9.5±0.2	5.0 ± 0.2	2.6 ± 0.3	52 ± 9	58 ± 10	58 ± 4
18.9±0.2	9.7 ± 0.2	5.0	46 ± 6	57 ± 1	56 ± 6
38.3±0.3	20.0 ± 0.3	10.4 ± 0.2	51 ± 6	47 ± 5	57 ± 7

Reaction conditions: 20 ml 100 mM potassium phosphate buffer pH 7.0, 1.7 U ml^{-1} (NBD) PaDa-I, 20 mM H_2O_2, 200 rpm, 25 ^{o}C

The complete residual enzyme activity profiles over 2 h for all three delivery systems at final H_2O_2 concentrations 10 mM, 20 mM and 40 mM are shown in Figure 4.7 **a**, **b** and **c**. Across the delivery methods investigated, it was observed that the residual activity decreased as the H_2O_2 concentration increased. In addition, the residual enzyme activity was measured as 10% lower using the once-off delivery approach compared to both stepwise and continuous addition across each H_2O_2 concentration. In terms of H_2O_2 utilisation, the amount of H_2O_2 transformed was obtained by measuring the difference between the control and experimental H_2O_2 concentration profiles for each delivery method tested. It appeared that there was a steady hydrogen peroxide transformation by the enzyme in the first 30 – 60 min for all three concentrations investigated. Thereafter, the amount of H_2O_2 transformed remained constant until the end of the reaction (Figure 4.7 **d**, **e**, **f**). Interestingly, within that same time interval was when the residual enzyme activity had levelled off (Figure 4.7 **a**, **b**, **c**). Using the continuous and stepwise delivery approaches, the enzyme managed to retain slightly higher catalytic activity (approximately 60% residual activity) than with the once-off delivery approach (ca. 55%) and yet still transformed similar amounts of H_2O_2 by the end of the 2 h incubation period.

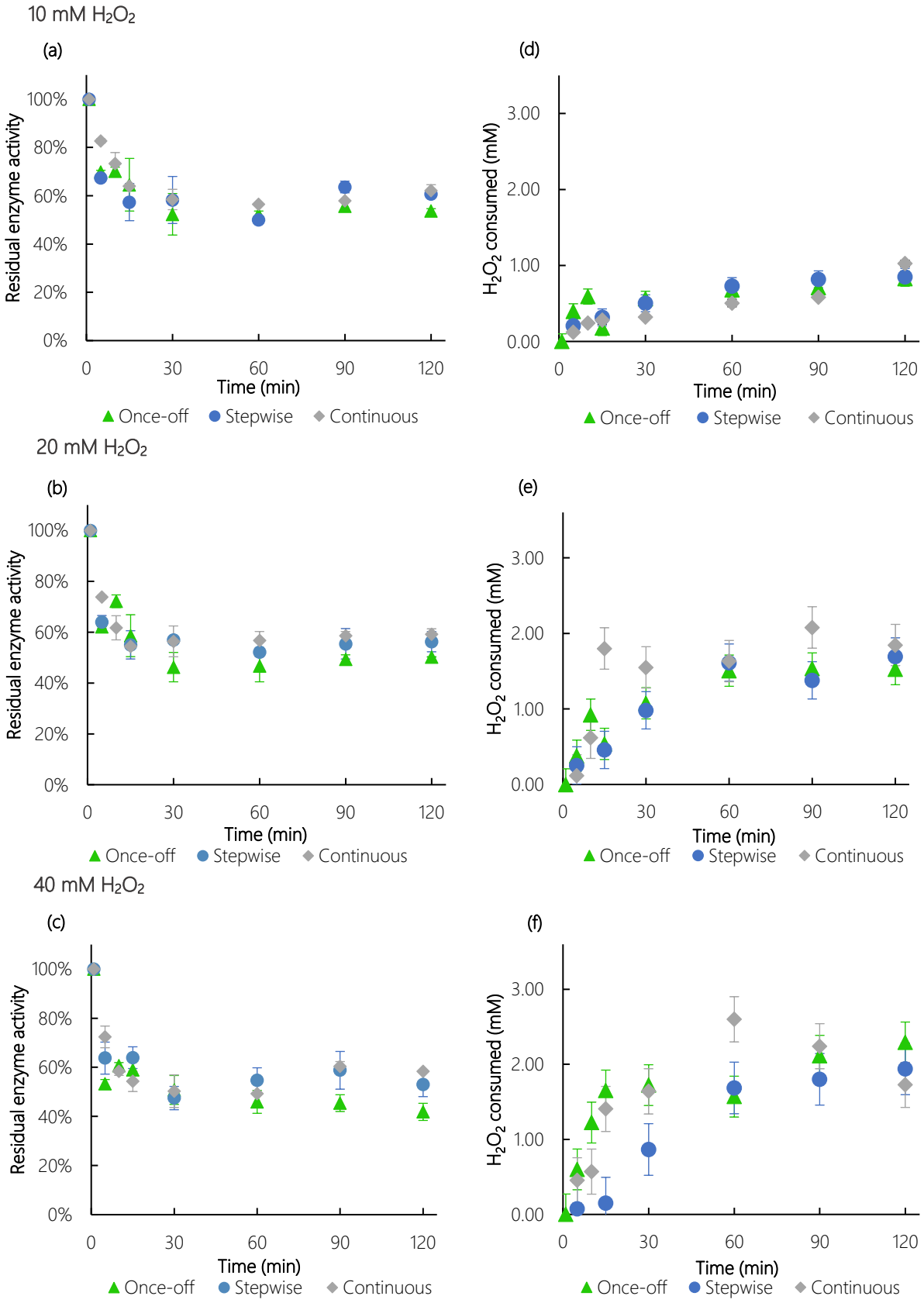

Figure 4.7: The residual peroxygenase activity for PaDa-I enzyme at H_2O_2 concentrations 10 mM (a), 20 mM (b) and 40 mM (c) and the H_2O_2 transformation profiles at H_2O_2 concentrations 10 mM (d), 20 mM and 40 mM (f) for PaDa-I enzyme using once-off (▲), stepwise (●) and continuous (◆) delivery methods. H_2O_2 transformation is the difference between the control and experimental H_2O_2 concentration profiles. Reaction conditions: 20 ml 100 mM potassium phosphate buffer pH 7.0, 1.7 U ml^{-1} PaDa-I, 20 mM H_2O_2, 200 rpm, 25 ^{o}C.

Approximately 1 mM H_2O_2 was utilised by the enzyme after 2 h for the delivery systems where 10 mM H_2O_2 was fed. From the samples collected at this point, which were used in the peroxygenase activity assay, it was determined that only <6 µM H_2O_2 was converted based on the 1:1 NBD:H_2O_2 stoichiometric ratio (Scheme 3.1, Section 3.3.1). This low conversion may be attributed to an excess of H_2O_2 in the assay (0.5 mM NBD vs 1 mM H_2O_2 in assay and ± 9 mM H_2O_2 in sample collected). It was noted that 4.96 µM H_2O_2 was converted using once-off delivery, which increased to 5.04 µM with stepwise delivery, and 5.83 µM using continuous delivery. This further emphasized that the enzyme was more stable using the continuous H_2O_2 delivery approach. Furthermore, it is probable that the rest of the H_2O_2 may have been used to form the less reactive enzyme intermediate Compound III (Valderrama, 2010)or the enzyme may have catalysed H_2O_2 decomposition or disproportionation (Crole *et al.*, 2016). Figures 4.7 **e** and **f** show that almost 2 mM H_2O_2 was transformed by the enzyme where H_2O_2 concentrations of 20 mM and 40 mM were fed to the enzyme/buffer mixture. This could potentially mean that the enzyme had reached the saturation point in terms of H_2O_2 transformation i.e. increasing the H_2O_2 concentration beyond 40 mM would not substantially impact the amount transformed by the enzyme as the enzyme's deactivation potentially became more pronounced. At these higher H_2O_2 concentrations, <5.5 µM of H_2O_2 was converted in the NBD reaction, which was approximately 8% less than what was converted at the lower H_2O_2 concentration, 10 mM. It is probable that more of the less reactive enzyme intermediate Compound III was formed at the higher H_2O_2 concentrations. Overall, the key insight from this investigation is that continuous delivery of H_2O_2 at low concentrations could potentially maximise enzyme productivity and stability in a biotransformation reaction system.

4.4 Conclusion

The impact of temperature, pH and H_2O_2 concentration and means whereby the oxidant may be introduced to the reaction on the PaDa-I enzyme's stability and residual activity were investigated. The evaluation of these conditions provided insight into how to best employ the PaDa-I UPO in a biotransformation reaction.

In the temperature studies, it was shown the enzyme was more stable at the lower temperatures 20 °C and 25 °C compared to 30 °C. This may be as a result of the protein molecule slightly losing the integrity of its shape thus affecting the enzyme stability at 30 °C. Additionally, the H_2O_2 consumption was similar at the lower temperatures but slightly lower at 30 °C as some of the H_2O_2 was lost through decomposition at the higher temperature. The enzyme could therefore potentially perform better in the biotransformation experiment at lower reaction temperatures 20 °C or 25 °C.

It was observed that the enzyme was more stable at pH 8.0, followed by pH 7.0 and lastly at pH 6.0. Despite the recommended optimum peroxygenase pH 7.0, the enzyme in fact favoured pH 8.0. However, less H_2O_2 (1.2 mM) was transformed at this pH value compared to pH 7.0 (1.5 mM H_2O_2) and pH 6.0 (1.8 mM H_2O_2) where more H_2O_2 was transformed. It can be proposed that the pH may influence the enzyme catalytic ability, therefore the enzyme should be tested at both the recommend pH 7.0 (EvoEnzyme) and pH 8.0 to determine whether the pH influences productivity of the biotransformation of styrene.

Overall, it was determined that the stability of the enzyme was most significantly impacted by H_2O_2 concentration and delivery method compared to reaction temperature and pH. The enzyme was more stable at lower H_2O_2 concentrations. At 10 mM H_2O_2, the enzyme exhibited a higher residual activity of

approximately 60% at the end of the incubation period compared to approximately 55% residual activity obtained at 20 mM H_2O_2 and approximately 50% obtained at 40 mM H_2O_2. However, less H_2O_2 was consumed by the enzyme at the lower H_2O_2 concentration which could mean that the productivity of the biotransformation may become oxidant limited. The conservative option is therefore 20 mM as the optimal H_2O_2 concentration where the enzyme was relatively stable and consumed more H_2O_2. In terms of the H_2O_2 delivery approach across all three concentrations investigated, similar amounts of H_2O_2 were consumed for all the delivery systems tested. In addition, the continuous delivery method resulted in the enzyme being most stable under the conditions tested, followed by stepwise and then once-off delivery. The continuous delivery method should therefore be considered as the optimal delivery approach for the biotransformation of styrene.

5 Evaluation of enzyme deactivation kinetics

Knowledge of enzyme stability, the associated deactivation pathways and kinetics are of paramount importance when considering scale-up of an enzymatic bioprocess. This is due to the generally high cost of enzyme generation and purification (Polizzi *et al.*, 2007; Schrewe *et al.*, 2013). In the case of the PaDa-I UPO, very little has been reported on its stability under bioprocess conditions. In this chapter the stability of PaDa-I under bioprocess conditions as well as the deactivation kinetics of PaDa-I will be investigated.

The residual enzyme activity profiles obtained in Chapter 4 suggested that the deactivation kinetics do not exhibit typical first order kinetics. There was initial rapid deactivation induced by the addition of the H_2O_2, followed by a region of stable residual enzyme activity. The observed dynamics in the presence of H_2O_2 appeared to follow the proposed deactivation pathway described in Section 2.2.3 whereby the enzyme may have initially formed a less reactive intermediate (Compound III) which then further decomposed through heme bleaching, protein oxidation or unimolecular decay (Scheme 5.1).

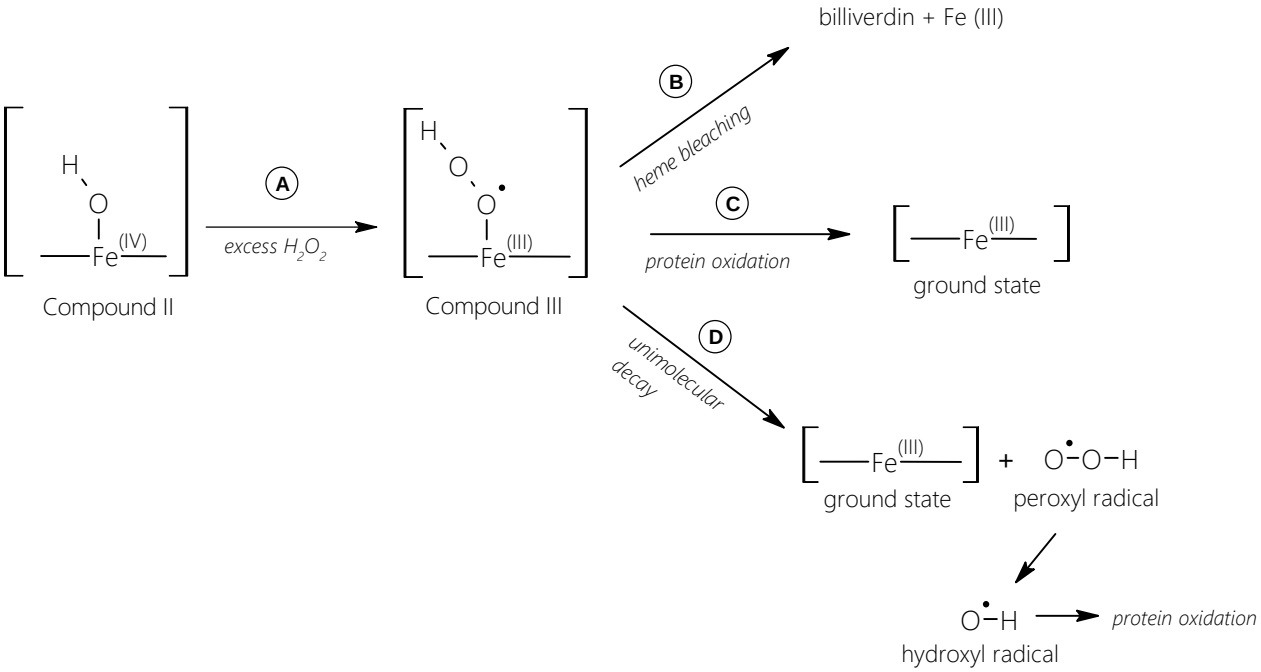

Scheme 5.1: An adaptation of the proposed enzyme deactivation mechanism for heme peroxidases (Valderrama, 2010)

Similar deactivation profiles have been described for the enzyme acetylcholinesterase whereby a two-step series deactivation was proposed to model the enzyme deactivation kinetics (Henley and Sadana, 1986; Sadana and Henley, 1987a). The deactivation mechanism can be expressed using three kinetic models as described in Table 5.1 (viz. deactivation schemes in Section 2.2.3). The first order model predicts that the enzyme is completely denatured thus loses all catalytic activity, which is in contrast to the results presented in Chapter 4. For the two-parameter and four-parameter models, the mechanism predicts that the initial enzyme activity is partially deactivated forming intermediate enzyme states (1 or 2, respectively) (Section 2.2.3). These states exhibit a lower specific activity (β_1 or β_2) relative to the initial enzyme state (β) as indicated by α_1 and α_2 in Equations (2.8) and (2.9).

$$\alpha_1 = \beta_1 / \beta \quad (2.8)$$

$$\alpha_2 = \beta_2 / \beta \quad (2.9)$$

These intermediate enzyme compounds were not characterised in this study as they were produced very quickly and were short lived and would have required complex analytical techniques. For example, rapid-mixing stopped-flow UV-visible spectroscopy was required to study the fast generation of UPO intermediate Compound II within approximately 0.5 s (Wang *et al.*, 2015), while electron spin resonance spectroscopy in conjunction with Mössbauer spectroscopy were used to examine the heme centre of the CYP119A1 enzyme to detect the presence of Compound I (Krest *et al.*, 2013).

Table 5.1: Summary of kinetic models that predict enzyme deactivation, where all model constants (A_t, A_0, k_1, α_1, k_2, α_2) are defined in the nomenclature

Kinetic model	Equation	
First order	$A_t/A_0 = \exp(-k_1 t)$	(2.14)
Two-parameter	$A_t/A_0 = (1 - \alpha_1) \exp(-k_1 t) + \alpha_1$	(2.12)
Four-parameter	$A_t/A_0 = \left(1 + \frac{\alpha_1 k_1}{k_2 - k_1} - \frac{\alpha_2 k_2}{k_2 - k_1}\right) \exp(-k_1 t) - \left(\frac{k_1}{k_2 - k_1}\right)(\alpha_1 - \alpha_2) \exp(-k_2 t) + \alpha_2$	(2.10)

Each of the proposed models introduced in Section 2.2.3 was fitted to the deactivation data presented in Chapter 4 by employing non-linear regression to obtain the deactivation kinetic parameters (k_1, k_2, α_1, α_2). The goodness of fit was then measured by comparing the coefficient of determination (R^2), chi-square (χ^2) value and average absolute relative deviation (AARD). In cases where multiple models fit the data well, the best model was selected based on the lowest Akaike's Information Criterion (AIC) and the Bayesian Information Criterion (BIC) values (Section 3.5) (Burnham and Anderson, 2002). These techniques were used to analyse the enzyme deactivation kinetic data at different operating conditions by varying temperature, pH, H_2O_2 concentration and delivery method. The findings from these analyses are detailed in the sections that follow.

5.1 Temperature-dependent enzyme deactivation kinetics

The enzyme deactivation data collected whilst varying the temperature (20 °C, 25 °C and 30 °C.) in the presence of only H_2O_2 is detailed in Section 4.1. To analyse this data, the kinetic models given in Table 5.1 were applied. Figure 5.1 shows the enzyme deactivation kinetics modelled using the calculated kinetic parameters obtained for the three kinetic models considered. Using non-linear regression, the variables k_1 and k_2 along with α_1 and α_2 were determined. The k_1 values obtained for the first order model were approximately 40% less than half the values obtained for the two- and four-parameter models, which implied that a slower enzyme deactivation rate was predicted using the first order model compared to the other two models (Table 5.2). Initial regression analyses revealed that a value of 0.18 min^{-1} for k_1 was consistently obtained for the two-parameter and four-parameter models. Consequently, this value was fixed across all subsequent nonlinear regressions performed on these models as this was considered an intrinsic property of the enzyme. This rate constant was similar to the deactivation constants reported in two studies where the enzyme was incubated in H_2O_2 (Ramirez-Ramirez *et al.*, 2020; Vidal-Limón *et al.*,

2013). Ramirez-Ramirez *et al.* (2020) reported 0.18 min^{-1} as the deactivation constant for a PaDa-I variant and Vidal-Limón *et al.* (2013) reported 0.21 min^{-1} and 0.26 min^{-1} values for CYP102A1 variants W96A and F405L, respectively. In both studies, the k values were obtained from first order enzyme deactivation kinetics. The k_2 value obtained for the four-parameter model was approximately an order of magnitude lower than k_1. This suggested that the initial rapid deactivation occurred at a significantly higher rate potentially leading to the formation of the first enzyme intermediate (referred to as Step **A** in Scheme 5.1). A second slower deactivation step then followed that potentially involves either steps **B**, **C** or **D** or a combination of these pathways. The final enzyme activity ratios α_1 for the two-parameter model and α_2 for the four-parameter model obtained for PaDa-I were closely aligned non-zero values (0.42 - 0.30) across the three temperatures investigated, which further supported that the enzyme exhibited some residual activity.

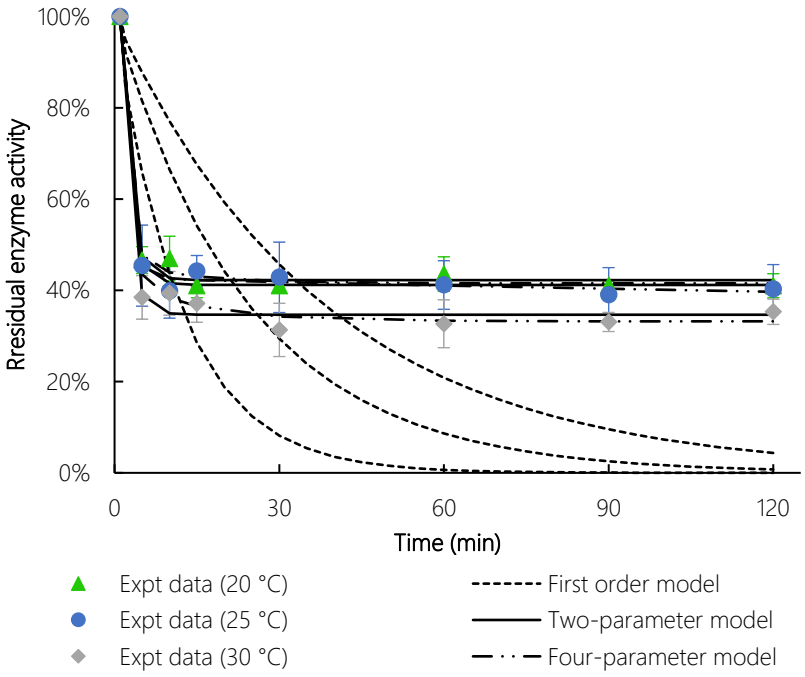

Figure 5.1: The enzyme deactivation kinetics for PaDa-I at 20 °C (▲), 25 °C (●) and 30 °C (◆) modelled by the first order (- - -), two-parameter (——) and four-parameter (— · · —) models. Reaction conditions: 20 ml 100 mM potassium phosphate buffer pH 7.0, 1.7 U ml^{-1} (NBD) PaDa-I, 20 mM H_2O_2 once-off addition, 200 rpm, 25 °C

The first order model represented the data poorly compared to the two-parameter and four-parameter models as evidenced by the low R^2 values <0.7 and high χ^2 values >1 (Table 5.2). This was expected because the UPO was not fully deactivated as presented by the potential deactivation pathway of the first order model. In contrast, the two-parameter and four-parameter models exhibited better alignment with the experimental data with higher R^2 values, and lower χ^2 and AARD values. These values were very similar, as indicated by the partial overlapping plots of the two models in Figure 5.1, therefore the AIC and BIC values were used to gauge which of the two models best represented the potential pathway for enzyme deactivation in the presence of H_2O_2. Given that the AIC and BIC were the lowest for the two-parameter model, it was concluded that this model best represented the deactivation kinetics of PaDa I when exposed to H_2O_2 only. Taking this into consideration, it can be inferred that the principal deactivation step is likely analogous to Step **A** in Scheme 5.1, giving rise to a less active intermediate compared to the initial enzyme. This is supported by the non-zero values of α_1 (Table 5.2). On the other

hand, the AIC and BIC values were highest for the first order model, which deemed this model unsuitable.

Table 5.2: Deactivation kinetic parameters for the peroxygenase activity of PaDa-I at temperatures 20 °C, 25 °C and 30 °C and once-off delivery 20 mM H_2O_2 where model constants k_1, k_2, α_1 and α_2 were determined by non-linear regression

	First order model			Two-parameter model			Four-parameter model		
Temperature (°C)	20	25	30	20	25	30	20	25	30
k_1 (min^{-1})	0.03	0.04	0.08	0.18	0.18	0.18	0.18	0.18	0.18
k_2 (min^{-1})							0.02	0.03	0.02
α_1				0.39	0.37	0.30	0.34	0.38	0.30
α_2							0.42	0.31	0.33
R^2	0.36	0.43	0.67	0.90	0.89	0.90	0.93	0.88	0.91
χ^2	4.80	27.85	>100	0.05	0.07	0.08	0.04	0.08	0.07
AARD (%)	<0.01	0.77	1.57	0.1	0.12	0.13	<0.01	0.09	0.25
AIC	11.49	11.53	10.56	3.16	4.01	4.26	6.13	8.22	7.89
BIC	8.20	8.24	7.27	-1.23	-0.38	-0.12	-0.45	1.64	1.31

A graphical presentation of the kinetic parameters obtained for the two-parameter model (best fit model) is shown in Figure 5.2. As previously mentioned, a constant deactivation constant 0.18 min^{-1} was obtained across all three temperatures (Figure 5.2 **a**). The ratio α_1 representing the enzyme activity at the end of the 2 h incubation period relative to the initial enzyme activity, aligns with the observation made on the residual enzyme activity profiles. This observation indicated that the enzyme was more stable at lower temperatures. This was highlighted by α_1 being at its lowest value of 0.30 at 30 °C compared to 0.37 and 0.39 obtained at 25°C and 20 °C, respectively (Figure 5.2 **b**). The enzyme's stability was impacted by slightly elevated reaction temperatures. It is therefore advisable to maintain lower reaction temperatures to potentially optimise enzyme performance. However, it should not be reduced to such an extent that it hinders the catalytic activity of the enzyme. When designing an optimised biocatalytic system, it becomes imperative to determine the right temperature balance to preserve the enzyme's functionality while maintaining high rates of conversion of the substrate.

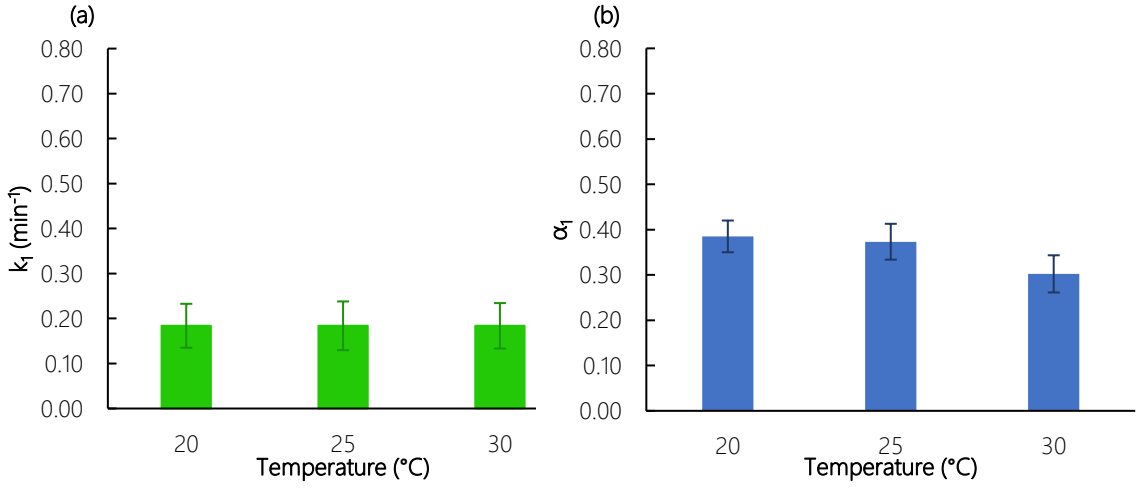

Figure 5.2: Summary of deactivation constants k_1 (a) and ratio of residual peroxygenase activity α_1 (b) for once-off delivery of 20 mM H_2O_2 at temperatures 20 °C, 25 °C and 30 °C obtained by non-linear regression of the best fit (two-parameter) model

5.2 pH-dependent enzyme deactivation kinetics

The kinetics analysis was performed on the enzyme deactivation data collected for the pH studies, where the stability of the PaDa-I enzyme in 20 mM H_2O_2 was investigated at pH 6.0, pH 7.0 and pH 8.0 (with the temperature maintained at 25 °C). The first order, two-parameter and four-parameter enzyme deactivation models were applied to this data as shown in Figure 5.3. As with the temperature studies, the first order model similarly predicted deactivation constant values an order of magnitude lower than the k_1 values obtained for the two-parameter and four-parameter models (Table 5.3). In terms of the α values, α_1 and α_2 were similar in the four-parameter model in the range 0.47 - 0.61. This range of values was similar to the α_1 values obtained in the two-parameter model. As a result of these similar values, the plots for these two kinetic models were seen to partially overlap in Figure 5.3. Furthermore, these non-zero α values indicated that the enzyme still retained some peroxygenase activity at the end of the 2 h incubation period as depicted by the residual enzyme activity profiles (Figure 5.3). The results from the regression analysis indicated that the first order model had a poor fit to the experimental data as evidenced by the low R^2 values (<0.6), whereas much higher R^2 values were obtained for the two-parameter and four-parameter models (R^2 values >0.8). The two-parameter model once again appeared to best describe the experimental data given that it had the lowest AIC and BIC values. The first order model was deemed unsuitable due to the high AIC and BIC along with the high R^2 values (Table 5.3).

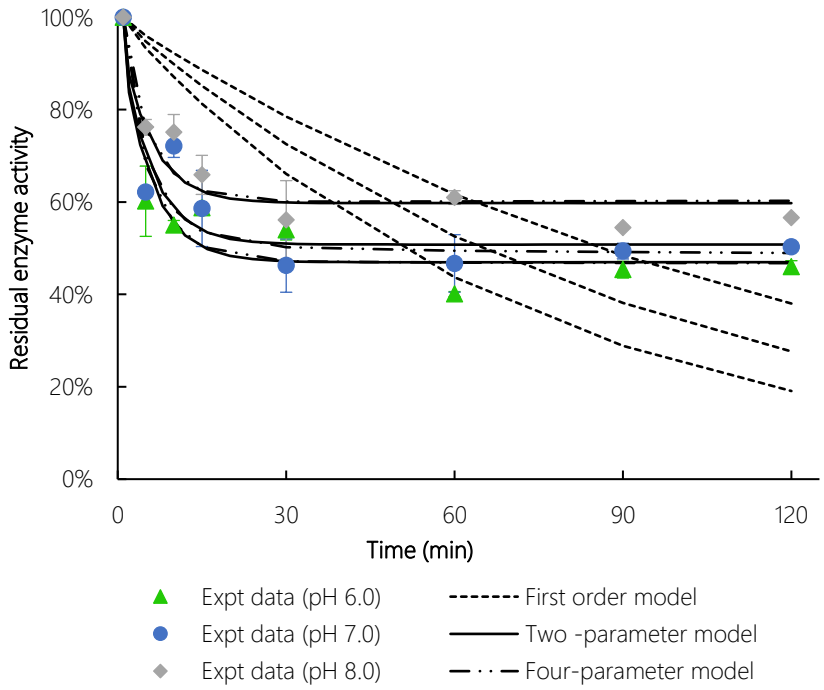

Figure 5.3: The enzyme deactivation kinetics for PaDa-I at pH 6.0 (▲), pH 7.0 (●) and pH 8.0 (◆) modelled by the first order (- - - -), two-parameter (——) and four-parameter (— · · —) models. Reaction conditions: 20 ml 100 mM potassium phosphate buffer, 1.7 U ml^{-1} (NBD) PaDa-I, 20 mM H_2O_2 once-off addition, 200 rpm, 25 °C

Table 5.3: Deactivation kinetic parameters for the peroxygenase activity of PaDa-I at pH 6.0, pH 7.0 and pH 8.0 and once-off delivery 20 mM H_2O_2 where model constants k_1, k_2, α_1 and α_2 were determined by non-linear regression

	First order model			Two-parameter model			Four-parameter model		
	pH 6.0	pH 7.0	pH 8.0	pH 6.0	pH 7.0	pH 8.0	pH 6.0	pH 7.0	pH 8.0
k_1 (min^{-1})	0.01	0.01	0.01	0.18	0.18	0.18	0.18	0.18	0.18
k_2 (min^{-1})							0.01	0.02	0.01
α_1				0.47	0.51	0.60	0.47	0.51	0.60
α_2							0.47	0.49	0.61
R^2	0.51	0.48	0.57	0.91	0.86	0.91	0.91	0.87	0.91
χ^2	0.80	0.55	0.29	0.04	0.05	0.02	0.16	0.20	0.16
AARD (%)	0.94	1.17	0.91	0.04	0.01	0.03	0.92	1.11	1.19
AIC	9.79	9.46	7.72	2.08	3.15	0.50	10.26	11.56	11.39
BIC	6.50	6.17	4.43	-2.31	-1.24	-3.89	3.68	4.98	4.81

The kinetic parameters obtained from the regression of the two-parameter model (best fit model) are shown in Figure 5.4. The deactivation constant was a constant value of 0.18 min^{-1} across all three pH values tested (Figure 5.4 a). The other kinetic parameter, α_1, indicates the ratio of the enzyme activity at the end of the incubation time in relation to the initial enzyme activity. The trend shown for α_1 values obtained, supports the observation made for the pH studies where the enzyme stability increased with increasing pH, as such α_1 was highest at pH 8.0 at 0.60, followed by 0.51 and 0.47 obtained at pH 7.0 and pH 6.0, respectively (Figure 5.4 b). There was a slight discrepancy of this kinetic parameter at reaction conditions pH 7.0 and 25 °C, whereby α_1 = 0.37±0.04 was noted for the temperature studies and 0.51±0.04 for the pH studies. This may have been a result of two different enzyme stock solutions that were used in each study. As such, each enzyme stock solution likely underwent distinct purification methods which could have contributed to the difference in enzyme stability measured over time at the same reaction conditions. Nonetheless, with the reaction temperature held constant at 25 °C, it was observed that the specific enzymea ctivity was affected by pH. Its stability appeared to be greater at pH 8.0 compared to pH 7.0 and pH 6.0.

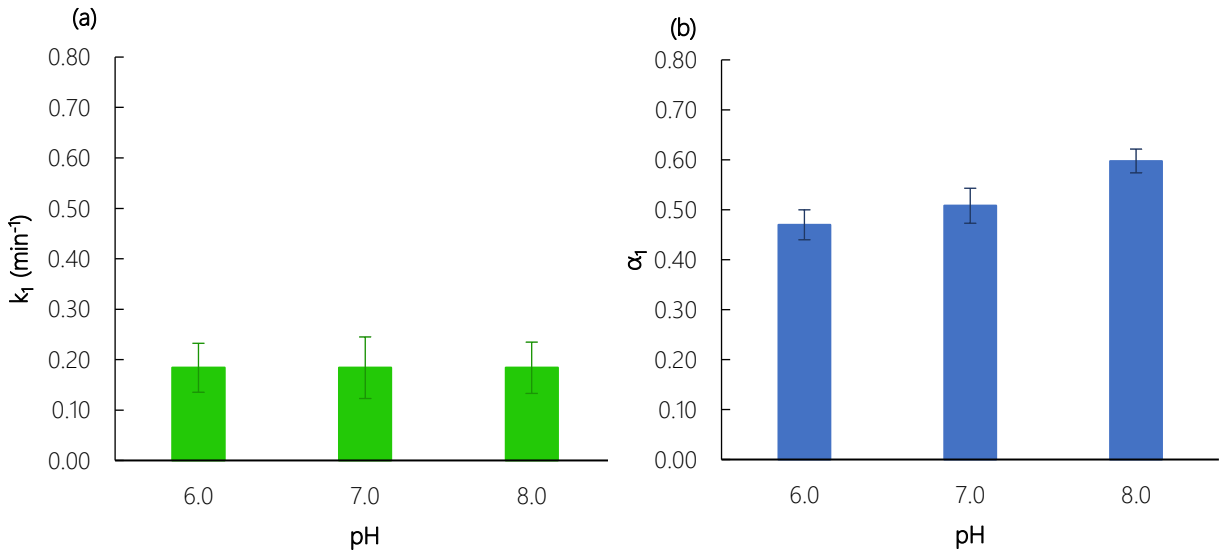

Figure 5.4: Summary of deactivation constants k_1 (a) and ratio of residual peroxygenase activity α1 (b) for once-off delivery of 20 mM H_2O_2 at pH 6.0, pH 7.0 and pH 8.0 obtained by non-linear regression of the best fit (two-parameter) model

5.3 Hydrogen peroxide-dependent enzyme deactivation kinetics

Hydrogen peroxide-dependent deactivation kinetics were evaluated at 10 mM, 20 mM and 40 mM concentrations using once-off, stepwise and continuous delivery. The outcomes of applying the first order, two-parameter and four-parameter deactivation models to the experimental data are illustrated in Figure 5.5.

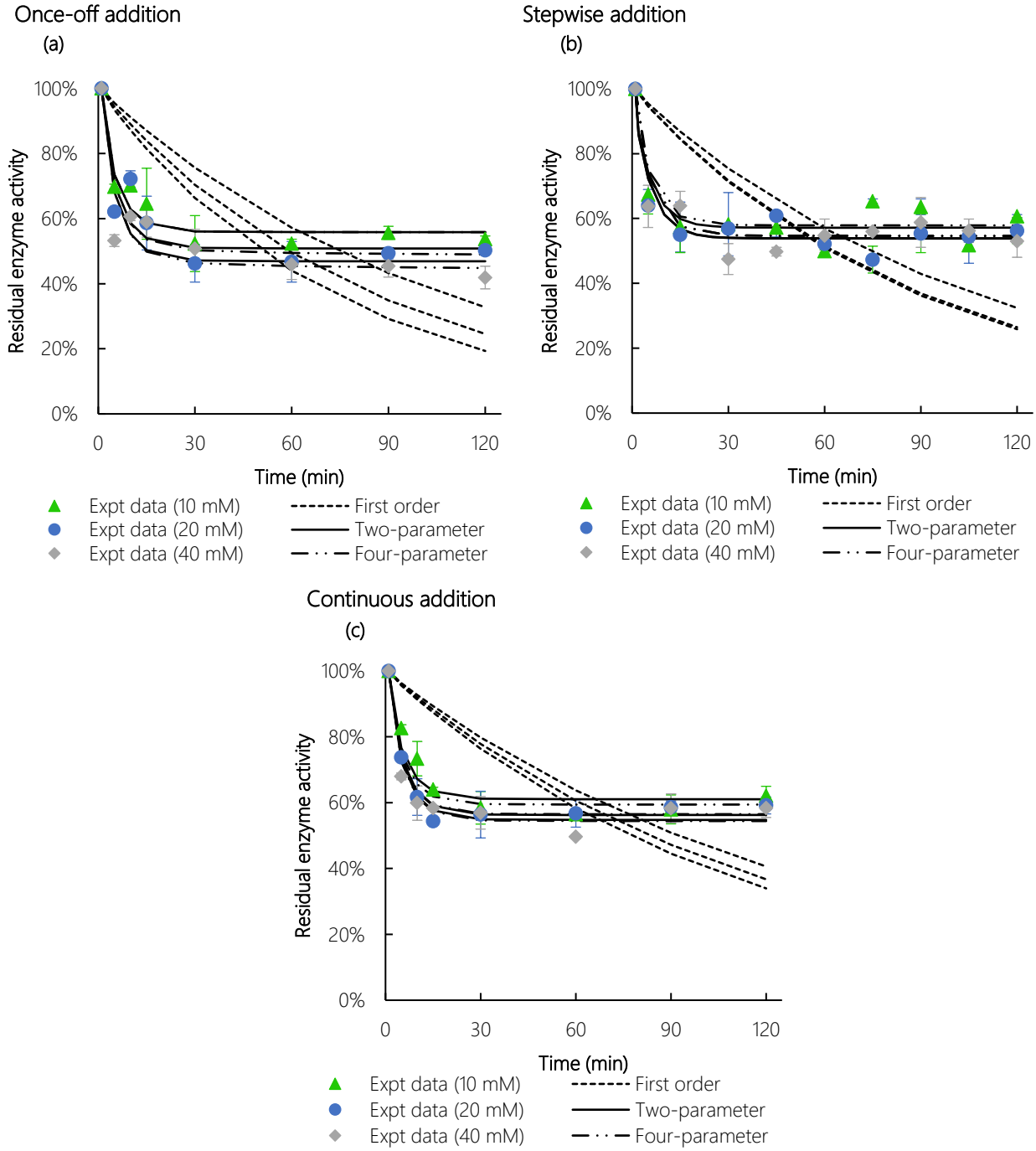

Figure 5.5: The enzyme deactivation kinetics of PaDa-I using (a) once-off (b) stepwise and (c) continuous delivery methods of H_2O_2 concentrations 10 mM (▲), 20 mM (●) and 40 mM (◆) modelled by the first order (- - - -), two-parameter (——) and four-parameter (— · · —) models. Reaction conditions: 20 ml 100 mM potassium phosphate buffer pH 7.0, 1.7 U ml^{-1} (NBD) PaDa-I, 200 rpm, 25 °C.

Tables 5.4, 5.5 and 5.6 present the kinetic parameters derived from the non-linear regression of the three deactivation models at the specified H_2O_2 concentrations using the different delivery approaches. The k_1 value obtained for the first order model was again lower than the 0.18 min^{-1} obtained for the other two-parameter and four-parameter models across all concentrations and delivery methods investigated. The results obtained from the first order model implied that the enzyme was less prone to deactivation over time compared to what was noted for the remaining two models. The other kinetic parameter, α, describes the ratio of the final enzyme activity relative to the initial enzyme activity. These α values decreased with increasing H_2O_2 concentration in both the two-parameter and four-parameter models - for instance, using stepwise H_2O_2 delivery, α decreased from 0.57 to 0.54 (Table 5.4). A similar trend was observed with the once-off and continuous delivery methods. These results appeared to support that high H_2O_2 concentrations increasingly deactivated the enzyme. In terms of the H_2O_2 delivery approaches, it was determined that the α values were lowest at once-off delivery (0.56 - 0.44), followed by stepwise delivery (0.57 - 0.54) and lastly continuous delivery (0.61 - 0.55) (Tables 5.4, 5.5, 5.6). This suggested that the method of H_2O_2 delivery could potentially influence the stability and performance of the enzyme in the presence of a substrate in a biotransformation reaction.

Table 5.4: Deactivation kinetic parameters for the peroxygenase activity of PaDa-I with once-off H_2O_2 delivery at concentrations 10 mM, 20 mM and 40 mM, where model constants k_1, k_2, α_1 and α_2 were determined by non-linear regression

	First order model			Two-parameter model			Four-parameter model		
$[H_2O_2]$ (mM)	10	20	40	10	20	40	10	20	40
k_1 (min^{-1})	0.01	0.01	0.01	0.18	0.18	0.18	0.18	0.18	0.18
k_2 (min^{-1})							0.02	0.02	0.02
α_1				0.56	0.51	0.47	0.56	0.51	0.47
α_2							0.56	0.49	0.44
R^2	0.51	0.49	0.51	0.93	0.86	0.86	0.93	0.87	0.86
χ^2	0.42	0.63	0.71	0.02	0.05	0.06	0.02	0.05	0.06
AARD (%)	1.00	0.95	1.00	<0.01	0.01	0.07	<0.01	0.08	0.04
AIC	8.68	9.43	9.83	0.15	3.15	3.67	4.15	7.05	7.61
BIC	5.39	6.14	6.54	-4.24	-1.24	-0.72	-2.43	0.47	1.03

The regression of the first order model resulted in poor agreement with the experimental data compared to the two-parameter and four-parameter models. Even though the statistical analysis revealed that there were low χ^2 (<1) and AARD (<2%) values obtained for all three models tested, the R^2 values were lowest for the first order model (<0.5) and high for the two-parameter and four-parameter models (>0.8) (Tables 5.4, 5.5, 5.6). Furthermore, the calculated AIC and BIC values revealed that the two-parameter model had the lowest values and was, therefore, best suited to model the experimental data.

Table 5.5: Deactivation kinetic parameters for the peroxygenase activity of PaDa-I with stepwise H_2O_2 delivery at concentrations 10 mM, 20 mM and 40 mM, where model constants k_1, k_2, α_1 and α_2 were determined by non-linear regression

	First order model			Two-parameter model			Four-parameter model		
$[H_2O_2]$ (mM)	10	20	40	10	20	40	10	20	40
k_1 (min^{-1})	0.01	0.01	0.01	0.18	0.18	0.18	0.18	0.18	0.18
k_2 (min^{-1})							0.02	0.02	0.02
α_1				0.57	0.54	0.54	0.57	0.54	0.54
α_2							0.58	0.55	0.55
R^2	0.30	0.41	0.36	0.86	0.91	0.89	0.86	0.91	0.89
χ^2	0.69	0.88	0.89	0.04	0.03	0.04	0.04	0.03	0.04
AARD (%)	0.11	0.05	0.02	0.02	0.10	0.07	0.09	0.19	0.15
AIC	8.37	7.77	8.35	0.07	-1.37	-0.60	4.22	2.91	3.58
BIC	5.37	4.77	5.35	-3.93	-5.37	-4.60	-1.78	-3.09	-2.42

Table 5.6: Deactivation kinetic parameters for the peroxygenase activity of PaDa-I with continuous H_2O_2 delivery at concentrations 10 mM, 20 mM and 40 mM, where model constants k_1, k_2, α_1 and α_2 were determined by non-linear regression

	First order model			Two-parameter model			Four-parameter model		
$[H_2O_2]$ (mM)	10	20	40	10	20	40	10	20	40
k_1 (min^{-1})	0.01	0.01	0.01	0.18	0.18	0.18	0.18	0.18	0.18
k_2 (min^{-1})							0.02	0.02	0.02
α_1				0.61	0.56	0.55	0.61	0.56	0.55
α_2							0.59	0.57	0.54
R^2	0.48	0.28	0.30	0.94	0.98	0.95	0.93	0.98	0.95
χ^2	0.32	0.51	0.56	0.02	0.01	0.01	0.02	0.01	0.01
AARD (%)	0.91	1.21	1.22	0.05	0.01	0.03	0.23	0.03	<0.01
AIC	7.95	9.67	9.83	-0.39	-4.19	-1.47	4.45	-0.13	2.50
BIC	4.65	6.38	6.54	-4.77	-8.58	-5.85	-2.13	-6.71	-4.08

An overall evaluation of the deactivation kinetic parameters of the best fit model (two-parameter model) across the different H_2O_2 delivery approaches at different H_2O_2 concentrations is summarised in Figure 5.6. As expected, the α_1 value decreased as the H_2O_2 concentration increased which suggested that high H_2O_2 concentrations potentially accelerated enzyme deactivation. In addition, Figure 5.6 **b** shows that the α_1 values are highest for the continuous delivery followed by stepwise and lastly once-off addition across all three H_2O_2 concentrations. It was further revealed that the enzyme was most stable at 10 mM where all α_1 values were highest at that concentration for each H_2O_2 delivery methods tested - 0.56 once-off delivery, 0.57 for stepwise delivery and 0.61 for continuous delivery. At the higher concentrations 20 mM and 40 mM, this value decreased; however, an α_1 value of 0.54 was obtained at both 20 mM and 40 mM H_2O_2 when the stepwise delivery approach as adopted (hence the plots at these concentrations overlapped in Figure5.5). Similarly, there was also a marginal difference in this value for the continuous delivery system with α_1 values of 0.56 and 0.55 obtained at these concentrations, respectively. This contrasted for once-off delivery where α_1 decreased from 0.51 to 0.47 at 20 mM and 40 mM, respectively. This indicated that the enzyme was more likely stable when the

H_2O_2 was introduced gradually. This would imply that a continuous H_2O_2 delivery approach may be essential in tandem one-pot processes where the enzyme would be in use for extended biotransformation reaction periods. By gradually introducing the oxidant to the reaction environment, the rate of enzyme deactivation would be reduced, and hence improve overall performance.

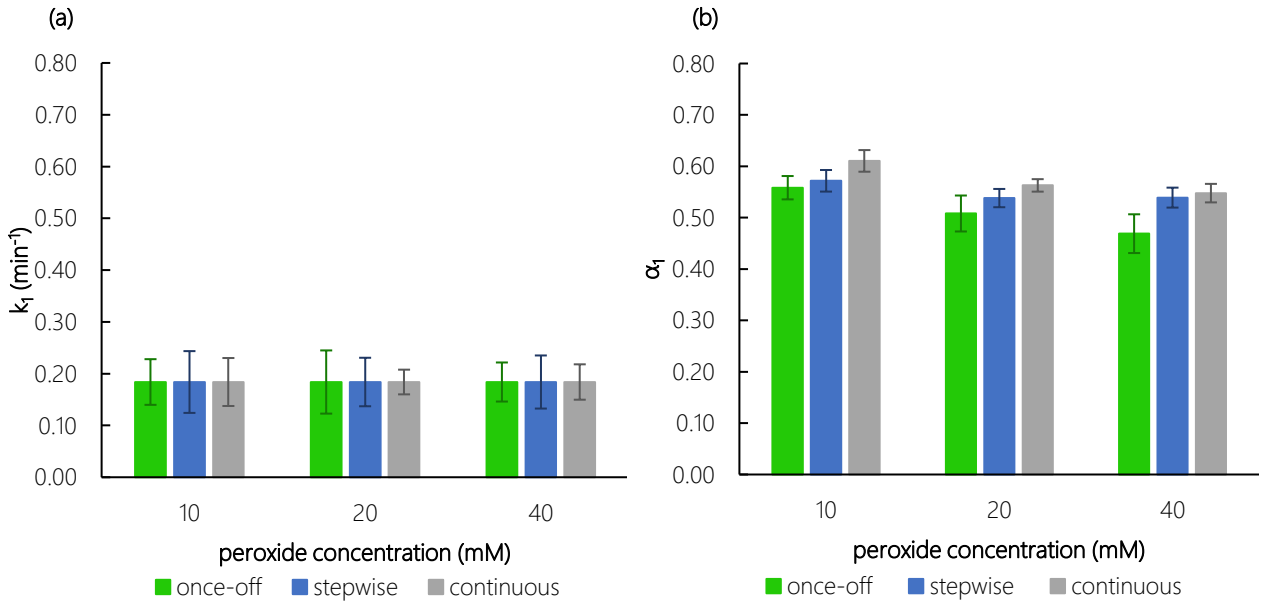

Figure 5.6: Summary of deactivation constants k_1 (a) and ratio of residual peroxygenase activity α_1 (b) for once-off, stepwise and continuous delivery at 10 mM, 20 mM and 40 mM H_2O_2 obtained by non-linear regression of the best fit (two-parameter) model

5.4 Conclusion

Three enzyme deactivation models, first order, two-parameter and four-parameter models, were used in an attempt to model the experimental enzyme deactivation kinetic data obtained in Chapter 4. It was determined that the two-parameter model was the best fit model across all data sets collected, while the first order model did not agree with the experimental data. Based on the potential deactivation pathways presented by these models, these results were expected because the enzyme exhibited residual activity at the end of the incubation period as opposed to complete deactivation.

In the two-parameter model, (best fit model) the deactivation rate constant k_1 was determined to be 0.18 min^{-1}. Slight differences in the α_1 value were observed across the temperature, pH and H_2O_2 studies due to enzyme inactivation that occurred at the different reaction conditions. For the temperature studies, an inverse relationship existed between α_1 and the reaction temperature whereby α_1 increased from 0.30 to 0.39 as the temperature was decreased from 30 °C to 20 °C, respectively. This was likely because the protein molecule could have unfolded and distorted the active site of the enzyme thus reducing the enzyme activity at the higher temperature (Bechtold and Panke, 2012). On the other hand, the pH studies revealed a direct relationship between α_1 and pH, where α_1 increased from 0.47 to 0.60 as the pH increased from pH 6.0 to pH 8.0. This may be due to the enzyme forming more stable intermediates at the higher pH (Hernández-Ruiz *et al.*, 2001). Lastly, it was noted that α_1 decreased as the H_2O_2 concentration was increased which implied that the enzyme was deactivated at higher H_2O_2 concentrations. The α_1 value was also influenced by the delivery approach. This was evidence by the

increase in α_1 as the H_2O_2 was gradually introduced into the system and was highest when a continuous delivery approach was adopted, followed by stepwise and lastly once-off addition.

Currently within the limited available literature, the isolation of deactivated intermediates for heme enzymes like PaDa-I has proven challenging. Nonetheless, the deactivation pathway proposed by the two-parameter model is a likely candidate due to the close alignment of experimental data with its predictions. This model suggests that the enzyme initially experiences rapid deactivation in the presence of the H_2O_2 and thereafter displays a non-zero specific activity. To improve the activity of the enzyme in a biotransformation reaction, it may be worthwhile investigating how to increase the kinetic parameter, α_1.

6 Investigating the kinetics of enzyme deactivation and inhibition in the biotransformation of styrene

The oxidation of styrene is an industrially important reaction and the formed chiral styrene oxides find broad application in the fine chemicals industry. Previous studies have shown that PaDa-I is highly selective towards the oxidation of sp^2 hybridized secondary carbons while showing very little activity towards the oxidation of primary and aromatic carbons. In addition, many test substrates tend to be oxidized in high enantiomeric excess. Styrene and the formed styrene oxide are commercially available, and due to the high regioselectivity, a simple product stream is expected making styrene an ideal model substrate to assess the catalytic activity of the PaDa-I enzyme while employing the different H_2O_2 delivery methods. In Chapters 4 and 5, it was established that there was a marginal difference (approximately 1%) in the enzyme stability at 20 °C and 25 °C, therefore the biotransformation in this investigation was performed at 25 °C. The pH, on the other hand, may influence the enzyme stability and catalytic activity, therefore the biotransformation was assessed at both pH 7.0 (base case pH) and pH 8.0. Furthermore, the H_2O_2 and styrene concentrations were varied to evaluate the type of inhibition that may be experienced by the enzyme. In each case, the performance of the enzyme was assessed by monitoring styrene oxide formation by gas chromatography (Section 3.3.3) while enzyme stability was monitored by means of the peroxygenase activity assay (Section 3.3.1).

6.1 Biocatalytic activity

The stability of the PaDa-I enzyme was investigated at different temperatures, pH levels, H_2O_2 concentrations and delivery methods in Chapters 4 and 5. The effect of the hydrocarbon substrate, styrene, on enzyme stability was also further investigated. Preliminary studies were, therefore, conducted to observe the behaviour of the enzyme in the presence of styrene over a 2 h incubation period in the absence of the H_2O_2 oxidant.

Figure 6.1 shows that the enzyme activity rapidly decreased from 100% to 59% in the presence of 20 mM styrene. The consequence of which was likely due to the droplets of nonpolar organic solvents giving rise to interfacial interactions with the enzyme which created hydrophobic forces that disturbed the secondary structure of the enzyme (Bechtold and Panke, 2012). Furthermore, this could not have been due to styrene oxide forming as oxidation did not occur in the absence of the oxidant (Appendix C.1) As the incubation progressed, the residual enzyme continued decreasing up until 30 min where 47% was measured. Thereafter, the enzyme appeared to have adapted to the styrene or the substrate was bound reversibly to the enzyme as the residual activity increased to 58% by the end of the 2 h incubation.

The residual activity profile for the enzyme exposed to styrene differed to those obtained when the enzyme was exposed to the control experiments containing either H_2O_2, or when the enzyme was exposed to only the potassium phosphate buffer (Figure 6.1). When 20 mM H_2O_2 was added (once-off delivery), in the absence of the styrene substrate, rapid deactivation was observed - the enzyme lost more than half of its peroxygenase activity within the first 5 min. The residual enzyme activity remained low until the end of the incubation period where it exhibited only 39% of its original peroxygenase activity. On the other hand, in the absence of both H_2O_2 or styrene, the enzyme retained about 70% of its initial activity after the 2 h incubation period. This illustrates that both the substrate and oxidant inhibit the enzyme over time. This observation was not unexpected, as it has been reported that a substrate

could potentially lead to enzyme inactivation for related enzymes (Waley, 1991). The combined effect of both styrene and H_2O_2 in the biotransformation reaction could also therefore reduce the enzyme's catalytic activity.

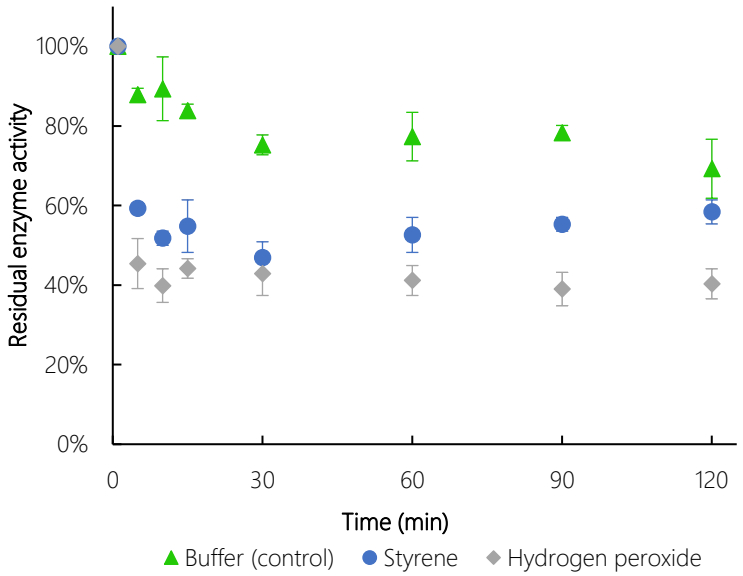

Figure 6.1: The residual enzyme activity in the absence (▲) and presence of 20 mM styrene (●) or 20 mM H_2O_2 (◆) as sole substrates. Reaction conditions: 20 ml 100 mM potassium phosphate buffer pH 7.0, 1.7 U ml^{-1} (NBD) PaDa-I, 20 mM styrene or 20 mM H_2O_2 (once-off addition), 200 rpm, 25 °C.

Following this observation, the biotransformation of styrene was evaluated using once-off addition of 20 mM H_2O_2 at the base case conditions (pH 7.0, and 25 °C) over an extended reaction time of 24 h. No product formation was detected under these conditions, which was likely due to the high H_2O_2 concentration inhibiting the enzyme. Consequently, the stepwise and semi-continuous delivery approaches of the oxidant were subsequently tested (Figure 6.2). For stepwise addition, H_2O_2 was delivered at 2.5 mM H_2O_2 (0.5 ml of a 200 mM H_2O_2 stock) every 30 min over the first 2 h, while for semi-continuous addition, 0.8 mM H_2O_2 (83 µl of a 200 mM H_2O_2 stock) was added every 1 h over the 24 h reaction period. This proved more successful than once-off addition, with styrene oxide detected as the only product under these conditions. It was established that about 56% more styrene oxide was obtained using semi-continuous H_2O_2 delivery compared to stepwise delivery (Figure 6.2 **a**). Within the first 2 h, the enzyme reached its maximum concentration at 0.48 mM styrene oxide with stepwise H_2O_2 delivery. In contrast, the styrene oxide concentration achieved in the semi-continuous delivery system was almost double (0.88 mM) what was observed in the stepwise delivery system within the same 2 h timeframe. This suggested that the catalytic activity was improved as less H_2O_2 was gradually introduced to the reaction mixture at a given time, which in turn could have reduced enzyme inhibition thus increasing substrate conversion. Using the semi-continuous delivery approach, the biotransformation proceeded to a maximum styrene oxide concentration of 1.09 mM after 8 h. Thereafter, the product concentration remained at pseudo-steady state before decreasing slightly by approximately 20% towards the end of the 24 h reaction period. This observed decrease could have resulted due to evaporation of the volatile substrate/product over time (refer to carbon balances in Appendix C.2).

There was a significant enzyme activity loss (>90%) measured as soon as both styrene and H_2O_2 were added to the enzyme/buffer mixture, irrespective of the H_2O_2 delivery approach (Figure 6.2 b). This is approximately double the enzyme activity lost within the same time frame of ca. 5 min, when the enzyme was exposed to styrene or H_2O_2 in isolation (Figure 6.1). This suggested that when combined, styrene and H_2O_2 have a strong inhibitory effect on the PaDa-I enzyme, which significantly reduced its catalytic activity. It is known that H_2O_2 may cause oxidative deactivation towards the enzyme (Valderrama, 2010; Valderrama *et al.*, 2002), and it is also probable that the styrene free radicals formed in the reaction (as per the catalytic cycle, Section 2.2.2) may have interacted with the enzyme which further decreased the activity (Aitken, 1993). Regardless of this, the enzyme was still capable of producing styrene oxide even though it was operating at ca. 10% of its initial activity. As the biotransformation proceeded from 5 min to 1 h, a recovery was observed as the residual activity slightly increased from 8% to 12% for semi-continuous H_2O_2 delivery. This was not the case for the stepwise H_2O_2 delivery approach, because the residual activity remained at 7% after the same reaction period. The enzyme activity remained low (<10%) for the rest of the reaction period with both methods of H_2O_2 delivery.

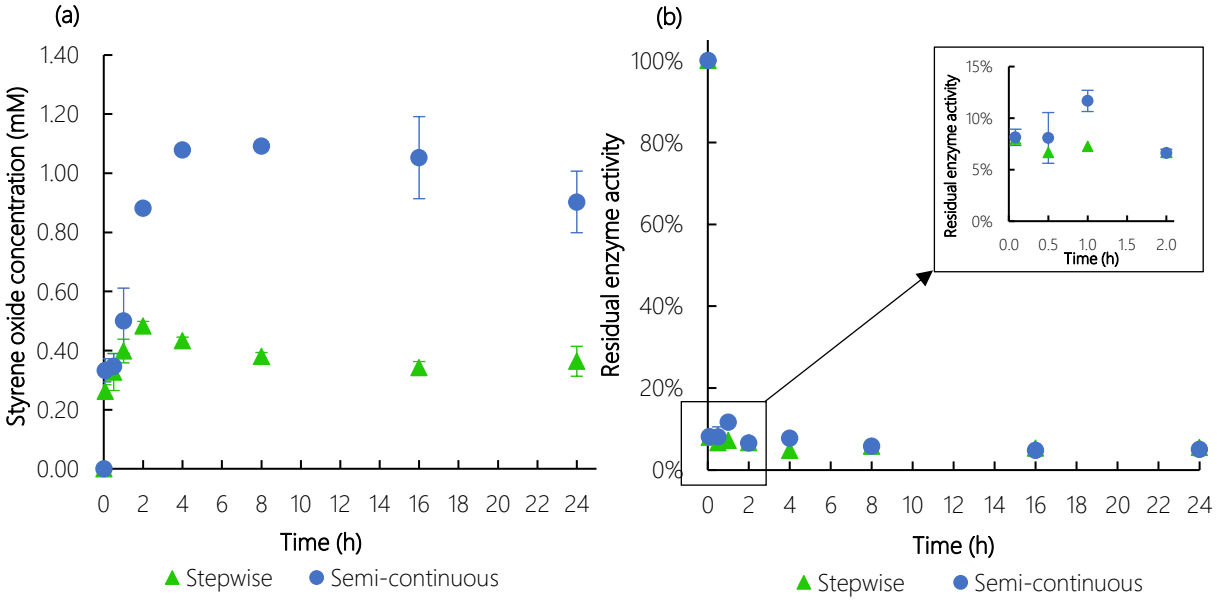

Figure 6.2: (a) Styrene oxide concentration profiles and (b) residual enzyme activity for the biotransformation of styrene from using the following H_2O_2 delivery methods: stepwise addition at 2.5 mM H_2O_2 every 30 min over the first 2 h (▲) and semi-continuous delivery at 0.83 mM H_2O_2 every 1 h over 24 h (●). Reaction conditions: 20 ml 100 mM potassium phosphate buffer pH 7.0, 12 U ml^{-1} (NBD) PaDa-I, 20 mM styrene, 20 mM H_2O_2, 200 rpm, 25 °C.

The biotransformation of styrene was then further optimised by evaluating the effect of temperature and pH. It was previously deduced that there was no significant difference between operating at 20 °C versus 25 °C (Figure 4.1, Section 4.1). It was therefore decided to continue working at 25 °C, as this would require less complex temperature control (chiller vs heating mantle). The effect of the reaction mixture pH was also evaluated, and it was observed that the enzyme was more stable at pH 8.0 (Figure 4.3, Section 4.2), therefore this was the pH used for further optimisation. Figure 6.2 already shows that semi-continuous H_2O_2 delivery resulted in >50% greater product yields compared to stepwise addition and once-off addition. Therefore, semi-continuous delivery was selected as the optimal method of H_2O_2 delivery. The product concentration profiles only showed differences in the first 2 h of the reaction

whereby 20% more styrene oxide was obtained at pH 8.0 compared to pH 7.0 (Figure 6.3 **a**). However, the maximum product concentration obtained did not exceed that obtained at pH 7.0. As the reaction progressed towards the end of the 24 h time period, there was no significant difference (<5%) in the styrene oxide concentration profiles obtained at both pH 8.0 and pH 7.0. Needless to say, similar residual enzyme activity profiles were obtained at the pH values investigated.

Figure 6.3 **b** illustrates an initial significant enzyme activity loss of approximately 90% after 5 minutes, where it remained low (7% residual enzyme activity) until the end of the biotransformation period. The catalytic activity of PaDa-I in the biotransformation of styrene was therefore not significant at both pH 7.0 and 8.0 conditions.

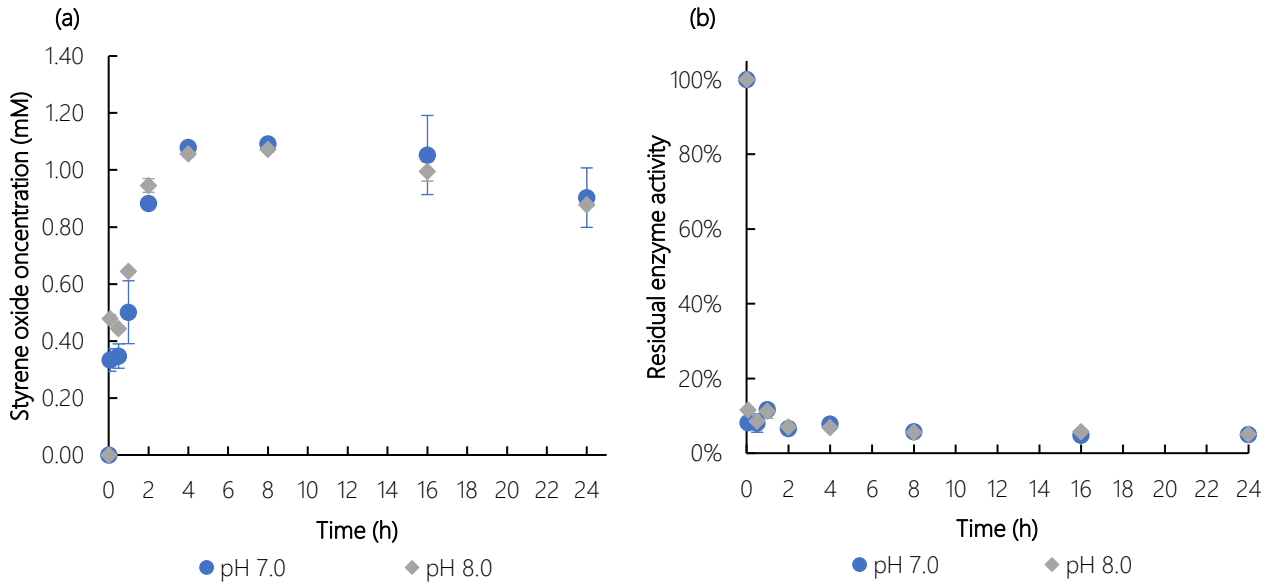

Figure 6.3: (a) Styrene oxide concentration profiles and (b) residual enzyme activity profiles for the biotransformation of styrene using the semi-continuous delivery approach at 0.83 mM H_2O_2 every 1 h over 24 h at pH 7.0 (●) and pH 8.0 (◆). Reaction conditions: 20 ml 100 mM potassium phosphate buffer pH 7.0/pH 8.0, 12 U ml^{-1} (NBD) PaDa-I, 20 mM styrene, 20 mM H_2O_2, 200 rpm, 25 °C.

It was important to consider the potential impact that 5-nitro-1,3-benzodioxide (NBD) could have on the enzyme, as this substrate was extensively used in the peroxygenase activity assay to evaluate the enzyme deactivation (Section 3.3.1). The presence of a co-substrate could lead to further enzyme deactivation, therefore the influence of NBD on the biotransformation of styrene was investigated. The same NBD concentration that was used in the residual peroxygenase activity assay was added to the biotransformation reaction mixture (0.5 mM, dissolved in acetonitrile) to assess whether styrene oxide formation would be impacted. This was performed using the semi-continuous delivery of H_2O_2. Figure 6.4 shows that a similar product concentration profile was obtained in both the absence and presence of the NBD, whereby high styrene oxide concentrations (>1 mM) were produced within the first 6-8 followed by a region of steady state until the end of the reaction.

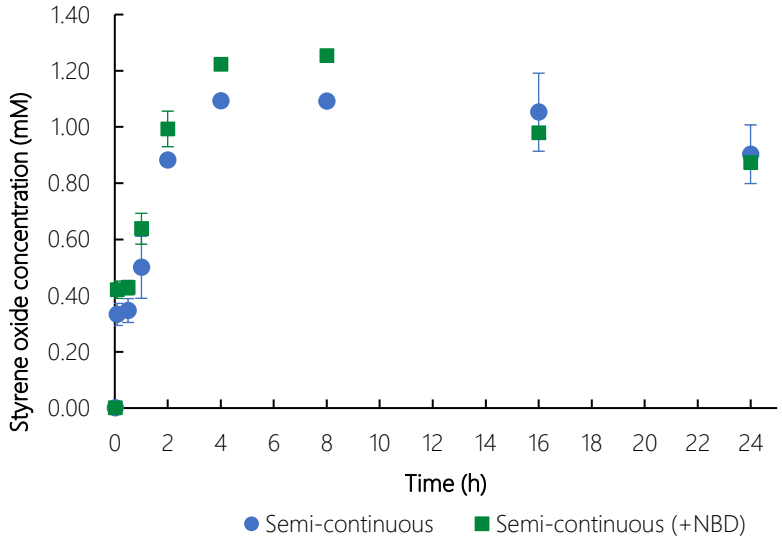

Figure 6.4: Styrene oxide concentration profiles using the semi-continuous delivery approach at 0.83 mM H_2O_2 every 1 h over 24 h in the absence (●) and presence (■) of 0.5 mM NBD. Reaction conditions: 20 ml 100 mM potassium phosphate buffer pH 7.0, 12 U ml^{-1} (NBD) PaDa-I, 20 mM styrene, 20 mM H_2O_2, 200 rpm, 25 °C.

It can therefore be deduced that double deactivation of the enzyme did not occur in the assay as the rate of product formation was seemingly maintained. In fact, a slight improvement was detected whereby a maximum styrene oxide concentration of 1.25 mM was obtained compared to 1.09 mM in the experiments without NBD (Figure 6.4). The acetonitrile solvent, used to dissolve the NBD, may have therefore acted as a substrate pool because less styrene evaporated for the experimental runs with NBD (refer to carbon balances in Appendix C.2). Initial results suggested that incorporation of solvents as products sink or substrate pool could be highly beneficial to productivity. Kluge *et al.* (2012) included 20 vol% acetonitrile in their reaction mixture for the biotransformation of alkylbenzenes and styrene derivatives by a UPO enzyme to ensure substrate solubility into the aqueous phase. They, however, did not take into consideration whether this solvent had an impact on the stability of the enzyme during the reaction. Future work in designing or improving a tandem chemo-bio system would need to focus on the utility of solvents in these biotransformation reactions, provided that the solvent does not affect the activity of the chemocatalyst

Table 6.1: Summary of key performance indicators of the enzyme-driven oxidation of styrene using stepwise and semi-continuous H_2O_2 delivery systems

Parameter	Stepwise	Semi-continuous (pH 7.0)	Semi-continuous (pH 8.0)	Semi-continuous (pH 7.0 +NBD)
Max. styrene oxide concentration (mM)	0.48±0.01	1.09±0.02	1.07±0.01	1.25±0.01
Max. conversion (%)	2.38±0.10	5.34±0.10	5.32±0.05	6.54±0.13
Max. yield ($mol_{product}\ mol_{substrate}^{-1}$)	0.02	0.05	0.05	0.07
Max. TON ($mol_{product}\ mol_{protein}^{-1}$)	1 307±29	3 070±40	3 010±29	3 520±29

Table 6.1 summarises the performance of the enzyme under the different conditions investigated. An overview of the different experimental runs investigating PaDa-I mediated styrene oxidations revealed that the maximum styrene oxide concentration obtained over 24 h did not exceed 1.25 mM. This was lower than 2.12 mM achieved within 2 h by a chemo-bio tandem system reported in the literature,

despite the AuPd chemocatalyst partially reducing the styrene to ethylbenzene (Freakley *et al*., 2019). Furthermore, in terms of the TON, the values shown in Table 6.1 were <4 000 $mol_{product}$ mol_{enzyme}^{-1} whereas the chemo-bio system developed by Freakley *et al*. (2019) achieved a higher TON of 11 700 $mol_{product}$ mol_{enzyme}^{-1} for this biotransformation. The discrepancy of these results may be an indication of how crucial the method of H_2O_2 delivery is to the enzyme - the lower H_2O_2 concentration produced *in-situ* in the tandem system (0.44 mM - 0.74 mM at steady state) could have possibly further enhanced enzyme performance compared to the manual stepwise and semi-continuous delivery approaches of higher H_2O_2 concentrations. In both studies, nevertheless, the specified enzyme performance requirements for fine chemicals synthesis outlined by Dong *et al*. (2018) were not met - a minimal turnover number of 27 000 $mol_{product}$ mol_{enzyme}^{-1}. From an economic perspective, this productivity target takes into account how much the biocatalyst contributes to the cost of the product compared to the added value achieved by employing biocatalysis over other production methods (Dong *et al*., 2018; Tufvesson *et al*., 2011). There is therefore a need to reduce enzyme deactivation in order to potentially enhance the TON in this biotransformation, with efforts to meet the performance requirements.

6.2 Enzyme deactivation kinetics evaluation

The specific enzyme activity was monitored throughout the biotransformation by using the peroxygenase assay. It was calculated in terms of the moles of 4-nitrocatechol product formed per minute per unit mass of total protein (U_{NBD} $mg_{protein}^{-1}$) (Section 3.3.1). The enzyme activity profiles shown in Figure 6.5 show the combined effect of both H_2O_2 and styrene on the peroxygenase activity of PaDa-I.

The specific enzyme activity drastically decreased in the presence of both substrate and oxidant compared to when they were added separately. The enzyme lost substantial activity within the first 5 min of the biotransformation. From an initial specific activity of approximately 8.7 U_{NBD} $mg_{protein}^{-1}$, the enzyme activity decreased to 0.96 U_{NBD} $mg_{protein}^{-1}$ at pH 8.0 and semi-continuous H_2O_2 delivery, 0.71 U_{NBD} $mg_{protein}^{-1}$ at pH 7.0, semi-continuous oxidant addition and 0.63 U_{NBD} $mg_{protein}^{-1}$ at pH 7.0 utilizing stepwise H_2O_2 addition. As the reaction progressed, slight recovery was observed after 1 h and 4 h for the semi-continuous delivery experiments. The specific activity did not; however, increase for stepwise H_2O_2 delivery at the same points. This corresponded with the product profile for stepwise delivery whereby no further styrene oxide formation was detected beyond 2 h as the enzyme had likely lost most of its initial activity. As the biotransformation proceeded beyond 8 h to the end of the 24 h reaction period, the enzyme exhibited similar activity of approximately 0.42 U_{NBD} $mg_{protein}^{-1}$ regardless of the method of H_2O_2 delivery and pH. This coincided with no further product formation after 8 h for the semi-continuous delivery experimental runs. The low remaining catalytic activity still was not sufficient to measurably increase styrene oxide production as the enzyme protein molecule had been irreversibly oxidised by the H_2O_2 and/or altered by the substrate whereby hydrophobic forces induced by the styrene may have disrupted the structure of the enzyme as described by Bechtold and Panke (2012).

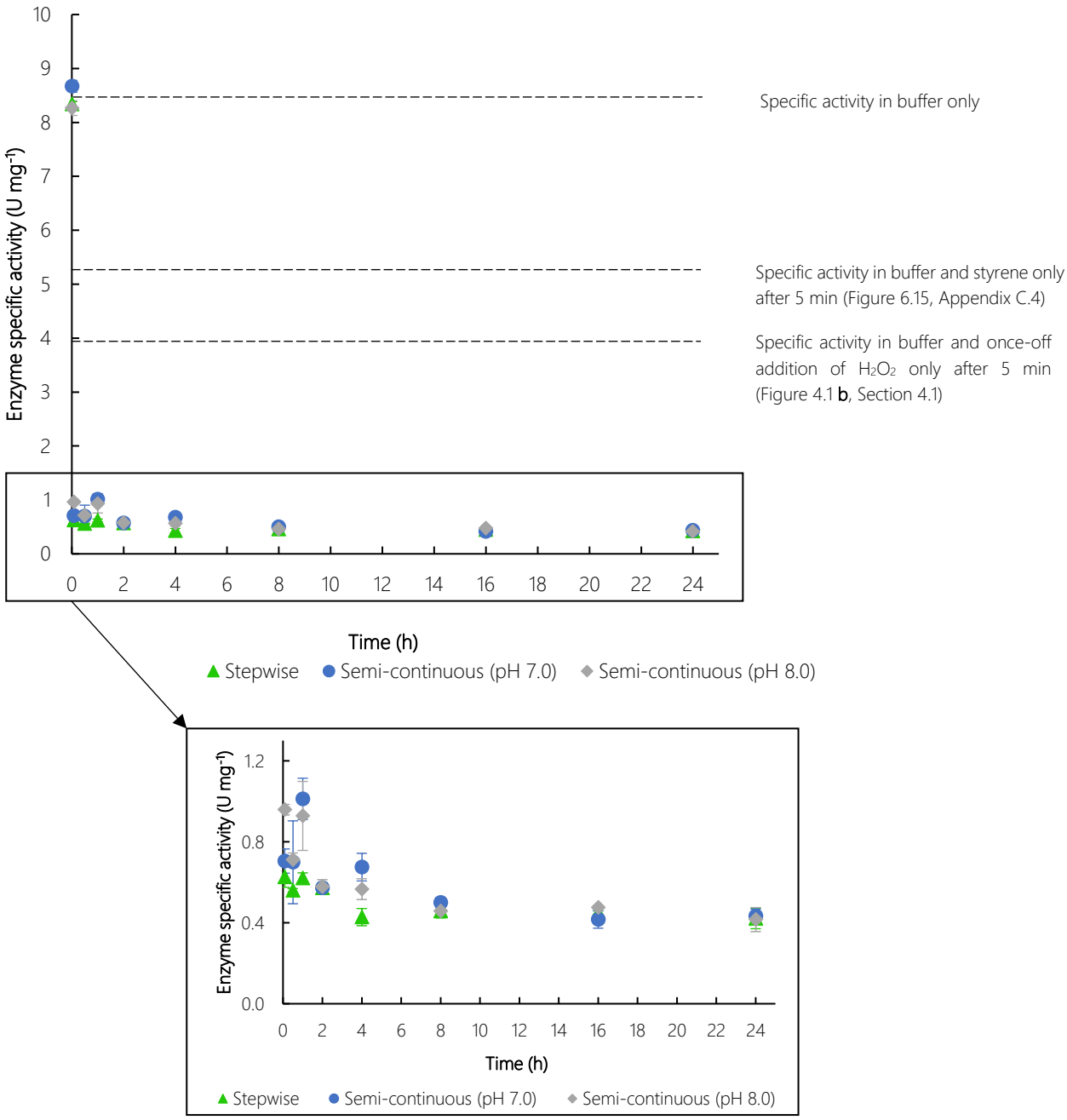

Figure 6.5: Specific activity of the PaDa-I enzyme during the biotransformation of styrene using the following H_2O_2 delivery methods: stepwise addition at 2.5 mM H_2O_2 every 30 min over the first 2 h (▲) and semi-continuous delivery at 0.83 mM H_2O_2 every 1 h over 24 h at pH 7.0 (●) and pH 8.0 (◆). Reaction conditions: 20 ml 100 mM potassium phosphate buffer pH 7.0, 12 U ml^{-1} (NBD) PaDa-I, 20 mM styrene, 20 mM H_2O_2, 200 rpm, 25 °C.

The kinetic data obtained from the enzyme activity profiles (Figure 6.5) were modelled using the first order, two-parameter and four-parameter deactivation models (Section 2.2.3). The kinetic parameters were obtained from non-linear regression and were fitted to the kinetic models as shown in Figure 6.6. The regression yielded similar deactivation constants (k_1) for the first order, the two-parameter and four-parameter models in the range of 0.09 – 0.18 min^{-1}. Lower R^2 values were; however, obtained for the first order model <0.75 compared to the other multi-parameter models (Table 6.2). Furthermore, the large χ^2 values (>100) obtained for the first order model indicated significant difference between the predicted and experimental values which suggested that it is the worst fit model. The α values obtained

for the two-parameter and four-parameter models were significantly low (<0.15) which indicated the reduced activity of the enzyme by the end of the 24 h reaction period (Table 6.2). This implied that the enzyme was not operating at its optimal, meaning that there is potential to improve its performance. This was emphasised by the fact that in each case tested, the enzyme operated at about 10% of its initial specific activity. Upon assessing the AIC and BIC values, it was determined that the two-parameter model was the best fit model.

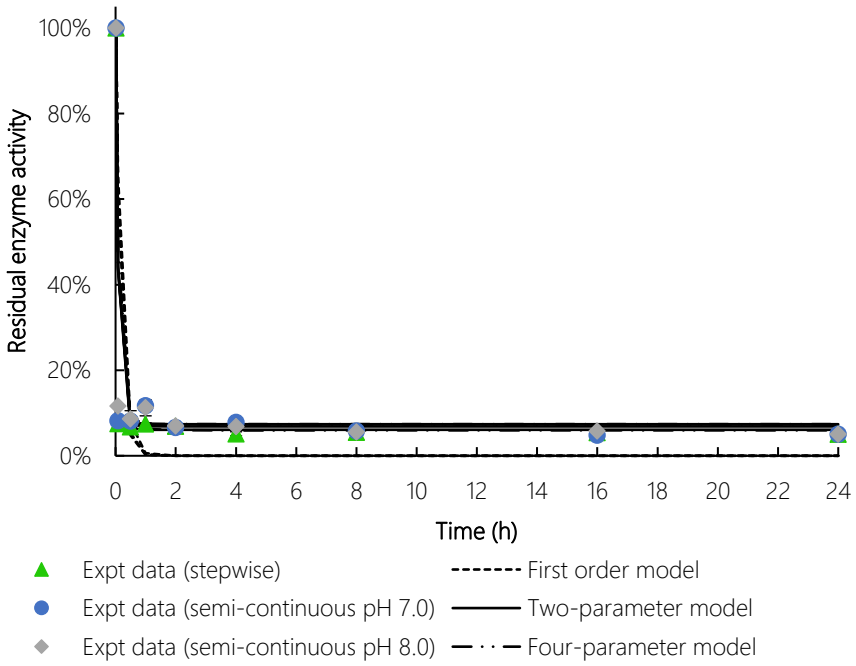

Figure 6.6: The enzyme deactivation kinetics of PaDa-I in the biotransformation of styrene using H_2O_2 delivery systems stepwise addition (▲) and semi-continuous (●) and semi-continuous (pH 8.0) addition (◆) modelled by the first order (- - - -), two-parameter (——) and four-parameter (— · · —) models. Reaction conditions: 20 ml 100 mM potassium phosphate buffer pH 7.0 or pH 8.0, 12 U ml^{-1} (NBD) PaDa-I, 20 mM styrene, 20 mM H_2O_2, 200 rpm, 25 °C.

Table 6.2: Deactivation kinetic parameters for the peroxygenase activity of PaDa-I in the presence of 20 mM H_2O_2 using different H_2O_2 delivery systems, where model constants k_1, k_2, α_1 and α_2 were determined by non-linear regression

	First order model			Two-parameter model			Four-parameter model		
	Stepwise	Semi. (pH 7.0)	Semi. (pH 8.0)	Stepwise	Semi. (pH 7.0)	Semi. (pH 8.0)	Stepwise	Semi. (pH 7.0)	Semi. (pH 8.0)
k_1 (min^{-1})	0.10	0.09	0.10	0.18	0.18	0.18	0.18	0.18	0.18
k_2 (min^{-1})							0.03	0.07	0.07
α_1				0.06	0.07	0.07	0.07	0.09	0.14
α_2							0.06	0.07	0.07
R^2	0.72	0.68	0.69	0.86	0.86	0.85	0.86	0.85	0.85
χ^2	>100	>100	>100	0.31	0.36	0.30	0.31	0.35	0.30
AARD (%)	0.20	0.20	0.07	0.45	0.45	0.41	0.47	0.49	0.48
AIC	8.89	9.58	8.61	7.63	7.82	6.99	11.78	11.87	11.61
BIC	5.76	6.44	5.48	3.44	3.63	2.81	5.51	5.59	5.33

The kinetic parameters obtained for the best fit two-parameter model show that there was little difference between α_1 for stepwise (α_1 = 0.06) and semi-continuous addition (α_1 = 0.07). Furthermore, this value was determined to be 0.07 at both pH 7.0 and pH 8.0 using the semi-continuous delivery method. This may be due to the combination of high concentrations of styrene and H_2O_2 combined, which adversely impacted the stability of the enzyme leading to reduced catalytic activity. Figure 6.7 b illustrates this combined effect as α_1 decreased from 0.51 in styrene and 0.37 in H_2O_2 (as sole substrates) to approximately 0.07 in experiments containing both. In order to further increase this kinetic parameter, future studies need to consider alternative delivery methods of the substrate. This has the potential to greatly improve enzyme stability and overall performance.

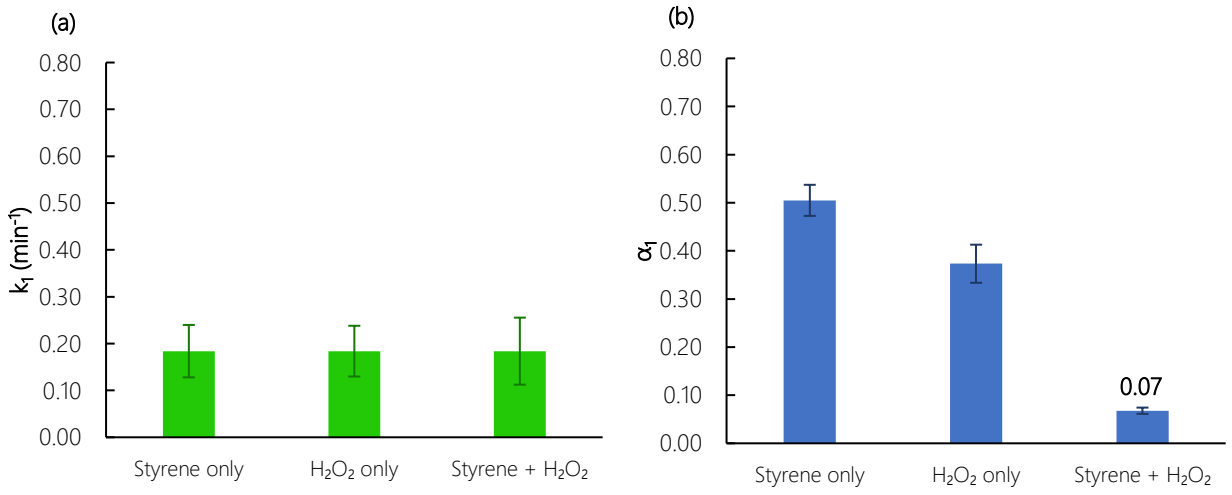

Figure 6.7: Summary of deactivation constants k_1 (a) and ratio of residual peroxygenase activity α_1 (b) for 20 mM H_2O_2 only, 20 mM styrene only and a combination of 20 mM H_2O_2 and 20 mM styrene obtained by non-linear regression of the best fit (two-parameter) model

6.3 Combined substrate and hydrogen peroxide-driven enzyme inhibition

The biocatalytic activity of the PaDa-I enzyme was tested at different substrate and oxidant concentrations to gain a better understanding of the enzyme inhibition that takes place during the biotransformation process. It was determined that an inverse relationship existed between product concentration and H_2O_2 concentration, whereby more styrene oxide was obtained as the H_2O_2 concentration was decreased from 10 mM to 5 mM and lastly 2.5 mM. Figure 6.8 shows that high H_2O_2 concentrations inhibited the enzyme performance by reducing its catalytic activity. The styrene concentration, on the other hand, did not influence the total conversion of the substrate as similar styrene oxide yields were obtained when the substrate concentration was increased from 2.5 mM to 20 mM. It is probable that the styrene concentration may have a less pronounced effect on the enzyme compared to the effect of once-off delivery of H_2O_2, as suggested by the 18% higher residual enzyme activity measured in the presence of styrene only compared to H_2O_2 only (Figure 6.1). This could prematurely eliminate competitive inhibition because the highest substrate concentration (20 mM styrene) did not outcompete the inhibitory effects of the lowest concentration of the H_2O_2 (2.5 mM H_2O_2) (Illanes *et al.*, 2008). The kinetics of this inhibition were therefore modelled to evaluate the type of inhibition that may have occurred.

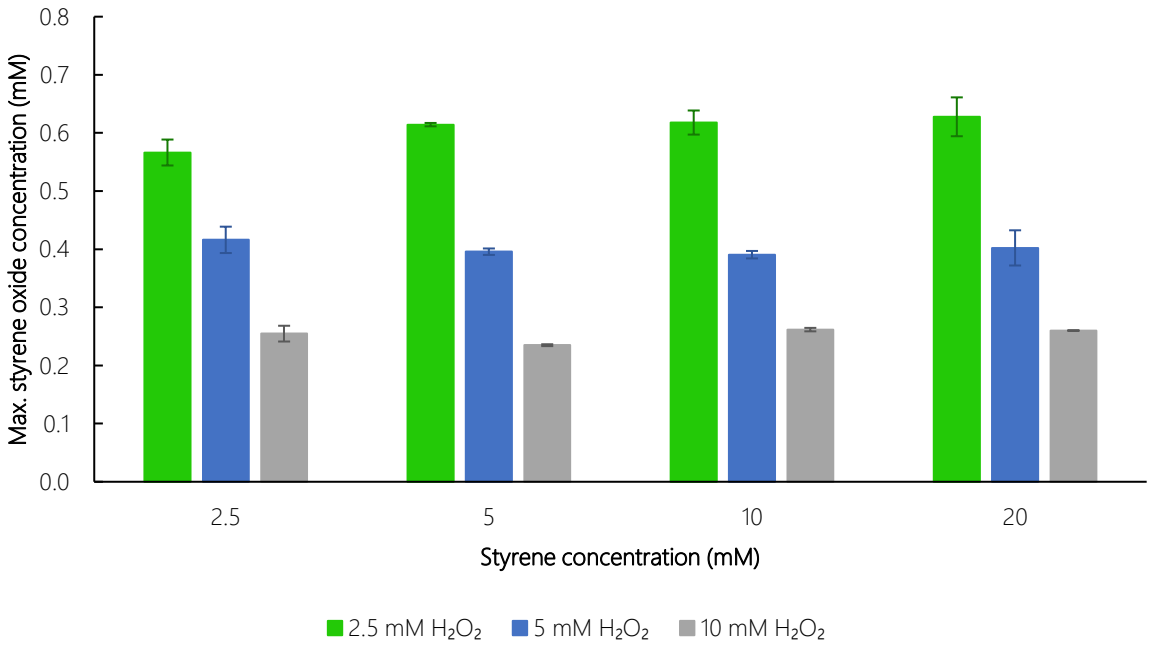

Figure 6.8: The influence of H_2O_2 concentrations in the presence of different initial styrene substrate concentrations. Reaction conditions: 20 ml 100 mM potassium phosphate buffer pH 7.0, 12 U ml^{-1} (NBD) PaDa-I, 20, 10, 5 or 2.5 mM styrene, 10, 5 or 2.5 mM mM H_2O_2 (once-off addition), 200 rpm, 25 °C.

The kinetic parameters were initially determined by constructing graphical representations of the modified Michaelis-Menten mechanisms described in Table 6.3 (refer to Section 2.2.3). From these, it was revealed that the type of inhibition caused by the H_2O_2 on the enzyme was non-competitive inhibition, yielding kinetic parameter of K_M = 0.21 mM, v_{max} = 0.24 mM min^{-1} and K_I = 2.30 mM (Appendix C.5 for detailed calculations). These values were therefore used as a guideline for the non-linear regression analysis on the modified Michaelis-Menten models. The non-linear regression was accompanied by statistical tools (R^2, χ^2, AARD, AIC and BIC) to validate whether the modified Michaelis-Menten model for non-competitive inhibition was indeed the best fit model or whether the competitive or uncompetitive inhibition versions of the model were more suitable for the experimental data.

Table 6.3: Summary of kinetic models that predict enzyme inhibition, where all model constants (I, K_I, K_M, S, v, v_{max}) are defined in the nomenclature

Michaelis-Menten kinetic model	Equation	
Competitive inhibition	$v = \frac{v_{max}[S]}{K_M\left(1+\frac{[I]}{K_I}\right)+[S]}$	(2.4)
Non-competitive inhibition	$v = \frac{v_{max}[S]}{(K_M+[S])\left(1+\frac{[I]}{K_I}\right)}$	(2.5)
Uncompetitive inhibition	$v = \frac{v_{max}[S]}{K_M+[S]\left(1+\frac{[I]}{K_I}\right)}$	(2.6)

The results from the regression of the three models show that the values for K_M were quite low (<0.5 mM) compared to the 20 mM styrene available to the enzyme thereby indicating that there was a strong affinity of the substrate to the enzyme. Despite this high affinity, the substrate transformation was slow as shown by the low v_{max} value <0.2 mM min^{-1} obtained. A similar inhibition constant K_I was obtained across the three inhibition models which implied that approximately <3.75 mM H_2O_2 would be required for the biotransformation of styrene to styrene oxide with minimal inhibition and increased v_{max}. Comparison of the models by statistical analyses, including inspection of the R^2, chi-square and AARD values obtained in Table 6.4, revealed that the non-competitive model was indeed the best fit model for the experimental data. This was further evidenced by the graphical validation of this model relative to experimental data presented in Figure 6.9.

Table 6.4: Preliminary analysis on the inhibition kinetics on the PaDa-I enzyme, where model constants v_{max}, K_M and K_I were determined by non-linear regression

Michaelis-Menten model	Competitive	Non-competitive	Uncompetitive
v_{max} (mM min^{-1})	0.07	0.18	0.17
K_M (mM)	0.06	0.22	0.42
K_I (mM)	3.64	3.75	3.75
R^2	0.30	0.80	0.60
χ^2	<0.10	<0.01	<0.01
AARD (%)	1.50	0.25	0.25
AIC	7.10	2.80	3.90
BIC	-5.28	-5.53	-5.35

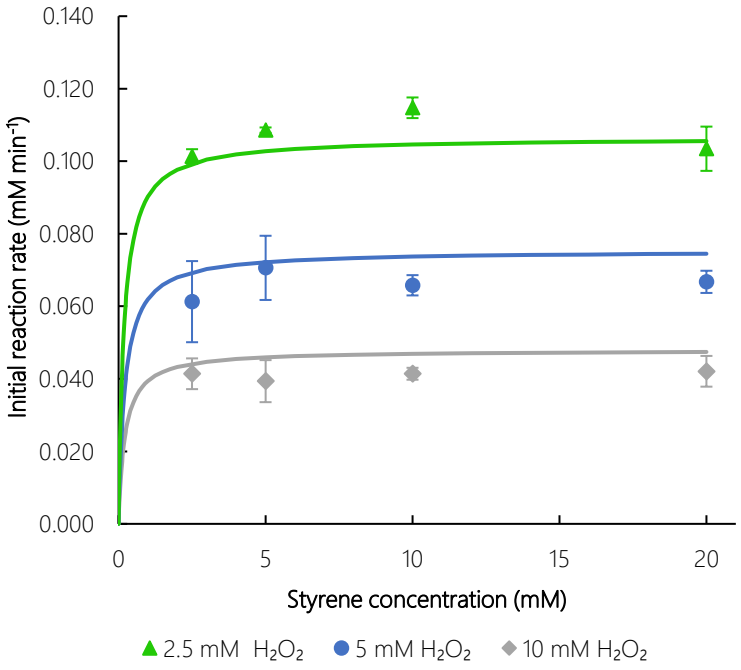

Figure 6.9: The fit of the non-competitive inhibition Michaelis-Menten model to the experimental data showing the influence of H_2O_2 concentrations 2.5 mM (▲), 5 mM (●) and 10 mM (◆) on the biotransformation of styrene. Reaction conditions: 20 ml 100 mM potassium phosphate buffer pH 7.0, 12 U ml^{-1} (NBD) PaDa-I, 20, 10, 5 or 2.5 mM styrene, 10, 5 or 2.5 mM mM H_2O_2, 200 rpm, 25 °C.

According to Illanes *et al*. (2008), non-competitive inhibition occurs when the inhibitor (in this case, H_2O_2) is bound to an allosteric site of the enzyme which potentially distorts the structure of the enzyme making it less effective in catalysing the reaction. This could consolidate the existing knowledge on the catalytic pathway of the PaDa-I enzyme whereby it was proposed that the less reactive intermediate, Compound III, was produced in response to exposure to excess H_2O_2 (Valderrama, 2010). This could explain the reduced styrene oxide concentrations and TONs observed in Figure 6.8 with increasing H_2O_2 concentration. To further validate the non-competitive inhibition model for PaDa- I, it would be necessary to perform extensive analyses to determine the different intermediate enzyme states and/or the products of further decomposition of Compound III by heme bleaching, protein oxidation or unimolecular decay (Valderrama *et al*., 2002).

Taking the kinetic parameters determined from the best fit model into consideration, it was estimated that the turnover rate k_{cat} was 8.22 $mol_{product}$ mol_{enzyme} s^{-1}. From that, the catalytic efficiency (k_{cat}/K_M) was determined to be 3.81 x 10^4 M^{-1} s^{-1} which approached the 7.24 x 10^4 M^{-1} s^{-1} obtained in the hydroxylation of cyclohexane (Peter *et al*., 2014) and an order of magnitude less efficient than the 5.90 x 10^5 M^{-1} s^{-1} achieved in the hydroxylation of ethylbenzene (Kluge *et al*., 2012) by a UPO from *Agrocybe aegerita*. Although this kinetic data shows comparable enzyme performance, improvements can still be made to increase the catalytic efficiency of the PaDa-I enzyme.

6.4 Conclusion

The three methods of H_2O_2 delivery were evaluated in the biotransformation of styrene to produce styrene oxide. It was determined that the enzyme did not produce any product when employing once-off addition of H_2O_2. Stepwise oxidant delivery was more successful, with 0.48 mM styrene oxide being produced over the same reaction time. The product concentration was nearly doubled when the H_2O_2 was delivered in a semi-continuous manner. It was also determined that similar product yields were obtained when the pH of the reaction mixture was changed from pH 7.0 to 8.0. Furthermore, the performance of the enzyme was seen to slightly improve by about 12% when an organic solvent, acetonitrile, was added to the reaction. This could be due to the water miscible solvent improving substrate solubility in the aqueous phase of the reaction, though this would need to be further investigated in future studies.

It was found that both the H_2O_2 as well as the styrene deactivated the enzyme. When the substrates were combined in the reaction mixture for the biotransformation, a severe decrease in enzyme activity was observed where the enzyme lost approximately 90% of its initial activity. This was further emphasized by kinetic parameters obtained from the best fit enzyme deactivation model (two-parameter model) whereby the ratio of the final to initial enzyme specific activity (α_1) was obtained at 0.06 for the stepwise delivery case and 0.07 for the semi-continuous delivery cases. These values imply that there was significant enzyme deactivation as the enzyme activity was decreased to <10% its initial activity. Furthermore, they were substantially lower than the α_1 values 0.37 obtained for H_2O_2 and 0.50 for styrene as sole substrates. The enzyme stability will therefore need to be improved to maximise productivity in order to progress to large scale biotransformations.

Another aspect considered in the biotransformation was the type of inhibition caused by the H_2O_2 on the enzyme. It was determined that non-competitive inhibition occurred. This was likely due to peroxide binding to an allosteric site on the enzyme which potentially distorted the active site thus lowering

styrene oxide production. The inhibition constant K_I was 3.75 mM which implied that significantly less than 20 mM H_2O_2 may be required to minimise inhibition in the biotransformation of styrene. Furthermore, it was deduced that there was a high substrate affinity due to the low K_M value of 0.22 mM, therefore the styrene concentration would need to be reduced from 20 mM, which will likely lead to a decrease in substrate induced enzyme deactivation. The catalytic efficiency of 3.81×10^4 M^{-1} s^{-1} was comparable to some of the literature (Peter *et al.*, 2014); however, there are still opportunities to improve the productivity of this biotransformation. These include lowering the H_2O_2 concentration and considering delivery methods of lower concentrations of styrene.

7 Conclusions and recommendations

The mild oxidation of hydrocarbons remains a great challenge, particularly at industrial scale, due to the low activity of the substrate. Unspecific peroxygenases, like PaDa-I are enzymes that can catalytically convert hydrocarbons to valuable oxygenates using H_2O_2 as the oxidant (Hobisch *et al.*, 2021; Hofrichter *et al.*, 2010; Hofrichter and Ullrich, 2014; Karich *et al.*, 2013; Kluge *et al.*, 2012; Ullrich *et al.*, 2004). These enzymes are highly active and selective. However, rapid inactivation occurs when the enzyme is exposed to high H_2O_2 concentrations. To potentially minimise this deactivation and enhance productivity, studies have shown that a one-pot tandem system combining *in-situ* H_2O_2 generation with the enzyme catalysed biotransformation holds great promise (Churakova *et al.*, 2011; Freakley *et al.*, 2019; Pesic *et al.*, 2019; Tieves *et al.*, 2019; Zhang *et al.*, 2017). There is; however, limited information available in the existing literature on the rate of enzyme deactivation induced by the H_2O_2. The overall objective was to investigate how different H_2O_2 delivery approaches affect enzyme activity and evaluate their impact on the overall enzyme productivity by analysing the catalytic performance and deactivation kinetics.

To address the key research questions posed in Section 2.4.4, the unspecific peroxygenase PaDa-I variant was exposed to H_2O_2 concentrations 10 mM, 20 mM and 40 mM over a 2 h incubation period. The residual enzyme activity was measured over time and it was determined that the enzyme's stability increased with decreasing H_2O_2 concentration. It was observed that the residual enzyme activity was highest at 10 mM H_2O_2 where the enzyme exhibited approximately 60% of its initial activity. This value decreased to 55% at 20 mM H_2O_2 and 50% at 40 mM H_2O_2. These results demonstrated that the enzyme's stability is influenced by high concentrations of H_2O_2.

In an attempt to circumvent the enzyme deactivation, different H_2O_2 delivery methods were investigated including adding all the H_2O_2 (20 mM) at once (once-off addition), adding a small amount of H_2O_2 at regular intervals (stepwise addition) and adding it gradually at a controlled flow rate using a syringe pump (continuous addition). The enzyme was most stable using the stepwise and continuous delivery approaches where the residual enzyme activity was approximately 60% after a 2 h incubation period in the presence of 10 mM H_2O_2. In contrast, the activity obtained using the once-off delivery method was about 50%. It was clear from these results that the H_2O_2 delivery method has an impact on enzyme activity where the PaDa-I enzyme exhibited the least deactivation with a gradual, controlled H_2O_2 delivery approach.

The enzyme stability was further assessed at different temperatures (20 °C, 25 °C and 30 °C) and pH levels (6.0, 7.0 and 8.0) to better understand how these reaction conditions influenced enzyme deactivation. The enzyme was more stable at the lower temperatures 20 °C and 25 °C compared to 30 °C. Furthermore, it was more stable at pH 8.0, followed by pH 7.0 and lastly at pH 6.0. These observations implied that, at higher temperature and lower pH, the protein molecule of the enzyme may have unfolded or lost some of its structural integrity (Bechtold and Panke, 2012). As such, under these conditions, the enzyme would not be effective in biocatalysis.

In the context of styrene biotransformation, a higher conversion was obtained when employing semi-continuous H_2O_2 delivery (5.40%) compared to stepwise H_2O_2 delivery (2.35%). On the other hand, there was no substrate conversion using the once-off delivery method. This demonstrated the importance of the H_2O_2 delivery approach, where more styrene oxide was formed when H_2O_2 was added gradually to the system. Despite the improved product yield, the combination of styrene and H_2O_2 led

to substantial deactivation. Preliminary tests had indicated a 40% activity loss with styrene and ca. 50% loss with H_2O_2, as sole substrates. The enzyme; however, lost >90% of its initial activity in the biotransformation reaction irrespective of the delivery method used. Nevertheless, the residual enzyme activity was approximately 5% higher using the semi-continuous H_2O_2 delivery approach compared to stepwise delivery within the first 4 h of the oxidation reaction. This indicated that, despite the overall deactivation, there was potential to enhance enzyme stability and productivity particularly at the earlier stages of the reaction by employing the semi-continuous delivery as the optimal delivery approach. The delivery rate (0.8 mM H_2O_2 every 1 h) should in future studies be modified such that less H_2O_2 is introduced to the system at either the same interval or less frequent intervals. Such a modification may improve the overall enzyme performance.

An investigation on the kinetics revealed that the two-parameter kinetic model was the most suitable model for determining the enzyme deactivation kinetics. The potential pathway represented by this kinetic model predicted that the enzyme did not undergo complete deactivation, but instead produced less reactive intermediates over time (Henley and Sadana, 1986; Sadana and Henley, 1987a). This is in agreement with the existing knowledge of the enzyme's catalytic pathway, whereby it has been reported that a less reactive enzyme intermediate (Compound III) was formed in the presence of excess H_2O_2 (Hernández-Ruiz *et al.*, 2001; Valderrama, 2010). The deactivation constant k_1 was determined to be 0.18 min^{-1} which was similar to literature values 0.18 min^{-1} (Ramirez-Ramirez *et al.*, 2020), 0.21 min^{-1} and 0.26 min^{-1} (Vidal-Limón *et al.*, 2013). The final to initial enzyme specific activity ratio α_1 decreased from approximately 0.60 - 0.50 with increasing H_2O_2 concentration from 10 mM - 40 mM. The higher α_1 value indicated a higher final enzyme activity at 10 mM H_2O_2, which was in agreement with the experimental observations. Among the various H_2O_2 delivery methods, α_1 was highest with continuous delivery (0.61 - 0.55), followed by stepwise delivery (0.57 - 0.54) and lastly once-off delivery (0.56 - 0.47). This corresponded with the observed enzyme activity, where the enzyme was most stable using the continuous delivery approach. During the biotransformation of styrene, this kinetic parameter α_1 reduced significantly to 0.07 with semi-continuous H_2O_2 addition and 0.06 with stepwise H_2O_2 addition. These low α_1 values indicated the decreased enzyme specific activity to a greater extent by the combination of styrene and H_2O_2. This reduced activity likely influenced the overall catalytic efficiency (3.81×10^4 M^{-1} s^{-1}), which was an order of magnitude lower than that reported in a similar biocatalytic system (Kluge *et al.*, 2012). Further insights on the kinetics of this biotransformation revealed that H_2O_2 behaved as a non-competitive inhibitor. This suggested that H_2O_2 was bound to an allosteric site on the enzyme, which distorted the structure of the enzyme making it less effective for styrene oxidation. Given that the inhibition constant K_I was determined to be 3.75 mM, it may be worthwhile further lowering the H_2O_2 concentration during delivery. This could minimise the effects of the non-competitive inhibition to maintain a more stable and possibly more catalytically active enzyme.

The data presented, analysed and discussed in this thesis confirmed the initially proposed hypothesis that the stability and catalytic performance of the PaDa-I enzyme was indeed enhanced by adding the H_2O_2 at regular intervals or low, controlled flow rates. It was observed that the enzyme was most stable when employing the (semi-)continuous H_2O_2 delivery method and that the product yields for the oxidation of styrene were more than doubled under these conditions. Consequently, there is opportunity to improve biotransformations, such as, styrene to styrene oxide. By decreasing the delivery rate of H_2O_2, higher residual activities may be achieved which could potentially maximise productivity. While falling outside the scope of this study, it is clear that evaluating and implementing different delivery approaches for the organic substrate may further contribute to improved productivity given that styrene was

observed to contribute to enzyme deactivation both as a sole substrate and in combination with H_2O_2. This delivery strategy could also be transferred to existing tandem systems that combine *in-situ* H_2O_2 production with hydrocarbon biotransformation using UPOs. This could potentially improve the stability and performance of current catalytic biotransformation systems. Further to these recommendations, it is advisable to analyse the enzyme deactivation kinetics of such tandem systems to provide guidance in the development of optimisation strategies. Future research should apply these insights to improve the catalytic efficiency and perform a technoeconomic analysis on unspecific peroxygenases used in large scale oxidative biotransformation processes.

References

Afewerki, S., Córdova, A., 2016. Combinations of Aminocatalysts and Metal Catalysts: A Powerful Cooperative Approach in Selective Organic Synthesis. Chem Rev 116, 13512–13570. https://doi.org/10.1021/acs.chemrev.6b00226

Aitken, M.D., 1993. Waste treatment applications of enzymes: opportunities. The Chemical Engineering Journal 52, 49–58. https://doi.org/https://doi.org/10.1016/0300-9467(93)80057-U

Aranda, C., Carro, J., González-Benjumea, A., Babot, E.D., Olmedo, A., Linde, D., Martínez, A.T., Gutiérrez, A., 2021. Advances in enzymatic oxyfunctionalization of aliphatic compounds. Biotechnol Adv 51, 1–19. https://doi.org/10.1016/j.biotechadv.2021.107703

Ayala, M., Torres, E., 2004. Enzymatic activation of alkanes: Constraints and prospective. Appl Catal A Gen 272, 1–13. https://doi.org/10.1016/j.apcata.2004.05.046

Babot, E.D., Del Río, J.C., Kalum, L., Martínez, A.T., Gutierrez, A., 2013. Oxyfunctionalization of Aliphatic Compounds by a Recombinant Peroxygenase From Coprinopsis cinerea. Biotechnol Bioeng 110, 2323–2332. https://doi.org/10.1002/bit.24904/abstract

Bankar, S.B., Bule, M. V., Singhal, R.S., Ananthanarayan, L., 2009. Glucose oxidase - An overview. Biotechnol Adv 27, 489–501. https://doi.org/10.1016/j.biotechadv.2009.04.003

Batra, M.S., Dwivedi, R., Prasad, R., 2019. Recent Developments in Heterogeneous Catalyzed Epoxidation of Styrene to Styrene Oxide. Chemistry Europe 4, 11636–11673. https://doi.org/10.1002/slct.201902396

Bechtold, M., Panke, S., 2012. 7.5 Reaction Engineering of Biotransformations, in: Comprehensive Chirality. Elsevier, pp. 71–100. https://doi.org/10.1016/B978-0-08-095167-6.00705-9

Bell, E.L., Finnigan, W., France, S.P., Green, A.P., Hayes, M.A., Hepworth, L.J., Lovelock, S.L., Niikura, H., Osuna, S., Romero, E., Ryan, K.S., Turner, N.J., Flitsch, S.L., 2021. Biocatalysis. Nature Reviews Methods Primers 1, 1–21. https://doi.org/10.1038/s43586-021-00044-z

Bennett, J.A., Mikheenko, I.P., Deplanche, K., Shannon, I.J., Wood, J., Macaskie, L.E., 2013. Nanoparticles of palladium supported on bacterial biomass: New re-usable heterogeneous catalyst with comparable activity to homogeneous colloidal Pd in the Heck reaction. Appl Catal B 140–141, 700–707. https://doi.org/10.1016/j.apcatb.2013.04.022

Bergman, R.G., 2007. C–H activation. Nature 446, 391–393. https://doi.org/10.1038/446391a

Bernhardt, R., 2006. Cytochromes P450 as versatile biocatalysts. J Biotechnol 124, 128–145. https://doi.org/10.1016/j.jbiotec.2006.01.026

Bhatia, S., 2018. Introduction to enzymes and their applications, in: Introduction to Pharmaceutical Biotechnology, Volume 2. IOP Publishing, pp. 1–29. https://doi.org/10.1088/978-0-7503-1302-5ch1

Blanksby, S.J., Ellison, G.B., 2003. Bond dissociation energies of organic molecules. Acc Chem Res 36, 255–263. https://doi.org/10.1021/ar020230d

Bormann, S., Gomez Baraibar, A., Ni, Y., Holtmann, D., Hollmann, F., 2015. Specific oxyfunctionalisations catalysed by peroxygenases: opportunities, challenges and solutions. Catal Sci Technol 5, 2038–2052. https://doi.org/10.1039/C4CY01477D

Burek, B.O., Bormann, S., Hollmann, F., Bloh, J.Z., Holtmann, D., 2019. Hydrogen peroxide driven biocatalysis. Green Chemistry 21, 3232–3249. https://doi.org/10.1039/c9gc00633h

Burnham, K.P., Anderson, D.R., 2002. Model Selection and Multimodel Inference: A Practical Information-Theoretic Approach, Second Edition. pp. 60–347. https://doi.org/http://dx.doi.org/10.1007/b97636

Cai, D., Tien, M., 1989. On the reactions of lignin peroxidase Compound III (isozyme H8). Biochem Biophys Res Commun 162, 464–469. https://doi.org/10.1016/0006-291X(89)92020-2

Chen, J., Kong, F., Ma, N., Zhao, P., Liu, C., Wang, X., Cong, Z., 2019a. Peroxide-Driven Hydroxylation of Small Alkanes Catalyzed by an Artificial P450BM3 Peroxygenase System. ACS Catal 9, 7350–7355. https://doi.org/10.1021/acscatal.9b02507

Chen, J., Kong, F., Ma, N., Zhao, P., Liu, C., Wang, X., Cong, Z., 2019b. Peroxide-Driven Hydroxylation of Small Alkanes Catalyzed by an Artificial P450BM3 Peroxygenase System. ACS Catal 9, 7350–7355. https://doi.org/10.1021/acscatal.9b02507

Churakova, E., Kluge, M., Ullrich, R., Arends, I., Hofrichter, M., Hollmann, F., 2011. Specific Photobiocatalytic Oxyfunctionalization Reactions. Angewandte Chemie 123, 10904–10907. https://doi.org/10.1002/ange.201105308

Cirino, P.C., Arnold, F.H., 2003. A Self-Sufficient Peroxide-Driven Hydroxylation Biocatalyst. Angewandte Chemie International Edition 42, 3299–3301. https://doi.org/https://doi.org/10.1002/anie.200351434

Cirino, P.C., Arnold, F.H., 2002. Regioselectivity and Activity of Cytochrome P450 BM-3 and Mutant F87A in Reactions Driven by Hydrogen Peroxide. Adv Synth Catal 344, 932–937. https://doi.org/10.1002/1615-4169(200210)344:9<932::AID-ADSC932>3.0.CO;2-M

Clarke, K.G., 2013. Enzymes as biocatalysts, in: Bioprocess Engineering. Elsevier, pp. 75–96. https://doi.org/10.1533/9781782421689.75

Cong, Z., Shoji, O., Kasai, C., Kawakami, N., Sugimoto, H., Shiro, Y., Watanabe, Y., 2015. Activation of Wild-Type Cytochrome P450BM3 by the Next Generation of Decoy Molecules: Enhanced Hydroxylation of Gaseous Alkanes and Crystallographic Evidence. ACS Catal 5, 150–156. https://doi.org/10.1021/cs501592f

Creamer, N.J., Mikheenko, I.P., Yong, P., Deplanche, K., Sanyahumbi, D., Wood, J., Pollmann, K., Merroun, M., Selenska-Pobell, S., Macaskie, L.E., 2007. Novel supported Pd hydrogenation bionanocatalyst for hybrid homogeneous/heterogeneous catalysis. Catal Today 128, 80–87. https://doi.org/10.1016/j.cattod.2007.04.014

Crole, D.A., Freakley, S.J., Edwards, J.K., Hutchings, G.J., 2016. Direct synthesis of hydrogen peroxide in water at ambient temperature. Proceedings of the Royal Society A: Mathematical, Physical and Engineering Sciences 472, 1–8. https://doi.org/10.1098/rspa.2016.0156

Denard, C.A., Hartwig, J.F., Zhao, H., 2013. Multistep one-pot reactions combining biocatalysts and chemical catalysts for asymmetric synthesis. ACS Catal 3, 2856–2864. https://doi.org/10.1021/cs400633a

Denard, C.A., Huang, H., Bartlett, M.J., Lu, L., Tan, Y., Zhao, H., Hartwig, J.F., 2014. Cooperative tandem catalysis by an organometallic complex and a metalloenzyme. Angewandte Chemie - International Edition 53, 465–469. https://doi.org/10.1002/anie.201305778

Deplanche, K., Bennett, J.A., Mikheenko, I.P., Omajali, J., Wells, A.S., Meadows, R.E., Wood, J., Macaskie, L.E., 2014. Catalytic activity of biomass-supported Pd nanoparticles: Influence of the biological component in catalytic efficacy and potential application in "green" synthesis of fine chemicals and pharmaceuticals. Appl Catal B 147, 651–665. https://doi.org/10.1016/j.apcatb.2013.09.045

Dezvarei, S., Shoji, O., Watanabe, Y., Bell, S.G., 2019. The effect of decoy molecules on the activity of the P450Bm3 holoenzyme and a heme domain peroxygenase variant. Catal Commun 124, 97–102. https://doi.org/10.1016/j.catcom.2019.03.004

Dong, J., Fernández-Fueyo, E., Hollmann, F., Paul, C.E., Pesic, M., Schmidt, S., Wang, Y., Younes, S., Zhang, W., 2018a. Biocatalytic Oxidation Reactions: A Chemist's Perspective. Angewandte Chemie 130, 9380–9404. https://doi.org/10.1002/ange.201800343

Dong, J., Fernández-Fueyo, E., Hollmann, F., Paul, C.E., Pesic, M., Schmidt, S., Wang, Y., Younes, S., Zhang, W., 2018b. Biokatalytische Oxidationsreaktionen – aus der Sicht eines Chemikers. Angewandte Chemie 130, 9380–9404. https://doi.org/10.1002/ange.201800343

Doran, P.M., 1995. Homogeneous Reactions, in: Bioprocess Engineering Principles. Elsevier, London, pp. 257–295. https://doi.org/10.1016/B978-0-12-220855-3.X5000-7

Edwards, J.K., Freakley, S.J., Carley, A.F., Kiely, C.J., Hutchings, G.J., 2014. Strategies for designing supported gold-palladium bimetallic catalysts for the direct synthesis of hydrogen peroxide. Acc Chem Res 47, 845–854. https://doi.org/10.1021/ar400177c

Edwards, J.K., Thomas, A., Solsona, B.E., Landon, P., Carley, A.F., Hutchings, G.J., 2007. Comparison of supports for the direct synthesis of hydrogen peroxide from H2 and O2 using Au-Pd catalysts. Catal Today 122, 397–402. https://doi.org/10.1016/j.cattod.2007.01.046

Fakhroleslam, M., Sadrameli, S.M., 2020. Thermal Cracking of Hydrocarbons for the Production of Light Olefins; A Review on Optimal Process Design, Operation, and Control. Ind Eng Chem Res 59, 12288–12303. https://doi.org/10.1021/acs.iecr.0c00923

Ferreira, R. da G., Azzoni, A.R., Freitas, S., 2018. Techno-economic analysis of the industrial production of a low-cost enzyme using E. coli: the case of recombinant β-glucosidase. Biotechnol Biofuels 11, 81–94. https://doi.org/10.1186/s13068-018-1077-0

Fogg, D.E., dos Santos, E.N., 2004. Tandem catalysis: A taxonomy and illustrative review. Coord Chem Rev 248, 2365–2379. https://doi.org/10.1016/j.ccr.2004.05.012

Foulkes, J.M., Deplanche, K., Sargent, F., Macaskie, L.E., Lloyd, J.R., 2016. A novel aerobic mechanism for reductive palladium biomineralization and recovery by escherichia coli. Geomicrobiol J 33, 230–236. https://doi.org/10.1080/01490451.2015.1069911

Franke, R., Selent, D., Börner, A., 2012. Applied hydroformylation. Chem Rev 112, 5675–5732. https://doi.org/10.1021/cr3001803

Freakley, S.J., Kochius, S., van Marwijk, J., Fenner, C., Lewis, R.J., Baldenius, K., Marais, S.S., Opperman, D.J., Harrison, S.T.L., Alcalde, M., Smit, M.S., Hutchings, G.J., 2019. A chemo-enzymatic oxidation cascade to activate C–H bonds with in situ generated H2O2. Nat Commun 10, 1–8. https://doi.org/10.1038/s41467-019-12120-w

Glieder, A., Farinas, E.T., Arnold, F.H., 2002. Laboratory evolution of a soluble, self-sufficient, highly active alkane hydroxylase. Nat Biotechnol 20, 1135–1139. https://doi.org/10.1038/nbt744

Gröger, H., Hummel, W., 2014. Combining the "two worlds" of chemocatalysis and biocatalysis towards multi-step one-pot processes in aqueous media. Curr Opin Chem Biol 19, 171–179. https://doi.org/10.1016/j.cbpa.2014.03.002

Groves, J.T., Myers, R.S., 1983. Catalytic asymmetric epoxidations with chiral iron porphyrins. J Am Chem Soc 105, 5791–5796. https://doi.org/10.1021/ja00356a016

Guengerich, F.P., Waterman, M.R., Egli, M., 2016. Recent Structural Insights into Cytochrome P450 Function. Trends Pharmacol Sci 37, 625–640. https://doi.org/10.1016/j.tips.2016.05.006

Gutiérrez, A., Babot, E.D., Ullrich, R., Hofrichter, M., Martínez, A.T., del Río, J.C., 2011a. Regioselective oxygenation of fatty acids, fatty alcohols and other aliphatic compounds by a basidiomycete heme-thiolate peroxidase. Arch Biochem Biophys 514, 33–43. https://doi.org/10.1016/j.abb.2011.08.001

Gutiérrez, A., Babot, E.D., Ullrich, R., Hofrichter, M., Martínez, A.T., del Río, J.C., 2011b. Regioselective oxygenation of fatty acids, fatty alcohols and other aliphatic compounds by a basidiomycete heme-thiolate peroxidase. Arch Biochem Biophys 514, 33–43. https://doi.org/10.1016/j.abb.2011.08.001

Hammerer, L., Winkler, C.K., Kroutil, W., 2018. Regioselective Biocatalytic Hydroxylation of Fatty Acids by Cytochrome P450s. Catal Letters 148, 787–812. https://doi.org/10.1007/s10562-017-2273-4

Henley, J.P., Sadana, A., 1986. Deactivation theory. Biotechnol Bioeng 28, 1277–1285. https://doi.org/10.1002/bit.260280821

Hernández-Ruiz, J., Arnao, M.B., Hiner, A.N.P., Garcia-Canovas, F., Acosta, M., 2001. Catalase-like activity of horseradish peroxidase: relationship to enzyme inactivation by H2O2. Biochemical Journal 354, 107–114. https://doi.org/10.1042/bj3540107

Hildebrand, F., Lütz, S., 2009. Stable electroenzymatic processes by catalyst separation. Chemistry - A European Journal 15, 4998–5001. https://doi.org/10.1002/chem.200900219

Hobisch, M., Holtmann, D., Gomez de Santos, P., Alcalde, M., Hollmann, F., Kara, S., 2021. Recent developments in the use of peroxygenases – Exploring their high potential in selective oxyfunctionalisations. Biotechnol Adv 51, 1–13. https://doi.org/10.1016/j.biotechadv.2020.107615

Hodgman, C.E., Jewett, M.C., 2012. Cell-free synthetic biology: Thinking outside the cell. Metab Eng 14, 261–269. https://doi.org/10.1038/jid.2014.371

Hofrichter, M., Ullrich, R., 2014. Oxidations catalyzed by fungal peroxygenases. Curr Opin Chem Biol 19, 116–125. https://doi.org/10.1016/j.cbpa.2014.01.015

Hofrichter, M., Ullrich, R., Pecyna, M.J., Liers, C., Lundell, T., 2010. New and classic families of secreted fungal heme peroxidases. Appl Microbiol Biotechnol. https://doi.org/10.1007/s00253-010-2633-0

Hollmann, F., Arends, I.W.C.E., Buehler, K., Schallmey, A., Bühler, B., 2011. Enzyme-mediated oxidations for the chemist. Green Chemistry 13, 226–265. https://doi.org/10.1039/c0gc00595a

Hosseinkhani, B., Søbjerg, L.S., Rotaru, A.E., Emtiazi, G., Skrydstrup, T., Meyer, R.L., 2012. Microbially supported synthesis of catalytically active bimetallic Pd-Au nanoparticles. Biotechnol Bioeng 109, 45–52. https://doi.org/10.1002/bit.23293

Hrycay, E.G., Bandiera, S.M., 2012. The monooxygenase, peroxidase, and peroxygenase properties of cytochrome P450. Arch Biochem Biophys 522, 71–89. https://doi.org/10.1016/j.abb.2012.01.003

Illanes, A., Altamirano, C., Wilson, L., 2008. Homogeneous Enzyme Kinetics, in: Enzyme Biocatalysis Principles and Applications. Springer, Dordrecht, pp. 107–151. https://doi.org/10.1017/CBO9781107415324.004

Jahangiri, H., Bennett, J., Mahjoubi, P., Wilson, K., Gu, S., 2014. A review of advanced catalyst development for Fischer-Tropsch synthesis of hydrocarbons from biomass derived syn-gas. Catal Sci Technol 4, 2210–2229. https://doi.org/10.1039/c4cy00327f

Jeffery, G.H., Basset, J., Mendham, J., Denney, R.C., 1989. Oxidations and Reduction Processes involving Iodine: Iodometric Titrations, in: Vogel's Textbook of Quantitative Chemical Analysis. pp. 384–393. https://doi.org/https://doi.org/10.1016/0160-9327(90)90087-8

Karich, A., Kluge, M., Ullrich, R., Hofrichter, M., 2013. Benzene oxygenation and oxidation by the peroxygenase of Agrocybe aegerita. AMB Express 3, 1–8. https://doi.org/10.1186/2191-0855-3-5

Karich, A., Scheibner, K., Ullrich, R., Hofrichter, M., 2016. Exploring the catalase activity of unspecific peroxygenases and the mechanism of peroxide-dependent heme destruction. J Mol Catal B Enzym 134, 238–246. https://doi.org/10.1016/j.molcatb.2016.10.014

Khodakov, A.Y., Chu, W., Fongarland, P., 2007. Advances in the development of novel cobalt Fischer-Tropsch catalysts for synthesis of long-chain hydrocarbons and clean fuels. Chem Rev 107, 1692–1744. https://doi.org/10.1021/cr050972v

Kluge, M., Ullrich, R., Scheibner, K., Hofrichter, M., 2012. Stereoselective benzylic hydroxylation of alkylbenzenes and epoxidation of styrene derivatives catalyzed by the peroxygenase of Agrocybe aegerita. Green Chemistry 14, 440–446. https://doi.org/10.1039/c1gc16173c

Krest, C.M., Onderko, E.L., Yosca, T.H., Calixto, J.C., Karp, R.F., Livada, J., Rittle, J., Green, M.T., 2013. Reactive Intermediates in Cytochrome P450 Catalysis. Journal of Biological Chemistry 288, 17074–17081. https://doi.org/10.1074/jbc.R113.473108

Landon, P., Collier, P.J., Carley, A.F., Chadwick, D., Papworth, A.J., Burrows, A., Kiely, C.J., Hutchings, G.J., 2003. Direct synthesis of hydrogen peroxide from H2 and O2 using Pd and Au catalysts. Physical Chemistry Chemical Physics 5, 1917–1923. https://doi.org/10.1039/b211338b

Li, X., Xu, L., Wang, G., Zhang, H., Yan, Y., 2013. Conformation studies on Burkholderia cenocepacia lipase via resolution of racemic 1-phenylethanol in non-aqueous medium and its process optimization. Process Biochemistry 48, 1905–1913. https://doi.org/10.1016/j.procbio.2013.09.001

Lundemo, M.T., Woodley, J.M., 2015. Guidelines for development and implementation of biocatalytic P450 processes. Appl Microbiol Biotechnol 99, 2465–2483. https://doi.org/10.1007/s00253-015-6403-x

Ma, N., Chen, Z., Chen, Jie, Chen, Jingfei, Wang, C., Zhou, H., Yao, L., Shoji, O., Watanabe, Y., Cong, Z., 2018. Dual-Functional Small Molecules for Generating an Efficient Cytochrome P450BM3 Peroxygenase. Angewandte Chemie 130, 7754–7759. https://doi.org/10.1002/ange.201801592

Mano, N., 2019. Engineering glucose oxidase for bioelectrochemical applications. Bioelectrochemistry 128, 218–240. https://doi.org/10.1016/j.bioelechem.2019.04.015

Maurer, S.C., Kühnel, K., Kaysser, L.A., Eiben, S., Schmid, R.D., Urlacher, V.B., 2005. Catalytic hydroxylation in biphasic systems using CYP102A1 mutants. Adv Synth Catal 347, 1090–1098. https://doi.org/10.1002/adsc.200505044

Mckenna, R., Pugh, S., Thompson, B., Nielsen, D.R., 2013. Microbial production of the aromatic building-blocks (S)-styrene oxide and (R)-1,2-phenylethanediol from renewable resources. Biotechnol J 8, 1465–1475. https://doi.org/10.1002/biot.201300035

Mireles, R., Ramirez-Ramirez, J., Alcalde, M., Ayala, M., 2021. Ether Oxidation by an Evolved Fungal Heme-Peroxygenase: Insights into Substrate Recognition and Reactivity. J. Fungi 7, 608. https://doi.org/10.3390/jof7080608

Molina-Espeja, P., Garcia-Ruiz, E., Gonzalez-Perez, D., Ullrich, R., Hofrichter, M., Alcalde, M., 2014. Directed Evolution of Unspecific Peroxygenase from Agrocybe aegerita. Appl Environ Microbiol 80, 3496–3507. https://doi.org/10.1128/AEM.00490-14

Molina-Espeja, P., Ma, S., Mate, D.M., Ludwig, R., Alcalde, M., 2015. Tandem-yeast expression system for engineering and producing unspecific peroxygenase. Enzyme Microb Technol 73–74, 29–33. https://doi.org/10.1016/j.enzmictec.2015.03.004

Munro, A.W., Girvan, H.M., Mason, A.E., Dunford, A.J., McLean, K.J., 2013. What makes a P450 tick? Trends Biochem Sci 38, 140–150. https://doi.org/10.1016/j.tibs.2012.11.006

Munro, A.W., McLean, K.J., Grant, J.L., Makris, T.M., 2018. Structure and function of the cytochrome P450 peroxygenase enzymes. Biochem Soc Trans 46, 183–196. https://doi.org/10.1042/BST20170218

Musser, M.T., 2011. Cyclohexanol and Cyclohexanone. Ullmann's Encyclopedia of Industrial chemistry 10, 673–710. https://doi.org/10.1002/14356007.a08

Nagababu, E., Rifkind, J.M., 2004. Heme Degradation by Reactive Oxygen Species. Antioxid Redox Signal 6, 967–978. https://doi.org/10.1089/ars.2004.6.967

Ni, Y., Fernández-Fueyo, E., Baraibar, A.G., Ullrich, R., Hofrichter, M., Yanase, H., Alcalde, M., van Berkel, W.J.H., Hollmann, F., 2016. Peroxygenase-Catalyzed Oxyfunctionalization Reactions Promoted by the Complete Oxidation of Methanol. Angewandte Chemie 128, 809–812. https://doi.org/10.1002/ange.201507881

Olaofe, O.A., Fenner, C.J., Gudiminchi, R., Smit, M.S., Harrison, S.T., 2013. The influence of microbial physiology on biocatalyst activity and efficiency in the terminal hydroxylation of n-octane using

Escherichia coli expressing the alkane hydroxylase, CYP153A6. Microb Cell Fact 12, 1–12. https://doi.org/10.1186/1475-2859-12-8

O'Reilly, E., Köhler, V., Flitsch, S.L., 2011. Cytochromes P450 as useful biocatalysts: Addressing the limitations. Chemical Communications 47, 2490–2501. https://doi.org/10.1039/c0cc03165h

Pesic, M., Willot, S.J.P., Fernández-Fueyo, E., Tieves, F., Alcalde, M., Hollmann, F., 2019. Multienzymatic in situ hydrogen peroxide generation cascade for peroxygenase-catalysed oxyfunctionalisation reactions. Zeitschrift fur Naturforschung - Section C Journal of Biosciences 74, 101–104. https://doi.org/10.1515/znc-2018-0137

Peter, S., Karich, A., Ullrich, R., Gröbe, G., Scheibner, K., Hofrichter, M., 2014. Enzymatic one-pot conversion of cyclohexane into cyclohexanone: Comparison of four fungal peroxygenases. J Mol Catal B Enzym 103, 47–51. https://doi.org/10.1016/j.molcatb.2013.09.016

Peter, S., Kinne, M., Wang, X., Ullrich, R., Kayser, G., Groves, J.T., Hofrichter, M., 2011. Selective hydroxylation of alkanes by an extracellular fungal peroxygenase. FEBS Journal 278, 3667–3675. https://doi.org/10.1111/j.1742-4658.2011.08285.x

Polizzi, K.M., Bommarius, A.S., Broering, J.M., Chaparro-Riggers, J.F., 2007. Stability of biocatalysts. Curr Opin Chem Biol 11, 220–225. https://doi.org/10.1016/j.cbpa.2007.01.685

Poraj-Kobielska, M., Kinne, M., Ullrich, R., Scheibner, K., Hofrichter, M., 2012. A spectrophotometric assay for the detection of fungal peroxygenases. Anal Biochem 421, 327–329. https://doi.org/10.1016/j.ab.2011.10.009

Puértolas, B., Hill, A.K., García, T., Solsona, B., Torrente-Murciano, L., 2015. In-situ synthesis of hydrogen peroxide in tandem with selective oxidation reactions: A mini-review. Catal Today 248, 115–127. https://doi.org/10.1016/j.cattod.2014.03.054

Punekar, N.S., 2018. Elucidation of Kinetic Mechanisms, in: ENZYMES: Catalysis, Kinetics and Mechanisms. Springer Singapore, Singapore, pp. 137–274. https://doi.org/10.1007/978-981-13-0785-0

Pyser, J.B., Chakrabarty, S., Romero, E.O., Narayan, A.R.H., 2021. State-of-the-Art Biocatalysis. ACS Cent Sci 7, 1105–1116. https://doi.org/10.1021/acscentsci.1c00273

Ramirez-Ramirez, J., Martin-Diaz, J., Pastor, N., Alcalde, M., Ayala, M., 2020. Exploring the role of phenylalanine residues in modulating the flexibility and topography of the active site in the peroxygenase variant pada-i. Int J Mol Sci 21, 1–15. https://doi.org/10.3390/ijms21165734

Rolf, J., Rosenthal, K., Lütz, S., 2019. Application of Cell-Free Protein Synthesis for Faster Biocatalyst Development. Catalysts 9, 1–18. https://doi.org/10.3390/catal9020190

Sadana, A., Henley, J.P., 1987a. Single-step unimolecular non-first-order enzyme deactivation kinetics. Biotechnol Bioeng 30, 717–723. https://doi.org/10.1002/bit.260300604

Sadana, A., Henley, J.P., 1987b. Analysis of Enzyme Deactivations by a Series-Type Mechanism:. Ann N Y Acad Sci 501, 73–79. https://doi.org/10.1111/j.1749-6632.1987.tb45687.x

Samanta, C., 2008. Direct synthesis of hydrogen peroxide from hydrogen and oxygen: An overview of recent developments in the process. Appl Catal A Gen 350, 133–149. https://doi.org/10.1016/j.apcata.2008.07.043

Sato, H., Hummel, W., Gröger, H., 2015. Cooperative Catalysis of Noncompatible Catalysts through Compartmentalization: Wacker Oxidation and Enzymatic Reduction in a One-Pot Process in Aqueous Media. Angewandte Chemie 127, 4570–4574. https://doi.org/10.1002/ange.201409590

Schrewe, M., Julsing, M.K., Bühler, B., Schmid, A., 2013. Whole-cell biocatalysis for selective and productive C–O functional group introduction and modification. Chem Soc Rev 42, 6346–6377. https://doi.org/10.1039/c3cs60011d

Sheldon, R.A., Woodley, J.M., 2018. Role of Biocatalysis in Sustainable Chemistry. Chem Rev 118, 801–838. https://doi.org/10.1021/acs.chemrev.7b00203

Soussan, L., Pen, N., Belleville, M.-P., Marcano, J.S., Paolucci-Jeanjean, D., 2016. Alkane biohydroxylation: Interests, constraints and future developments. J Biotechnol 222, 117–142. https://doi.org/10.1016/j.jbiotec.2016.02.007

Stenner, A., Lewis, R.J., Brehm, J., Qin, T., López-Martín, Á., Morgan, D.J., Davies, T.E., Chen, L., Liu, X., Hutchings, G.J., 2023. Chemo-Enzymatic One-Pot Oxidation of Cyclohexane via in-situ H2O2 Production over Supported AuPdPt Catalysts. ChemCatChem 15, 1–12. https://doi.org/10.1002/cctc.202300162

Strelec, I., Crevar, B., Kovac, T., Bilic Rajs, B., Primorac, L., Flanjak, I., 2018. Glucose oxidase activity and hydrogen peroxide accumulation in Croatian honeys. Croatian Journal of Food Science and Technology 10, 33–41. https://doi.org/10.17508/CJFST.2018.10.1.06

Tieves, F., Willot, S.J., van Schie, M.M.C.H., Rauch, M.C.R., Younes, S.H.H., Zhang, W., Dong, J., Gomez de Santos, P., Robbins, J.M., Bommarius, B., Alcalde, M., Bommarius, A.S., Hollmann, F., 2019. Formiat-Oxidase (FOx) aus *Aspergillus oryzae*: ein Katalysator für verschiedene H_2O_2-abhängige biokatalytische Oxidationen. Angewandte Chemie 131, 7955–7959. https://doi.org/10.1002/ange.201902380

Truppo, M.D., 2017. Biocatalysis in the Pharmaceutical Industry: The Need for Speed. ACS Med Chem Lett 8, 476–480. https://doi.org/10.1021/acsmedchemlett.7b00114

Tufvesson, P., Lima-Ramos, J., Nordblad, M., Woodley, J.M., 2011. Guidelines and cost analysis for catalyst production in biocatalytic processes. Org Process Res Dev 15, 266–274. https://doi.org/10.1021/op1002165

Ullrich, R., Nüske, J., Scheibner, K., Spantzel, J., Hofrichter, M., 2004. Novel haloperoxidase from the agaric basidiomycete Agrocybe aegerita oxidizes aryl alcohols and aldehydes. Appl Environ Microbiol 70, 4575–4581. https://doi.org/10.1128/AEM.70.8.4575-4581.2004

Urlacher, V.B., Girhard, M., 2019. Cytochrome P450 Monooxygenases in Biotechnology and Synthetic Biology. Trends Biotechnol 37, 882–897. https://doi.org/10.1016/j.tibtech.2019.01.001

Valderrama, B., 2010. Deactivation of hemeperoxidases by hydrogen peroxide: Focus on compound III, in: Biocatalysis Based on Heme Peroxidases: Peroxidases as Potential Industrial Biocatalysts. Springer Berlin Heidelberg, pp. 291–304. https://doi.org/10.1007/978-3-642-12627-7_11

Valderrama, B., Ayala, M., Vazquez-Duhalt, R., 2002. Suicide Inactivation of Peroxidases and the Challenge of Engineering More Robust Enzymes. Chem Biol 9, 555–565. https://doi.org/https://doi.org/10.1016/S1074-5521(02)00149-7

Vidal-Limón, A., Águila, S., Ayala, M., Batista, C. V., Vazquez-Duhalt, R., 2013. Peroxidase activity stabilization of cytochrome P450BM3 by rational analysis of intramolecular electron transfer. J Inorg Biochem 122, 18–26. https://doi.org/10.1016/j.jinorgbio.2013.01.009

Waley, S.G., 1991. The kinetics of substrate-induced inactivation. Biochem. J 279, 87–94. https://doi.org/https://doi.org/10.1042/bj2790087

Wang, X., Ullrich, R., Hofrichter, M., Groves, J.T., 2015. Heme-thiolate ferryl of aromatic peroxygenase is basic and reactive. Proc Natl Acad Sci U S A 112, 3686–3691. https://doi.org/10.1073/pnas.1503340112

Wasilke, J.-C., Obrey, S.J., Baker, R.T., Bazan, G.C., 2005. Concurrent Tandem Catalysis. Chem Rev 105, 1001–1020. https://doi.org/10.1021/cr020018n

Westphal, A.H., Berkel, W.J.H., 2021. Techniques for Enzyme Purification, in: Biocatalysis for Practitioners. Wiley, pp. 1–31. https://doi.org/10.1002/9783527824465.ch1

Whitehouse, C.J.C., Bell, S.G., Wong, L.-L., 2012. P450 BM3 (CYP102A1): connecting the dots. Chem. Soc. Rev. 41, 1218–1260. https://doi.org/10.1039/C1CS15192D

Wilbers, D., Brehm, J., Lewis, R.J., van Marwijk, J., Davies, T.E., Morgan, D.J., Opperman, D.J., Smit, M.S., Alcalde, M., Kotsiopoulos, A., Harrison, S.T.L., Hutchings, G.J., Freakley, S.J., 2021. Controlling product selectivity with nanoparticle composition in tandem chemo-biocatalytic styrene oxidation. Green Chemistry 23, 4170–4180. https://doi.org/10.1039/d0gc04320f

Winkler, C.K., Schrittwieser, J.H., Kroutil, W., 2021. Power of Biocatalysis for Organic Synthesis. ACS Cent Sci 7, 55–71. https://doi.org/10.1021/acscentsci.0c01496

Woodley, J.M., 2008. New opportunities for biocatalysis: making pharmaceutical processes greener. Trends Biotechnol. https://doi.org/10.1016/j.tibtech.2008.03.004

Yi, D., Bayer, T., Badenhorst, C.P.S., Wu, S., Doerr, M., Höhne, M., Bornscheuer, U.T., 2021. Recent trends in biocatalysis. Chem Soc Rev 50, 8003–8049. https://doi.org/10.1039/d0cs01575j

Zhang, W., Burek, B.O., Fernández-Fueyo, E., Alcalde, M., Bloh, J.Z., Hollmann, F., 2017. Selective Activation of C−H Bonds in a Cascade Process Combining Photochemistry and Biocatalysis. Angewandte Chemie - International Edition 56, 15451–15455. https://doi.org/10.1002/anie.201708668

Zhu, J., Wood, J., Deplanche, K., Mikheenko, I., Macaskie, L.E., 2016. Selective hydrogenation using palladium bioinorganic catalyst. Appl Catal B 199, 108–122. https://doi.org/10.1016/j.apcatb.2016.05.060

8 Appendices

Appendix A

Appendix A.1: Standard curves for styrene and styrene oxide

Known concentrations of styrene and styrene oxide (analytic standards) were analysed by the Varian GC. The retention times of the analytes, including the solvent ethyl acetate and internal standard 1-decanol are highlighted in Table 8.1. The relative area was calculated as the ratio of the peak area of the analyte to the peak area of 1-decanol, and this was used to develop the standard curves in Figure 8.1. The response factors for styrene and styrene oxide were 0.0477 and 0.0413, respectively.

Table 8.1: The retention times for the analytes detected by GC analysis

Analyte	Retention time (min)
Ethyl acetate	3.8
Styrene	8.9
Styrene oxide	18.9
1-decanol	35.8

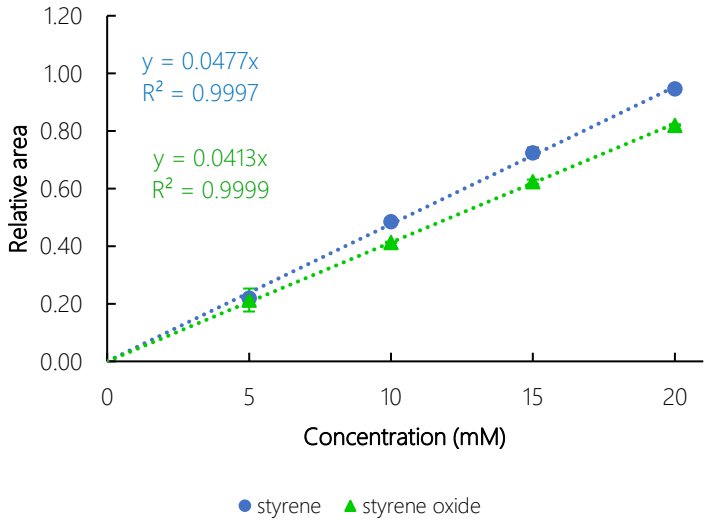

Figure 8.1: Standard curves for styrene and styrene oxide after GC analysis

Appendix B

Appendix B.1: Enzyme stability at different reaction conditions

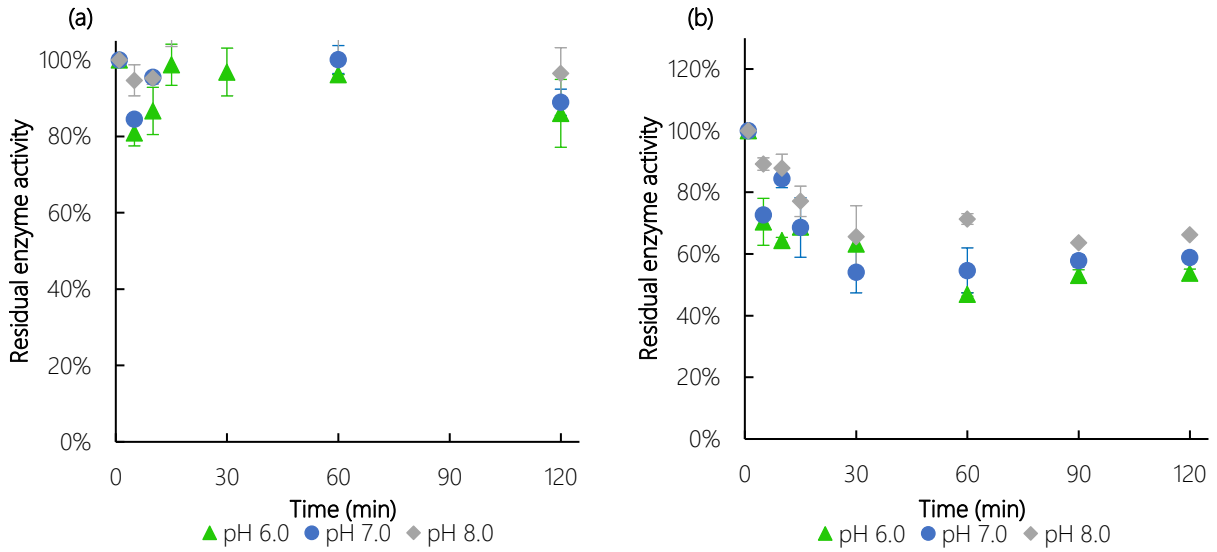

Figure 8.2: The raw data showing the residual peroxygenase activity of PaDa-I in the absence (a) and presence (b) of 20 mM H_2O_2 once-off addition at pH 6 (▲), pH 7 (●) and pH 8 (◆). Reaction conditions: 20 ml 100 mM potassium phosphate buffer, 1.7 U ml^{-1} (NBD) PaDa-I, 200 rpm, 25 °C.

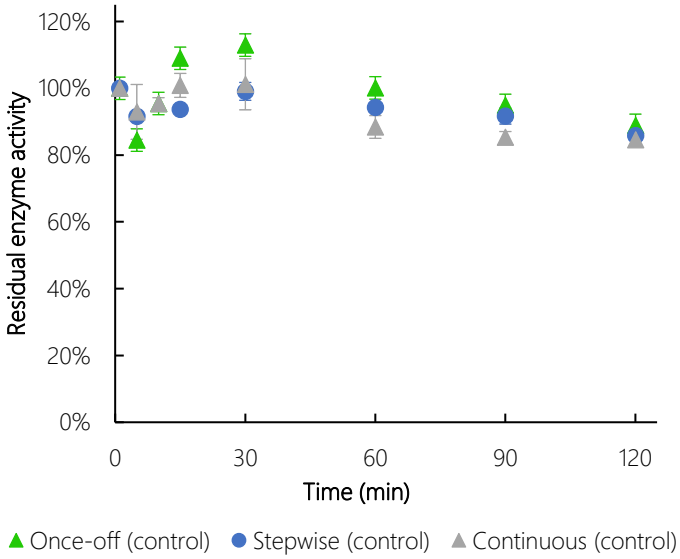

Figure 8.3: The raw data showing the residual peroxygenase activity of the PaDa-I enzyme in the absence of hydrogen peroxide, using delivery methods once-off (▲), stepwise (●) and continuous (◆) addition of potassium phosphate buffer pH 7. Reaction conditions: 20 ml 100 mM potassium phosphate buffer pH 7.0, 1.7 U ml^{-1} (NBD) PaDa-I, 200 rpm, 25 °C.

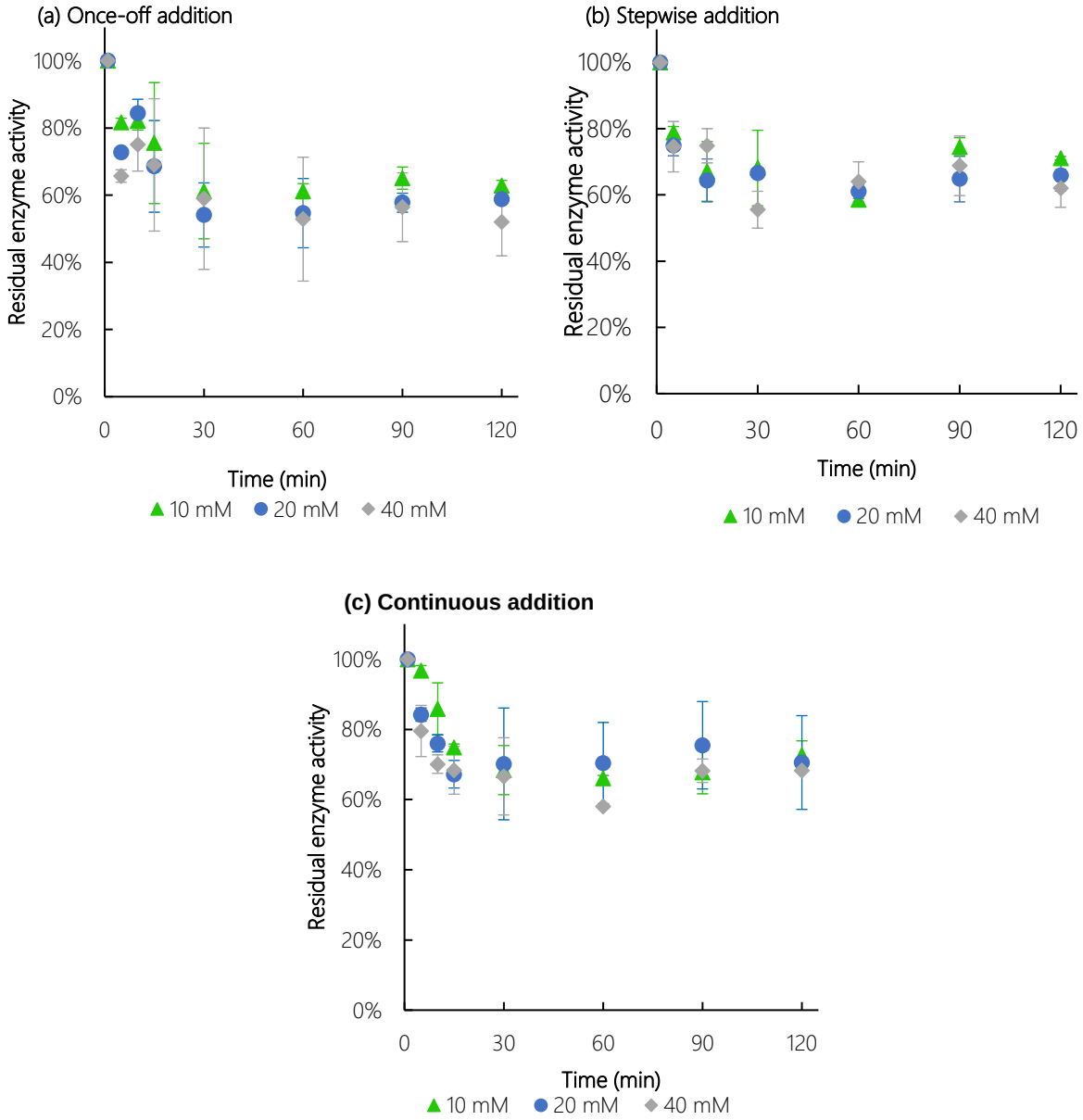

Figure 8.4: The raw data showing the effect of H_2O_2 delivery systems (a) once-off, (b) stepwise and (c) continuous addition and H_2O_2 concentrations 10 mM (▲), 20 mM (●) and 40 mM (◆) on the residual peroxygenase activity of PaDa-I enzyme. Reaction conditions: 20 ml 100 mM potassium phosphate buffer pH 7, 1.7 U ml^{-1} (NBD) PaDa-I, 20 mM H_2O_2, 200 rpm, 25 °C.

Appendix B.2: pH profiles for the enzyme studies at different reaction conditions

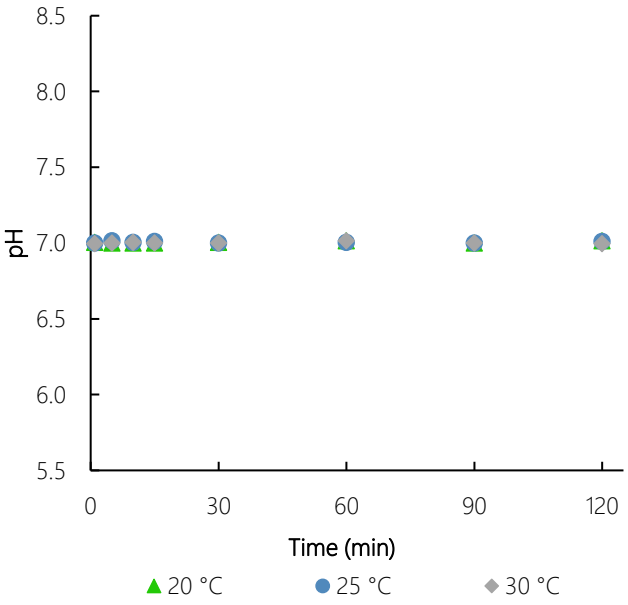

Figure 8.5: The pH profiles of the PaDa-I enzyme/buffer reaction mixture for temperature studies at 20 °C (▲), 25 °C (●), 30 °C (◆). Reaction conditions: 20 ml 100 mM potassium phosphate buffer pH 7.0, 1.7 U ml^{-1} (NBD) PaDa-I, 20 mM H_2O_2 (once-off addition), 200 rpm.

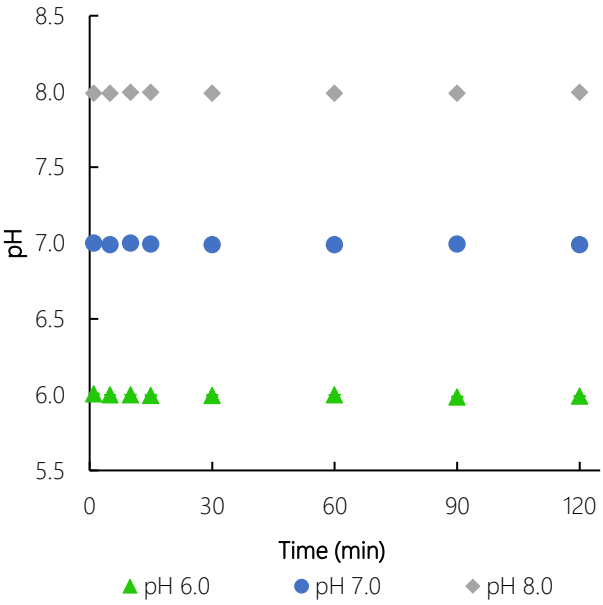

Figure 8.6: The pH profiles of the PaDa-I enzyme/buffer reaction mixture for the pH studies at pH 6.0 (▲), pH 7.0 (●), pH 8.0 (◆). Reaction conditions: 20 ml 100 mM potassium phosphate buffer, 1.7 U ml^{-1} (NBD) PaDa-I, 20 mM H_2O_2 (once-off addition), 200 rpm, 25 °C

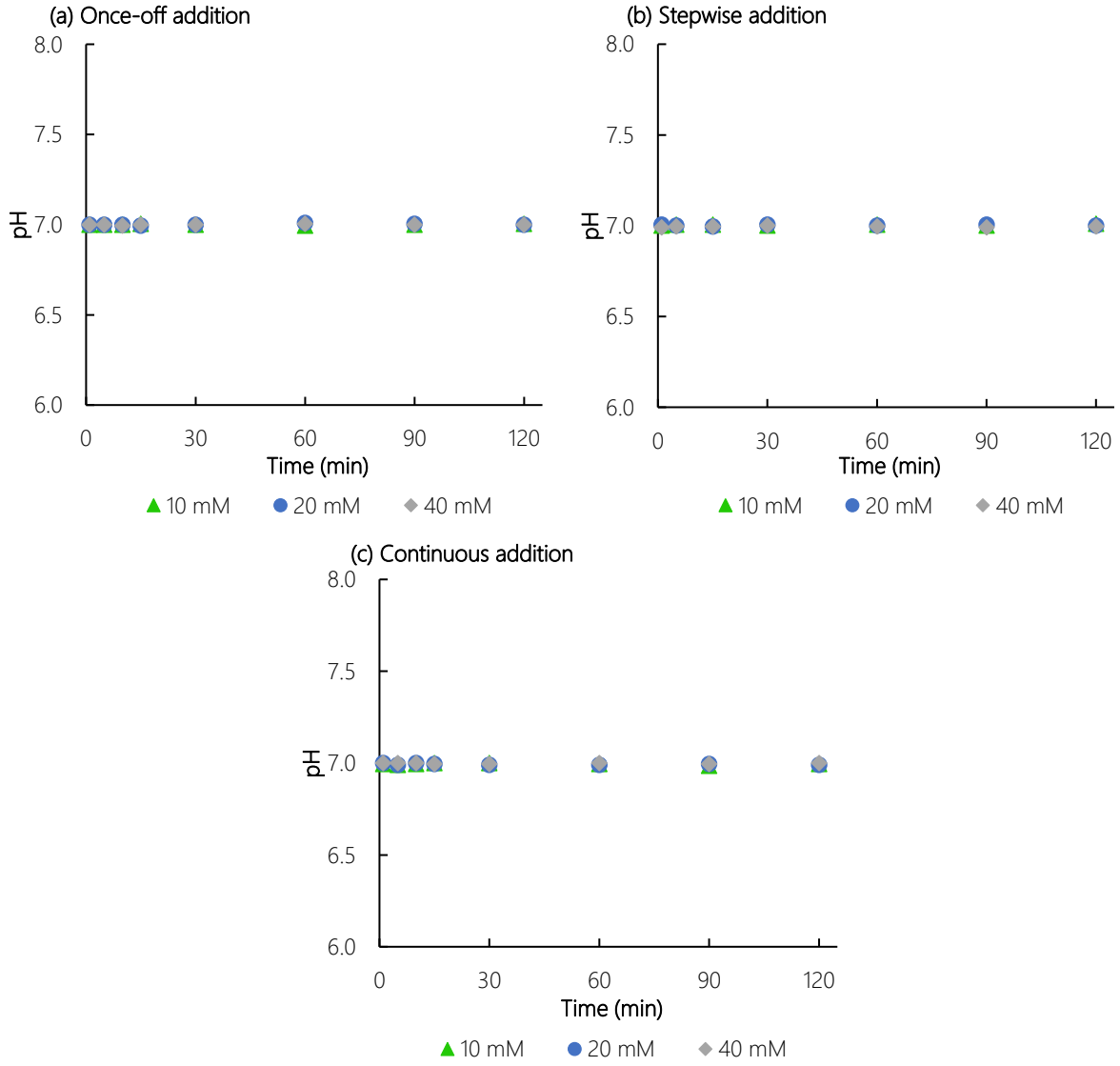

Figure 8.7: The pH profiles of the PaDa-I enzyme/buffer mixture using H_2O_2 delivery systems (a) once-off, (b) stepwise and (c) continuous addition and H_2O_2 concentrations 10 mM (▲), 20 mM (●) and 40 mM (◆). Reaction conditions: 20 ml 100 mM potassium phosphate buffer pH 7.0, 1.7 U ml^{-1} (NBD) PaDa-I, 200 rpm, 25 °C.

Appendix C

Appendix C.1: Residual styrene concentration profiles in the biotransformation study

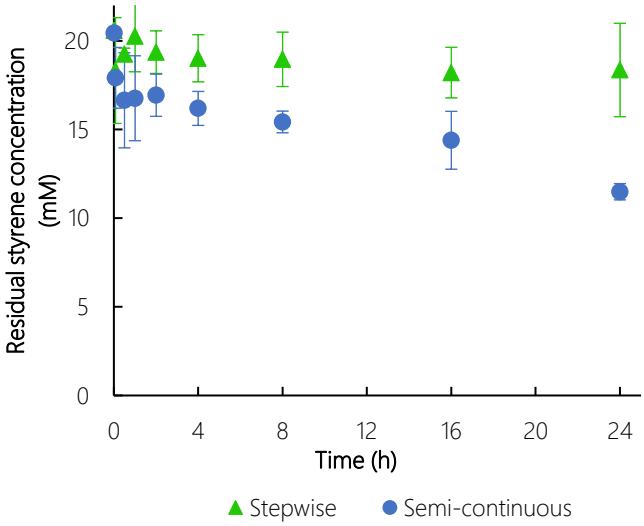

Figure 8.8: Residual styrene concentration profiles of the biotransformation of styrene using stepwise (▲) and semi-continuous (●) hydrogen peroxide addition. Reaction conditions: 20 ml 100 mM potassium phosphate buffer pH 7.0, 12 U ml^{-1} (NBD) PaDa-I, 20 mM styrene, 20 mM H_2O_2 stepwise (2.5 mM H2O2 every 30 min over the first 2 h) or semi-continuous (0.83 mM H_2O_2 every 1 h over 24 h) addition, 200 rpm, 25 °C.

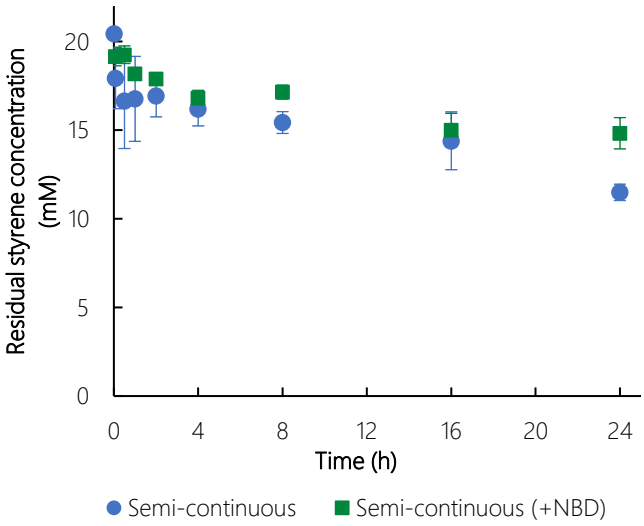

Figure 8.9: Residual styrene concentration profiles of the biotransformation of styrene using semi-continuous hydrogen peroxide addition in the absence (●) and presence (■) of 0.5 mM NBD. Reaction conditions: 20 ml 100 mM potassium phosphate buffer pH 7.0, 12 U ml^{-1} (NBD) PaDa-I, 20 mM styrene, 0.5 mM NBD, 20 mM H_2O_2 semi-continuous (0.83 mM H_2O_2 every 1 h over 24 h), 200 rpm, 25 °C.

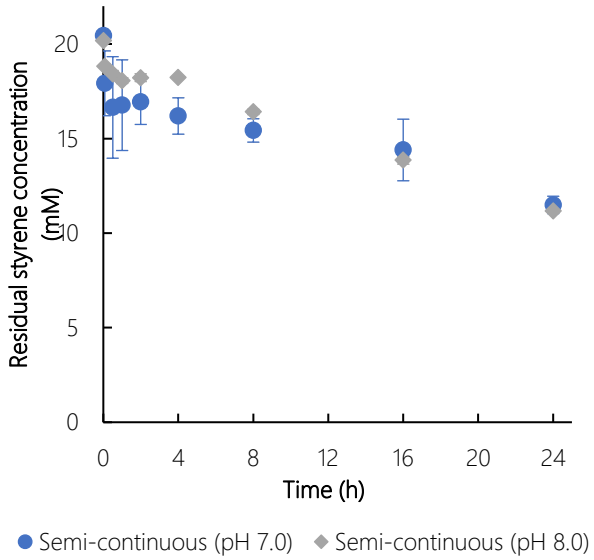

Figure 8.10: Residual styrene concentration profiles of the biotransformation of styrene using semi-continuous hydrogen peroxide addition at pH 7.0 (●) and pH 8.0 (◆). Reaction conditions: 20 ml 100 mM potassium phosphate buffer pH 7.0 or pH 8.0, 12 U ml^{-1} (NBD) PaDa-I, 20 mM styrene, 20 mM H_2O_2 semi-continuous (0.83 mM H_2O_2 every 1 h over 24 h), 200 rpm, 25 °C.

Appendix C.2: Carbon balances in the styrene biotransformation study

The carbon balance was calculated as the total product and residual substrate concentration relative to the initial substrate concentration.

Sample calculation:

$$Carbon\ balance\ (\%) = \frac{Concentration_{styrene} + Concentration_{styrene\ oxide}}{Concentration_{styrene,initial}}$$

It was determined that the carbon balance for the experiments that employed semi-continuous H_2O_2 delivery were lower compared to stepwise delivery. This may be attributed to opening and sealing the reaction vessels every hour (i.e. 24 times) to add the hydrogen peroxide compared to opening and closing the vessels only 4 times for stepwise delivery. As a result, carbon balances of about 60% were obtained for the semi-continuous delivery approach at the end of the 24 h reaction time and 90% for stepwise addition. It is, however, worth noting that the carbon balance improved to 80% for the semi-continuous delivery approach when NBD was present in the reaction mixture. Perhaps more of the substrate was dissolved in the acetonitrile solvent in which the NBD was added. It may be worthwhile establishing a better experimental set up for semi-continuous delivery and consider the use of organic solvents to minimise substrate and/or product loss thus potentially ensuring effective enzyme use.

Table 8.2: The carbon balances for all cases for the biotransformation of styrene experimental runs

	Stepwise				Semi-continuous			
Time (h)	Rep. 1	Rep. 2	Ave.	Std. dev	Rep. 1	Rep. 2	Ave.	Std. dev
0.02	100%	100%	100%	0%	100%	100%	100%	0%
0.08	100%	81%	90%	14%	96%	83%	89%	9%
0.5	96%	95%	95%	1%	93%	74%	83%	14%
1	106%	94%	100%	9%	93%	76%	84%	13%
2	100%	93%	96%	5%	92%	83%	87%	6%
4	98%	90%	94%	6%	88%	81%	85%	5%
8	99%	89%	94%	7%	83%	78%	81%	3%
16	94%	86%	90%	6%	70%	81%	76%	8%
24	100%	82%	91%	12%	59%	62%	61%	3%
	Semi-continuous (+NBD)				Semi-continuous (pH 8.0)			
Time (h)	Rep. 1	Rep. 2	Ave.	Std. dev	Rep. 1	Rep. 2	Ave.	Std. dev
0.02	100%	100%	100%	0%	100%	100%	100%	0%
0.08	102%	102%	102%	0%	96%	95%	96%	0%
0.5	99%	107%	103%	5%	94%	93%	93%	1%
1	96%	100%	98%	3%	93%	92%	93%	1%
2	97%	100%	99%	2%	96%	94%	95%	1%
4	91%	98%	94%	5%	95%	96%	96%	0%
8	96%	96%	96%	1%	87%	86%	87%	1%
16	78%	89%	84%	7%	74%	73%	74%	1%
24	84%	80%	82%	2%	60%	60%	60%	0%

Reaction conditions: 20 ml 100 mM potassium phosphate buffer pH 7.0 or pH 8.0, 12 U ml^{-1} (NBD) PaDa-I, 20 mM styrene, with or without 0.5 mM NBD, 20 mM H_2O_2 stepwise (2.5 mM H2O2 every 30 min over the first 2 h) or semi-continuous (0.83 mM H_2O_2 every 1 h over 24 h) addition, 200 rpm, 25 °C.

Appendix C.3: pH profiles for the styrene biotransformation study

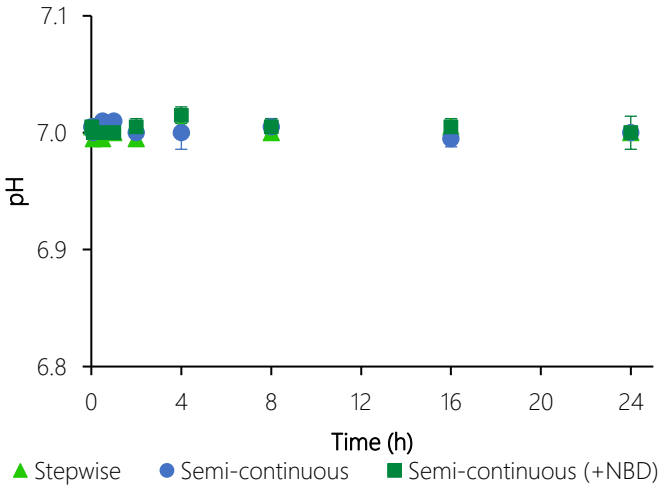

Figure 8.11: pH profiles of the biotransformation of styrene using stepwise (▲) and semi-continuous hydrogen peroxide delivery in the absence (●) and presence (■) of 0.5 mM NBD and continuous hydrogen peroxide addition in the absence (a) and presence (b) of 0.5 mM NBD. Reaction conditions: 20 ml 100 mM potassium phosphate buffer pH 7.0, 12 U ml^{-1} (NBD) PaDa-I, 20 mM styrene, 20 mM H_2O_2 stepwise (2.5 mM H_2O_2 every 30 min over the first 2 h) or semi-continuous (0.83 mM H_2O_2 every 1 h over 24 h) addition , 200 rpm, 25 °C.

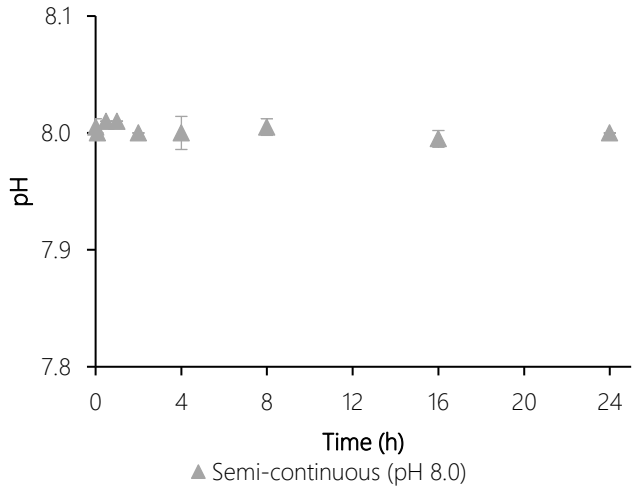

Figure 8.12: pH profile of the biotransformation of styrene using semi-continuous peroxide delivery at pH 8.0 in. Reaction conditions: 20 ml 100 mM potassium phosphate buffer pH 8.0, 12 U ml^{-1} (NBD) PaDa-I, 20 mM styrene, 20 mM H_2O_2 semi-continuous (0.83 mM H_2O_2 every 1 h over 24 h) addition , 200 rpm, 25 °C.

Appendix C.4: Enzyme deactivation kinetics in the presence of styrene only

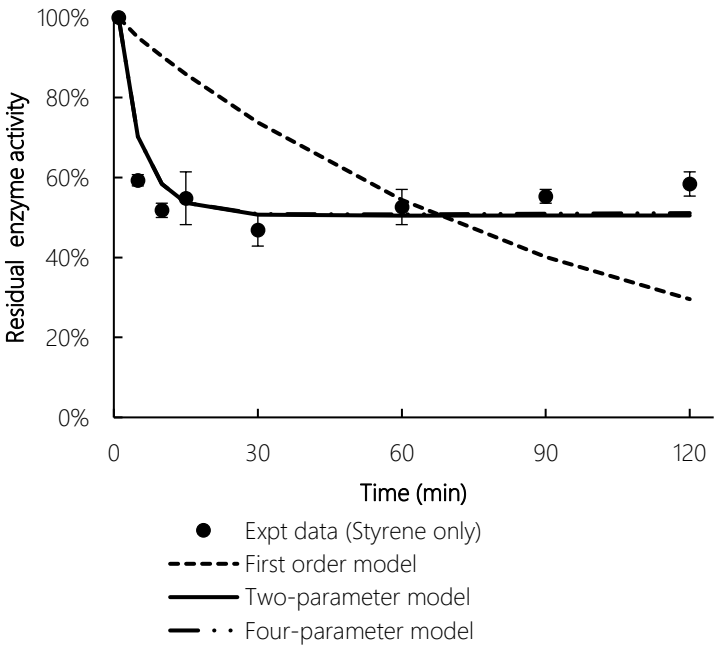

Figure 8.13: The enzyme deactivation kinetics of PaDa-I in the presence of 20 mM styrene only modelled by the first order (- - - -), two-parameter (——) and four-parameter (— · · —) models. Reaction conditions: 20 ml 100 mM potassium phosphate buffer pH 7.0, 1.7 U ml^{-1} (NBD) PaDa-I, 200 rpm, 25 °C.

Table 8.3: Deactivation kinetic parameters for the peroxygenase activity of PaDa-I in the presence of 20 mM styrene as a sole substrate, where model constants k_1, k_2, α_1 and α_2 were determined by non-linear regression

Kinetic parameter	First order model	Two-parameter model	Four-parameter model
k_1 (min^{-1})	0.01	0.18	0.18
k_2 (min^{-1})			0.001
α_1		0.51	0.51
α_2			0.56
R^2	0.15	0.87	0.88
χ^2	0.85	0.05	0.04
AARD (%)	1.41	0.08	0.11
AIC	11.09	2.59	6.43
BIC	7.80	-1.79	-0.15

Appendix C.5: Enzyme inhibition kinetics calculations

Rate equations for reactions affected by inhibition can initially be expressed through the unmodified Michaelis Menten equation in terms of apparent parameters v_{app} and K_{app} (Equation 8.4) (Illanes *et al.*, 2008). The initial reaction rates data was obtained from the first 5 minutes of the biotransformation (Table 8.4) and linearised by the Lineweaver-Burke equation (Equation 8.5).

$$v = \frac{v_{app}\,[S]}{K_{app}+[S]} \tag{8.4}$$

$$\frac{1}{v} = \frac{K_M}{v_{max}}\frac{1}{[S]} + \frac{1}{v_{max}} \tag{8.5}$$

Table 8.4: Initial rates data for biotransformation of styrene at different H_2O_2concentrations

	2.5 mM H_2O_2 [v] initial reaction rate (mM min^{-1})				5 mM H_2O_2 [v] initial reaction rate (mM min^{-1})				10 mM H_2O_2 [v] initial reaction rate (mM min^{-1})			
[S] (mM)	Rep. 1	Rep. 2	Ave.	Std. dev.	Rep. 1	Rep. 2	Ave.	Std. dev.	Rep. 1	Rep. 2	Ave.	Std. dev.
2.5	0.107	0.095	0.101	0.006	0.064	0.058	0.061	0.003	0.033	0.025	0.029	0.004
5	0.111	0.106	0.109	0.003	0.073	0.068	0.071	0.003	0.038	0.041	0.039	0.002
10	0.115	0.114	0.115	0.001	0.075	0.057	0.066	0.009	0.047	0.036	0.041	0.006
20	0.105	0.101	0.103	0.002	0.078	0.056	0.067	0.011	0.038	0.046	0.042	0.004

Reaction conditions: 20 ml 100 mM potassium phosphate buffer pH 7.0, 12 U ml^{-1} (NBD) PaDa-I, 20, 10, 5 or 2.5 mM styrene, 10, 5 or 2.5 mM mM H_2O_2, 200 rpm, 25 ^{o}C.

Based on the Lineweaver-Burke double reciprocal plots shown in Figure 8.14, it was determined that the apparent kinetic parameters for the biotransformation were v_{app} = 0.11 mM min^{-1} and K_{app} = 0.21 mM. Thereafter, the kinetic parameters for non-competitive inhibition were obtained from the secondary plot in Figure 8.15 - K_I = 2.30 mM and v_{max} = 0.24 mM min^{-1}. The results from the graphical analysis agree with what Illanes *et al.* (2008) prescribed: for non-competitive inhibition $K_M = K_{app}$ and $v_{max} > v_{app}$. These values were therefore used as a guideline for the nonlinear regression analysis.

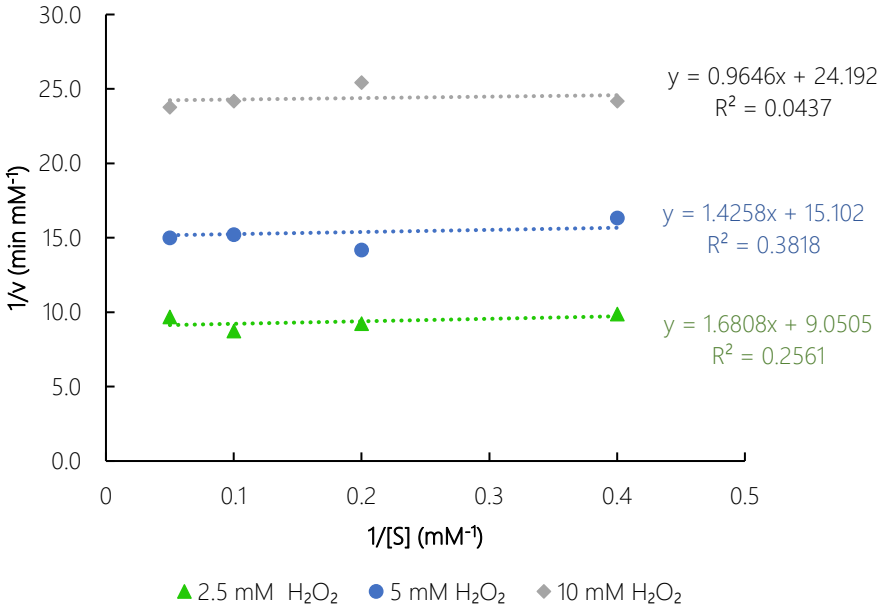

Figure 8.14: Lineweaver-Burke reciprocal plots

Table 8.5: Results for determining apparent kinetics from the Lineweaver-burke method of linearisation

H_2O_2 (mM)	intercept	v_{app}	slope	K_{app}	$1/v_{app}$	$1/K_{app}$	K_{app}/V_{app}
10	24.19	0.041	11.16	-0.46	24.19	-2.17	-11.16
5	15.10	0.067	-6.15	0.42	14.50	2.36	6.15
2.5	9.05	**0.111**	-1.90	**0.21**	9.05	4.76	1.90

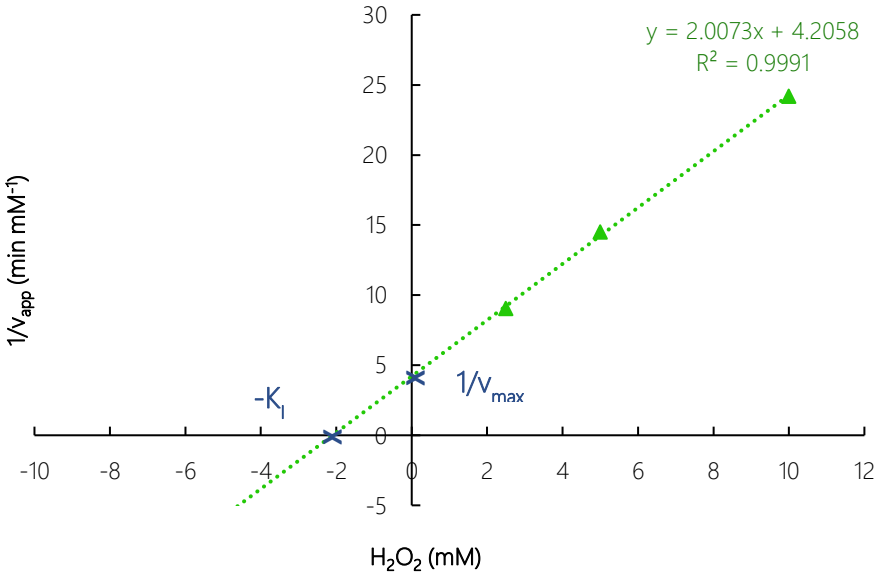

Figure 8.15: Secondary plot to determine the kinetic parameters for non-competitive inhibition